ABSTRACT

Title of Dissertation:	FUNCTIONAL CHARACTERIZATION OF HEME TRANSPORTERS IN ZEBRAFISH
	Jianbing Zhang, Doctor of Philosophy, 2017
Dissertation directed by:	Professor Dr. Iqbal Hamza, Department of Animal and Avian Sciences

Hrg1 and Mrp5 are identified as eukaryotic heme importer and exporter, respectively. Two Hrg1 paralogs have been annotated in zebrafish genome, Hrg1a (Slc48a1b) and Hrg1b (Slc48a1a) with 84% homology in protein sequences. *Hrg1a* and *hrg1b* are widely expressed in embryonic and adult zebrafish. Yeast growth assays reveal that zebrafish Hrg1a and Hrg1b are both capable of heme import. However, *hrg1a* and *hrg1b* double knockout (*hrg1* DKO) zebrafish generated by CRISPR/Cas9 has no overt defects in differentiation and maturation of erythroid cells. Knockdown of *hrg1a* in *hrg1b* mutants or *vice versa* does not impair erythroid lineage in zebrafish embryos. These genetic results suggest that Hrg1 is not required for maturation and hemoglobinization of primitive erythroid cells.

Hrg1a and *hrg1b* mRNA are upregulated in adult kidneys and spleens upon PHZ-induced hemolysis, together with *hmox1*, a downstream heme degrading enzyme, suggesting that Hrg1 is involved in adult heme-iron recycling during erythrophagcytosis in kidney and spleen of adult zebrafish. DAB-enhanced Perl's

iron staining reveals that iron is accumulated in macrophages in the kidney and spleen in adult wild-type zebrafish. However, macrophages with positive Perl's staining are rarely found in the kidney of *hrg1* DKO and instead large amount of iron is deposited in renal tubules, suggesting defects in heme-iron recycling by kidney macrophages in *hrg1* DKO under PHZ-induced hemolysis. Whole transcriptome sequencing of mRNA extracted from spleens and kidneys reveals massive differentially expressed genes in *hrg1* DKO involved in immune response, lipid transport, oxidation-reduction process and proteolysis. These indicate that *hrg1* DKO are deficient in recycling heme-iron derived from damaged RBCs in the absence of functional Hrg1.

Phylogenetic analysis reveals that Mrp5 and Mrp9 are closed homologs in the zebrafish genome. Yeast growth assays reveal that both zebrafish Mrp5 and Mrp9 are capable of heme export. Morpholino knockdown of *mrp*5 and *mrp9* in zebrafish showed severe anemia in developing embryos indicating their involvements in erythropoietic development. Subsequent generation and characterization of *mrp*5 and *mrp*9 mutants by CRISPR/Cas9 will further define the function of Mrp5 and Mrp9 during zebrafish development.

FUNCTIONAL CHARACTERIZATION OF HEME TRANSPORTERS IN ZEBRAFISH

By

Jianbing Zhang

Dissertation submitted to the Faculty of the Graduate School of the
University of Maryland, College Park, in partial fulfillment
of the requirements for the degree of
Doctor of Philosophy
2017

Advisory Committee:
Dr. Iqbal Hamza, Chair
Dr. Karen Carleton
Dr. Tom Porter
Dr. Byung-Eun Kim
Dr. Paul Liu

Dedication

To my parents, my wife, my newborn son, my family
and mentors who made this possible

Acknowledgement

I would not attain this dissertation without the support and guidance of my committee, my advisor, and all mentors through my academic career. Thank you all who have generously supported me during the past six years, kept me up when I was frustrated, and enlightened me when I was puzzled.

I am especially grateful for my Ph.D advisor, Prof. Iqbal Hamza, for his thoughtful supervision and continuous support. I would like to thank Iqbal for the scientific training, improving my presentation and writing skills, and teaching me how to philosophically tackle scientific questions. I was impressed by his passion, enthusiasm for scientific research, and "Think Big" as provoked by UMD. Specific thanks also go to Iqbal for the advice he shared with me as experienced mentor for life.

Grateful thanks also come to my thesis committee members, Dr. Karen Carleton, Dr. Tom Porter, Dr. Byung-Eun Kim, and Dr. Paul Liu, for providing valuable and thoughtful scientific comments, discussions and suggestions. I appreciate all the time and effort you have put in throughout this degree. These will be of great benefit to me to become a better scientific researcher.

I would like to thank the current and previous members in the Hamza lab. Thanks to Kate Pinter who always took good care of the fish facility and urged me to take good care of it. Thanks to Dr. Paul Liu at NIH, Dr. Barry H. Paw and Dr. Leonard I. Zon of Harvard University, who shared me transgenic fish. Thanks to Dr. Xiaojing Yuan for the discussions and troubleshooting when I was working on the bench, and also for reading and editing almost everything I have written in the lab. I

would like to thank Dr. Tamika Samuel, Dr. Nicole Rietzschel, Dr. Jason Sinclair, Dr. Tamara Korolnek, Simon Beasley, Ian Chambers, Rini Pek and Shyrice Mitchell, for all the common time we have shared in the lab.

Thanks to Dr. Michael Krause and Dr. Sijung Yun from the NIH for sequencing and data analysis on RNAseq experiments. Thanks to Dr. Jeffery Wolf from EPL, INC. for providing technical and intellectual support for physiological and histological studies in zebrafish. I really enjoyed our discussions and have learned a lot from his in-depth knowledge of fish pathology.

Special thanks also go to all the fellows in the Department of Animal and Avian Sciences, to keep everything working and ready, for me to settle down and focus on the research. Thanks to Sheryl Grey who chased me for all the paperwork to be fulfilled; I might have lost my stipends several times without her help.

Six years of studying in the US has taught me to be independent and to take responsibility for my life. Tremendous gratitude goes to my parents who always supported me. Although I could not physically be with them, home is always the best "safe house" for me. Thanks to my wife, Linlin Lyu, to be with me during the last year and the hardest time of my Ph.D study. Thank you for bringing our newborn son, Charles Xingjian Zhang; your two always cheered me up when I was exhaustedly back from work. This love will encourage me to explore the coming part of our life and overcome difficulties.

Thank you all.

Table of Contents

List of Figures and Tables

Chapter 1

Chapter 3

Chapter 4

Chapter 5

List of Abbreviations

ABCC	ABC-transports subfamily C
AGM	aorta-gonad-mesonephros
ALA	δ-aminolevulinic acid
ALAD	ALA dehydratase
ALAS	δ-aminolevulinic acid synthase
APX	ascorbate peroxidase
BCRP	breast cancer resistance protein
BFU-E	burst- forming unit- erythroid
BMDM	bone marrow derived macrophages
CFU-E	colony- forming unit- erythroid
CHT	caudal hematopoietic tissue
CPgenIII	coproporphyrinogen III
CPOX	coproporphyrinogen oxidase
CRISPR	clustered regularly interspaced short palindromic repeats
cRNA	Capped RNA
CSA	sideroblastic anemia
DMT1	divalent metal transporter 1
dpf	day post fertilization
DKO	double knockout
DSB	double strand breaks
dSTORM	direct stochastic optical reconstruction microscopy
EBI	erythroblastic island
EP	erythrophagocytosis
EPO	erythropoietin
EPOR	erythropoietin receptor
FACS	Fluorescence activating cell sorting
FBXL5	F box and leucine-rich repeat protein 5
FDR	False Discovery Rate
FECH	ferrochelatase
Fe-S	iron-sulfur cluster
FLVCR	Feline leukemia virus subgroup C receptor-related protein 1
Fpn1	ferroportin1
GO	gene ontology
GRX5	glutaredoxin 5
HEP	hepatoerythropoietic porphyria
hpf	hour post fertilization
Hmox1, HO1	heme oxygenase 1
HRG1	Heme Responsive Gene -1
HRI	heme regulated inhibitor
HRP	horse radish peroxidase
HSC	hematopoietic stem cell
ICM	intermediate cell mass

IDA	Iron deficiency anemia
INDEL	insertion or deletion
IRE	iron responsive element
IRP	iron regulatory protein
LCR	globin locus control
MARE	MAF recognition elements
MFRN	nuclear receptor coactivator 4
MRP	Multidrug resistant protein
MudPIT	multidimensional protein identification technology
NALP12	NACHT, LRR and PYD domains-containing protein 12
NBF	Neutral buffered formalin
NCOA4	nuclear receptor coactivator 4
NHEJ	non-homologous end joining
PBG	porphobilinogen
PBGD	porphobilinogen deaminase
PBI	Posterior blood island
PCBP	Poly r(C)-binding protein
PCT	porphyria cutanea tarda
PHZ	Phenylhydrazine
PPgenIX	protoporphyrinogen IX
PPIX	protoporphyrin IX
PPOX	protoporphyrinogen oxidase
RBC	Red blood cell
RDA	rhodamine B-[(2, 2-bipyridin-4-yl) aminocarbonyl] benzyl ester
RES	reticuloendothelial system
RPM	red pulp macrophage
SA	succinylacetone
SLC	solute carrier
SPRY	SPla/RYanodine receptor
STEAP3	six-transmembrane epithelial antigen of prostate 3 reductase
TALEN	transcription-activator like effector nuclease
Tf	transferrin
TFR	transferrin receptor
TMHMM	Tied Mixture Hidden Markov Model
UROD	uroporphyrinogen decarboxylase
UROgen III	uroporphyrinogen III
UROS	uroporphyrinogen synthase
VDA	ventral wall of dorsal aorta
WISH	whole mount in situ hybridization
WT	wild-type
YSL	yolk-syncytial layer

Chapter 1: Introduction

Heme (iron-protoporphyrin IX) is an iron-containing porphyrin which can serve as a cofactor for various biological processes, such as oxygen transport, miRNA processing, electron transfer, and circadian clock control *et al* (1, 2). Although iron is abundant on this planet, it is not readily bioavailable to humans, rendering iron deficiency anemia (IDA) as a common nutritional disorder (3). Compared to inorganic iron, heme is the most absorbable form of iron for human nutrition, highlighting the importance of understanding how heme is transported and utilized in our daily diet (4). Moreover, human dietary iron only accounts for around 10 % of daily iron requirement which complements for daily iron losses, while the majority of iron supply comes from heme-iron recycling from clearance of senescent red blood cells (RBCs) (5, 6). Therefore, iron absorption and heme-iron recycling contribute to systematic iron homeostasis. One of the most evident symptoms for defects in iron transport and heme synthesis is anemia, which is due to aberrant production or function of RBCs in the circulating blood system (7). RBCs contain approximately 70 % of overall iron inside the body, which makes it particularly important to maintain organismal iron homeostasis (7). Thus, understanding how heme is synthesized, trafficked and recycled may shed light on the pathology of anemia.

Heme biosynthesis

In most eukaryotes, heme is synthesized via a widely conserved eight-step pathway in cytosol and mitochondria requiring coordinated substrate transport between the mitochondria and cytosol (8). The first step initiates in the mitochondrial matrix and is catalyzed by δ-aminolevulinic acid synthase (ALAS) to synthesize δ-aminolevulinic acid (ALA) from glycine and succinyl-coenzyme A. ALA is subsequently transported out of the mitochondria

to the cytosol for the following four enzymatic reaction steps: ALA to porphobilinogen (PBG) catalyzed by ALA dehydratase (ALAD); PBG to an unstable polymer hydroxymethylbilane by porphobilinogen deaminase (PBGD); hydroxymethylbilane to uroporphyrinogen III (UROgen III) by uroporphyrinogen synthase (UROS); and UROgen III to coproporphyrinogen III (CPgen III) by uroporphyrinogen decarboxylase (UROD). CPgen III is then transported into the mitochondria where coproporphyrinogen oxidase (CPOX), a mitochondrial intermembrane space enzyme, catalyzes the formation of protoporphyrinogen IX (PPgen IX). The inner mitochondrial membrane enzyme protoporphyrinogen oxidase (PPOX) catalyzes the formation of protoporphyrin IX (PPIX) from PPgen IX in the mitochondrial matrix. On the last step, ferrochelatase (FECH) catalyzes the insertion of ferrous iron (Fe^{2+}) into PPIX to form heme.

Regulation of heme biosynthesis in RBCs

Tremendous amount of heme is synthesized during differentiation and maturation of RBCs. The efficiency of converting iron to heme in maturing erythroid cells is extremely high, resulting in heme-iron concentrations to be over 40,000-fold greater than non-heme iron in mature RBCs (9, 10). One mode of tackling this large requirement for heme would be upregulating heme synthesis in mitochondria and then mobilizing heme out of the mitochondria for insertion into cytoplasmic globin to couple synthesis with increasing globin protein production. In contrast, it is also essential to downregulate heme synthesis and decrease intracellular iron content when globin production is low in the early stage of erythropoietic development, since both free heme and iron are toxic to erythroid cells by inducing oxidative stresses. Failure to regulate heme synthesis during erythropoiesis will cause either iron-deficient or iron-overload anemia (11).

Although there are eight enzymatic steps for heme biosynthesis, the rate-limiting step is the synthesis of ALA from glycine and succinyl-coenzyme A, catalyzed by ALAS (12). Two

forms of ALAS exist, ALAS1 and ALAS2. ALAS1 is ubiquitously expressed in all the tissues (13), while ALAS2 (or ALAS-E), is exclusively expressed in developing erythroid cells (14). ALAS2 is activated by the transcription factor GATA1, a master regulator for erythropoiesis. Chip-Seq analysis using G1E-ER4 erythroid progenitor cell line derived from *Gata1* mutant mice identified two GATA-1 *cis* elements in the first and eighth introns of *Alas2* (15–17). Disruption of these two GATA1-binding elements abrogates expression of ALAS2 and subsequent inhibition of heme synthesis, which can be rescued by supplementing cells with high concentrations of ALA, the product of ALAS (16, 17). Another regulation of ALAS2 occurs at post-transcription level, modulated by iron responsive elements (IREs) in the 5'UTR. IREs interact with iron regulatory proteins (IRPs), linking the regulation of heme biosynthesis in erythroid cells to iron availability (18). Under iron deficient conditions, IRPs bind to IREs and inhibit *Alas2* mRNA translation. Conversely, when intracellular iron level increases, IRPs are either degraded or converted to an aconitase by a [4Fe-4S] and *Alas2* mRNA translation resumes to promote heme synthesis. The regulation of ALAS2 expression is coordinated with the cellular iron levels to tightly control cellular heme content.

FECH is a second limiting enzyme in the heme biosynthetic pathway. Transcription of *Fech* spikes during terminal erythroid differentiation and is controlled by the transcription factors SP1, NFE2 and GATA1(19). Furthermore, the enzymatic activity of FECH is dependent on the presence of iron-sulfur cluster [4Fe–4S], again linking iron regulation to heme synthesis (20). Distinct erythroid-specific elements have been identified in the promoter region of *Fech*, together with erythroid-specific alternate splicing in the 3′ noncoding region of *Fech* mRNA in the mouse genome (21, 22), further underscoring the unique regulatory mechanisms for heme synthesis in RBCs maturation.

Beside regulation of heme synthesis in erythroid cells, globin synthesis is controlled by the Heme/BACH1 axis, in which heme binds to BACH1, a transcription suppressor, to relieve the depression for globin gene expression (23). These regulations collectively

coordinate the cellular iron level, heme synthesis, and globin protein expression, to maintain heme and iron homeostasis in erythroid cells.

Iron acquisition during erythropoiesis

The tremendous need for iron for heme synthesis during erythropoiesis mandates an efficient pathway to uptake extracellular iron. Erythroid cells rely on a high affinity system composed of transferrin (Tf) and transferrin receptor (TFR). One molecule of transferrin can bind to two ferric iron atoms with an association coefficient of 10^{-20} M at physiological pH (24). Transferrin receptor 1 (TFR1, also known as CD71) tightly binds to TF, permitting developing erythroid cells to uptake iron efficiently from the circulation. The complex of iron-bound TF and TFR1 is internalized by receptor-mediated endocytosis and the ferric iron is then released from TF as the endosomes acidify. Since only ferrous iron can be utilized for erythropoietic heme synthesis, the released ferric iron is reduced to ferrous by STEAP3 (six-transmembrane epithelial antigen of prostate 3 reductase) (25). The ferrous iron is transported out of endosome by DMT1 (divalent metal transporter 1, also known as NRAMP2 and SLC11A2) (26). The apo-TF/TFR1 complex is then recycled back to the cell surface, where apo-TF dissociates from the TFR1 and re-enters the circulation. The holo-TF/TFR1 and apo-TF/TFR1 cycle ensures that erythroid cells optimize iron uptake from the circulation for maximal hemoglobin production.

Non-TF iron uptake also exists in erythroid cells, although the overall evidence is not conclusive and postulated to be more relevant during pathological conditions of iron overload, when serum TF is saturated by iron (27). By exposing erythroid cells to ferrous ammonium sulfate under in TF-free conditions, erythroid cells from all developmental stages can uptake non-TF iron and accumulate redox-active labile iron with generation of reactive oxygen species. However, the utilization of non-TF iron for heme synthesis during maturation of erythroid cells has not been probed. It is speculated that uptake of non-TF iron

may account for ineffective erythropoiesis of developing precursors in the bone marrow with shortened lifespan of mature RBCs in the circulation during iron-overload condition. *In vivo* study of non-TF iron uptake by erythroid cells should be carried out to further delineate this pathway.

Upon arrival in the cytosol, iron has to be either stored or further transported to the mitochondria for utilization, since free iron is cytotoxic due to Fenton chemistry (28). Iron is stored in the cytosol by binding to ferritin with the aid of Poly r(C)-binding protein (PCBP) (29). PCBP1 and PCBP2 exhibit high affinity for ferritin *in vitro* and PCBP1 and its paralog PCBP2 co-immuoprecipitate with ferritin in HEK293 cells. Co-expression of PCBP1 and PCBP2 together with human ferritins in yeast activates an iron deficiency response by increasing iron deposition into ferritin. However, knockdown of PCBP1 but not PCBP2 impaired iron utilization during RBCs maturation, and PCBP1 deficient mice show microcytic anemia (30).

Iron storage has to be released before entering mitochondria for heme or iron-sulfur cluster synthesis. While PCBP1 mediates delivery and integration of iron into ferritin, nuclear receptor coactivator 4 (NCOA4) promotes release of ferritin iron by directing ferritin to autophagosomes for protein degradation (30); NCOA4 can be immunoprecipitated with erythroid ferritin. Binding of PCBP1 precedes NCOA4-ferritin interaction, coinciding with globin synthesis during erythroid maturation. NCOA4-deficient cells exhibit massive accumulation of iron in ferritin with impaired hemoglobinization and enhanced erythroid cell death by ferritinophagy, since ferritin is an essential source of iron for heme production during terminal erythroid differentiation.

Upon release from ferritin, iron is then transported into mitochondria, which is mediated by SLC25A37 (mitoferrin1, MFRN1), a protein belonging to the family of mitochondrial solute carrier proteins. MFRN1 is expressed in the inner mitochondrial membrane and transports iron across mitochondrial membranes (31). Mouse erythroblasts

derived from *Mfrn1*-dificient embryonic stem cells show a complete blockage of iron incorporation into heme. Defect in Mfrn1 results in profound hypochromic anemia and erythroid maturation arrest owing to insufficient mitochondrial iron uptake in zebrafish. Deletion of two yeast Mfrn homologs, Mrs3 and Mrs4 impairs incorporation of iron into PPIX and formation of Fe-S cluster assembly, collectively resulting in poor growth under low iron conditions. Deletion of *Mfrn1* in mice is embryonic lethal and mice with targeted deletion of *Mfrn1* in adult hematopoietic tissues show severe anemia owing to deficits in erythroblast formation (32).

The majority of iron for heme synthesis in the mitochondria is acquired from the TF-ferritin-MFRN axis in erythroid cells. Alternate possible pathway of iron uptake by mitochondria was recently delineated as a "kiss and run" interaction between endosomes and mitochondria (33). Three-dimensional direct stochastic optical reconstruction microscopy (dSTORM) revealed that transient interactions between iron-bound TF within endosomes and mitochondria are capable of directing iron into mitochondria in erythroid cells. Tracing experiment with mitochondria-specific iron sensor RDA (rhodamine B-[(2, 2-bipyridin-4-yl) aminocarbonyl] benzyl ester) confirmed functional iron transfer from an interacting TF-endosome to mitochondria. The motility of TF-endosomes is significantly reduced upon encountering mitochondria, while blocking intra-endosomal iron release led to significantly increased motility of TF-endosomes and increased duration of endosome–mitochondria interactions.

Regulation of iron uptake in RBCs

The coordination between iron uptake, heme synthesis, and globin protein expression dictates a tightly regulated system during erythroid differentiation. Like the regulation of the rate-limiting enzymatic step of ALAS2 during heme synthesis, the IRE/IRP system is also essential in controlling cellular iron uptake and storage via a posttranscriptional manner. Two IRPs has been identified, IRP1 and IRP2. The binding of IRPs to IREs in 3'-UTR of *Tfr1* mRNA increases the stability and strengthens the translation of TFR1, promoting cellular iron uptake. IRPs can also bind to IREs situated in the 5'-UTR region of both H and L subunits of ferritin mRNAs to inhibit ferritin translation (34).

Although IRPs can regulate cellular iron level by modulating mRNA translation or degradation, the IRE-binding activity of IRPs can be also inversely regulated by iron, representing a typical negative feedback in biological processes (18). Both IRP1 and IRP2 are ubiquitously expressed. However, the mechanisms are distinct in controlling IRP1 and IRP2 activity in response to cellular iron pool. The binding activity of IRP1 is negatively regulated by iron-sulfur cluster [4Fe-4S] insertion. Under irons-replete condition, the binding of IRP1 to IREs is prevented by 4[Fe-S] cluster assembled into IRP1, which can decrease iron uptake by destabilizing TFR1 and enhancing ferritin translation for iron storage. IRP2 does not contain a Fe-S cluster and is regulated by iron via proteasome degradation, mediated by FBXL5 (F box and leucine-rich repeat protein 5) (35). In summary, the regulation of the IRE-binding activities of IRP1 and IRP2 assures the appropriate expression of IRP targeted genes and cellular iron balance.

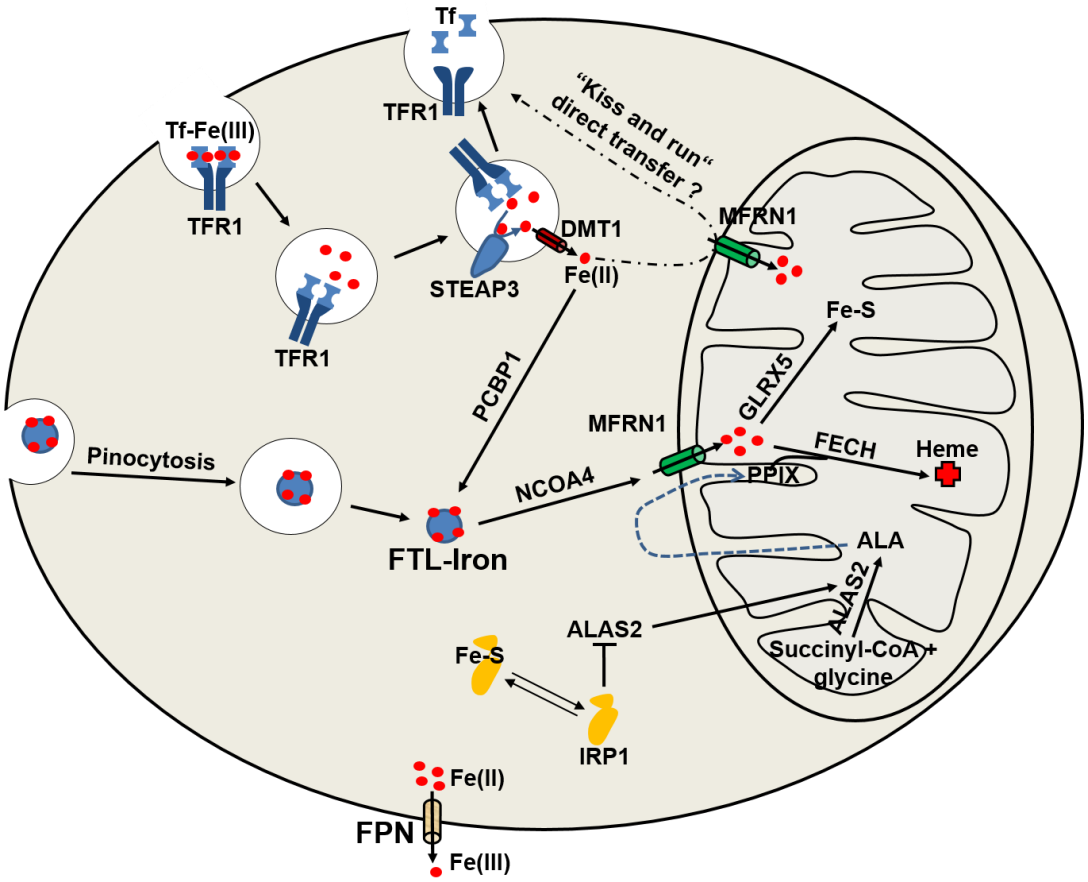

Figure 1.1 Iron metabolism in erythroid cells

Iron acquisition in erythroid cells is dependent on endocytosis of Tf-bound Fe (Tf-Fe(III)) via the transferrin receptor (TFR1). Iron (Fe(III)) is imported into the cytoplasm by DMT1 after reduction by STEAP3. Pinocytosis of extracellular ferritin may also contribute to iron-uptake in erythroid cells. Iron can be stored in the ferritin (FTL) (FTL-Iron) mediated by PCBP1 and can be released from FTL promoted by NCOA4. MFRN1 is responsible for bringing iron to the mitochondria for heme synthesis. It is uncertain whether "kiss and run" direct iron transfer exists between lysosomes and the mitochondria. Iron is inserted into PPIX by FECH to produce heme. Iron is also used for Fe-S cluster synthesis with involvement of GLRX5. IRP1 binding can inhibit translation of ALAS2 to prevent the accumulation of toxic heme intermediates. Cellular iron efflux is mediated by FPN and requires iron oxidation on the extracellular side.

Heme as a regulator during erythropoiesis

Heme itself can modulate gene expression by negatively regulating the transcriptional repressor BACH1. Heme strongly stimulates transcription of heme oxygenase 1 (HO-1 or HMOX1), the enzyme which catalyzes heme degradation. BACH1 represses *HMOX1* gene expression by binding to multiple MAF recognition elements (MAREs) sites located within *HMOX1* enhancers by forming heterodimers with another transcription factor MAF. Under heme-replete condition, heme binding to heme regulatory motifs within BACH1 releases it from the enhancers. This allows binding of MAF-NRF2 or MAF-NFE2 heterodimers which function as transcriptional activators of HMOX1 (36). Interestingly, *Hmox1* mRNA decreases during erythroid differentiation of MEL cells, a murine erythroleukaemia cell line, while heme biosynthesis is upregulated to make sufficient quantities of hemoglobin (37). HMOX1 overexpression impairs hemoglobin synthesis, while HMOX1 deficiency enhances hemoglobinization in cultured erythroid cells (38). Thus, HMOX1 can control the regulatory heme pool at appropriate levels for erythroid differentiation.

MAREs can also be found in the enhancer of the L subunit of ferritin and globin locus control region (LCR) (23, 39). Heme deficiency represses protein translation, especially globin synthesis, by activating heme regulated inhibitor (HRI), a stress protein kinase which phosphorylates eIF2a (40). Phosphorylation of eIF2a prevents the exchange of GDP into GTP and inhibits globin mRNAs translation, ensuring globin production can be coordinated with heme synthesis during erythroid differentiation. HRI deficient mice suffer from hyperchromic normocytic anemia with erythroid hyperplasia and erythrocytes are loaded with multiple globin inclusions (41).

Mobilization of heme biosynthetic intermediates during erythropoiesis

Although heme is an essential cofactor, the accumulation of free heme or its intermediates are cytotoxic (42). Therefore, the synthesis and transport of these molecules must be tightly controlled and the time when the intermediates are processed and the location where the particular enzymes appear for catalytic reactions have to be coordinately regulated.

ALA, product of ALAS from the first step of heme synthesis, has to be transported out of the mitochondria to be utilized by ALAD in the cytosol. This transporter was recently identified to be mediated by SLC25A38, a putative glycine/ALA transporter (43). Mutation in SLC25A38 results in mitochondria ALA deficiency and causes non-syndromic autosomal recessive congenital sideroblastic anemia (CSA). Interestingly, mutations in *slc25a38* in zebrafish causes phenotypes similar to CSA and the anemia phenotypes can be rescued by glycine together with folate, but surprisingly not ALA, questioning the direct role for SLC25A38 as an ALA transporter (44).

ABCB6, a mitochondrial outer membrane ATP-dependent transporter, was proposed to mediate the transport of CPgen III from the cytosol to the mitochondria (45, 46). However, a direct evidence of CPgen III transport by ABCB6 is lacking and the substrates transported by ABCB6 are still elusive. Defects in ABCB6 is not associated with hematological defects (47). ABCB6 is dispensable for erythropoiesis and localizes to the endosomal/lysosomal compartments and plasma membrane of erythrocytes rather than the mitochondria (48).

The ins and outs of heme transport

The hydrophobicity and cytotoxicity of free heme mandates the necessity of heme trafficking pathways (2). The final step of heme biosynthetic pathway occurs in the inner mitochondria. Thus heme must be exported out of the mitochondria for incorporation into hemoproteins located in various subcellular compartments (49).

Studies have shown that ABCB10 may facilitate transport of heme out of the mitochondria in erythroid cells (50). ABCB10 is a mitochondrial ABC transporter located in the inner mitochondrial membrane. ABCB10 interacts with MFRN1 and FECH and stabilizes the complex (51). Expression of ABCB10 is highly induced during erythroid differentiation and ABCB10 overexpression strengthens hemoglobin synthesis in erythroid cells. It has been shown that ABCB10-null mice display defective erythropoiesis and lack of hemoglobinized RBCs, indicating ABCB10 is essential for erythropoiesis *in vivo* (50). However, conclusive evidence for direct heme transport by ABCB10 is still lacking.

The Feline leukemia virus subgroup C receptor-related protein 1 (FLVCR1) was identified as a heme exporter (52). FLVCR1 belongs to the family of MFS (major facilitator superfamily) proteins which transport small solutes across membranes facilitated by a counter ion gradient. Overexpression of FLVCR1 induces significant reduction in cellular heme content, suggesting that FLVCR1 is involved in heme export (52). FLVCR1-null mice are embryonic lethal with deficiencies in definitive erythropoiesis, and suffer from craniofacial and limb deformities resembling those of patients with diamond-blackfan anemia (DBA). *Flvcr1*$^{-/-}$ mice develop a severe macrocytic anemia with proerythroblast maturation arrest, suggesting that erythroid precursors may be exporting excess heme to avoid heme toxicity (53).

Two isoforms of FLVCR has been identified, FLVCR1a and FLVCR1b. While FLVCR1a encodes a plasma membrane-localized heme transporter, FLVCR1b was identified to be a mitochondrial isoform encoded from an alternative transcription start site, resulting in a shortened N-terminus containing a mitochondrial targeting signal (54). Thus, FLVCR1a contributes to intercellular and FLVCR1b to intracellular heme transport. FLVCR1a is expressed in different hematopoietic cells and shows weak expression in the fetal liver, pancreas and kidney (55). Ectopically expressing FLVCR1a reduces intracellular heme level and mediates efflux of ZnMP, a fluorescent heme structural analog, in rat renal epithelial and

human hematopoietic K562 cells (52). FLVCR1a may export heme during erythrophagocytosis (EP), a process in which macrophages phagocytose senescent RBCs, as FLVCR1a has been showed to interact with the extracellular heme-binding protein hemopexin and mediate heme export at least 100-fold more efficient in the presence of hemopexin (56). FLVCR1a has a limited substrate range including heme, protoporphyrin IX and coproporphyrin, but not bilirubin, the product of heme catabolism. FLVCR1a expression is increased during erythropoiesis and is at its greatest during intermediate stages of RBCs maturation when HMOX1 expression is low, implying that FLVCR1a helps to maintain stoichiometric amounts of heme and globin by exporting excess heme and preventing heme toxicity to RBCs (57). Depletion of FLVCR1b in HeLa cells results in accumulation of mitochondrial heme, indicating that FLVCR1b may play a role in heme export from the mitochondria (54). Therefore, the embryonic lethality of FLVCR1 knockout mice may be due to lack of heme export from the mitochondria by FLVCR1b, as mice lacking FLVCR1a but not mitochondrial FLVCR1b appears to have normal erythropoiesis although with defects in erythroid maturation. It is not yet known whether FLVCR1b resides on the inner or outer mitochondrial membrane. Moreover, if mitochondrial heme export by FLVCR1b is indispensable and indeed attenuated in *Flvcr1*$^{-/-}$ mice, it cannot explain why embryos from *Flvcr1*$^{-/-}$ null mice can survive until E14.5. Yeast does not appear to have an obvious FLVCR homolog, yet is able to export heme from the mitochondria indicating that alternate mechanisms must exist for mitochondrial heme export.

ABCG2, also known as breast cancer resistance protein (BCRP) has been identified as a heme exporter in mammals (58). *ABCG2* is expressed in hematopoietic stem cells (HSCs) and erythroid progenitors. Compared to high FLVCR1 expression during erythropoietic differentiation, the expression level of ABCG2 is particularly high at the early stages of hematopoiesis (59). ABCG2 binds to heme directly through an extracellular loop 3 with a porphyrin-binding domain (60). Ectopically expressed ABCG2 exports ZnMP in K562 cells.

However, direct evidence that ABCG2 exports heme is still lacking (60). Whether FLVCR1 and ABCG2 can function synergistically to export heme during erythropoiesis is not clear. ABCG2-null human patients are defined as Jr(a–) blood group with a unique side population of HSCs, however, with no apparent deficiencies in erythropoiesis (61, 62).

MRP-5 was identified as a heme exporter in *Caenorhabditis elegans.* This roundworm is a unique model for uncovering unknown heme trafficking since it is a heme auxotroph but requires heme to grow. Thus, it needs to acquire dietary heme via the intestine and distribute heme from the intestine to other tissues (63, 64). *C. elegans* MRP-5 (CeMRP-5) localizes to the basolateral membrane of intestinal cells and loss of MRP-5 results in accumulation of ZnMP in intestinal cells and growth retardation. Overexpression of CeMRP-5 and human MRP5 in yeast caused reduced growth owing to heme depletion, which could be rescued by co-expression of the heme importer, HRG-4. Interestingly, overexpression of CeMRP-5 and human MPR5 causes heme levels to increase in the secretory pathway, as measured by a secretory pathway heme protein reporter. However, the physiological role of MRP5 in vertebrates and it involvement in erythropoiesis is not clear.

Heme carrier protein 1 (HCP1, SLC46A1) is a membrane protein expressed in enterocytes and was proposed to be an intestinal heme transporter (65). However, subsequent studies revealed that HCP1 is a proton-coupled folate transporter (PCFT) rather than a heme transporter (66). Erythroblasts from HCP1 knockout mice showed deficiency in differentiation and high apoptosis rate resulting in severe macrocytic normochromic anemia, which was ascribed to folate but not heme deficiency (67). Moreover, knockdown of HCP1 by shRNA in Caco-2 cells attenuated both heme and folate uptake but increased HO-1 expression, suggesting HCP1 could potentially function as a low affinity heme importer (66, 68)

The Heme Responsive Gene -1 (HRG1, SLC48A1) was identified as a heme importer in the intestine of *C.elegans* (69). Four HRG1 homologs, CeHRG-1, CeHRG-4, CeHRG-5

and CeHRG-6 were found in the *C. elegans* genome. Significant heme-induced inward currents were observed in *Xenopus* oocytes injected with *Cehrg-1*, *Cehrg-4*, and human *HRG1* mRNA, indicating heme-dependent transport across cell membranes (69). Human *HRG1* (*SLC48A1*) mRNA is abundant in the brain, kidney, heart, skeletal muscle, in addition to cell lines derived from duodenum and bone marrow (69). HRG1 localizes to acidic endosomal and lysosomal organelles in HEK293 cells, and its binding affinity to heme increases as pH decreases. Human HRG1 interacts with the C subunit of the vacuolar proton ATPase (V-ATPase) pump and enhances endosomal acidification (70). These studies collectively suggest that HRG1 transports heme from the exoplasmic space or the lumen of acidic endosome–lysosomal compartments into the cytoplasm. Global transcriptomic expression profiling shows that *Hrg1* mRNA is expressed at increasing levels during erythroblast maturation (71). Why a apparently heme importer would be necessary for erythropoiesis since developing RBCs are capable of iron-dependent de novo heme synthesis is puzzling.

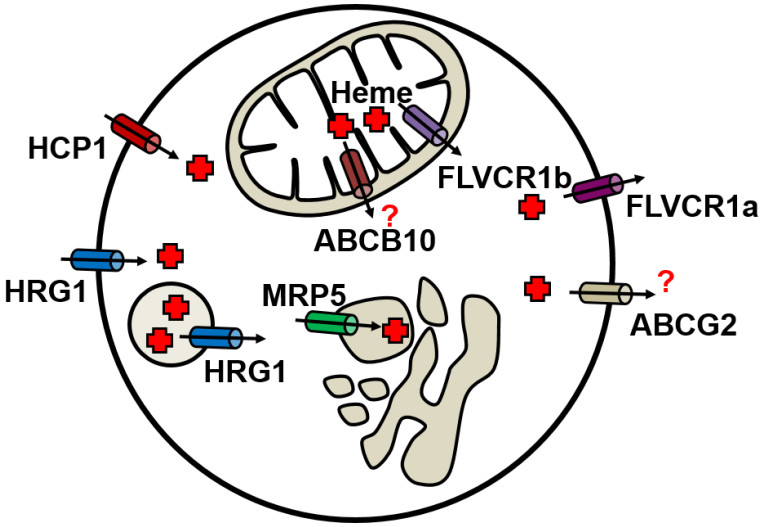

Figure 1.2 The ins and outs of heme transport

Mitochondrial isoform FLVCR1b transports heme into the cytosol. ABCB10 is reported to forms complex with FECH and MFRN1. It is not clear whether ABCB10 transport heme. The cell surface FLVCR1a and the ABC transporter ABCG2 have been implicated in heme export. MPR5 is a heme exporter which can transport heme from cytosol to the secretory pathway. HCP1 is a folate importer as well as a low-affinity heme importer. HRG-1 is a heme importer that localizes to endosomal/lysosomal compartments, but also traffics to the plasma membrane.

The dual play between erythroid cells and macrophages

Although macrophages and erythroid cells represent different developmental lineages during hematopoiesis, namely myelopoiesis and erythropoiesis, erythroid cells maintain an intimate dual relationship with macrophages from birth to death (72, 73). Adult definitive erythropoiesis is a tightly regulated process occurring in the bone marrow. The development of erythroid cells initiates from differentiation of HSCs to burst- forming unit- erythroid (BFU-E) and then colony- forming unit- erythroid (CFU-E). The CFU-Es continually develop in the following stages with different histological properties: proerythroblast, basophilic erythroblast, polychromatic erythroblast, orthochromatic erythroblast, reticulocyte and ultimately to mature RBCs in the peripheral blood (74). This developmental process can be described as terminal erythroid maturation and takes place in a special microenvironment of the bone marrow called erythroblastic islands (EBI) (75). The structure of EBIs was revealed as a structure of a macrophage (nurse macrophage) surrounded by developing and maturing erythroblasts. The process of differentiation from proerythroblast to reticulocyte has been known to take place in EBIs (75). Histological sectioning of bone marrow from mice has shown that roughly 10 erythroblasts were supported by central nurse macrophage, while this number is 5-30 for human EBIs (76, 77). Not only in bone marrow, EBIs have also been found in the red pulp of the spleen and liver of mice, especially under stress conditions with extramedullary erythropoiesis (78). Nurse macrophages play a critical role in enucleation of erythroblasts proceeding to the stage of reticulocytes (79). For a long time, EBIs were thought to be only responsible for RBC maturation from definitive erythropoiesis. However, recent studies suggested that the development of primitive erythrocytes in yolk sac also involves similar structure as EBIs with central macrophages, and primitive RBCs are also enucleated with nuclear extrusion promoted by central macrophages to generate erythrocytes and pyrenocytes after association with macrophages in EBIs (80).

Macrophages promote erythropoiesis by directly stimulating proliferation and survival of erythroblasts. Cultured erythroid precursors attached to macrophages are subjected to enhanced proliferation compared to non-attached erythroblasts, thereby suggesting that macrophages may augment the response to erythropoietic stimulation by direct interaction with erythroblasts (81). Although the major iron source for developing erythroblasts is by uptake of TF-bound iron from circulation, nurse macrophages were proposed to support erythropoiesis by directly transferring ferritin bound iron to erythroid progenitors, a process called pinocytosis. Cell culture studies have shown that extracellular ferritin is synthesized and secreted by macrophages, with capability of delivering iron to erythroblasts and supporting the differentiation of erythroid precursors in the absence of transferrin in the culture medium (82).

Lifespan of mature RBCs is limited in circulation, with ~40 and ~120 days for mouse and human respectively (83, 84). Circulating RBCs are also subject to damage in stressed conditions like hemolysis or some toxic effects to RBCs. When RBCs become senescent or the number of damaged RBCs increases in the circulation, macrophages in the reticuloendothelial system (RES) (liver or spleen) contribute to clear the RBCs and promote iron recycling through EP. The majority of iron required to sustain erythropoiesis is derived from recycled RBCs, and defects in EP lead to aberrant iron metabolism, including anemia and iron overload (72, 73). Upon degradation of RBCs in erythrophagosome, heme must be imported into the cytoplasm for degradation by HMOX1. Mice with HMOX1 deficiency lose the ability to recycle heme iron and consequently suffer from anemia, reduced serum iron, and accumulation of iron in the liver and spleen (85). HMOX1 null mice lack liver and splenic red pulp macrophages and most pups die from heme-associated toxicity due to the inability to degrade heme from RBCs (86). Heme extracted from hemoglobin during EP is reported to be degraded by HMOX1 inside the phagolysosome, and iron could then be imported into the cytosol by NRAMP1, the iron transporter found on the phagolysosomal

membrane, for storage in ferritin or export into the circulation by ferroportin 1 (Fpn1) (87). However, there are several gaps existed in this model of heme-iron recycling. First, HMOX1 is embedded in the ER membrane via a transmembrane segment, with the enzymatic active site facing the cytosol (88, 89). Second, the optimal pH for HMOX1 (pH 7.4) is closer to cytosolic pH than acidic lysosomal pH (90). Third, maximal HMOX1 activity is achieved only in the presence of biliverdin reductase, which is located in the cytosol (89). Moreover, immunocytochemistry studies suggest that HMOX1 is not found in or on the phagolysosome during EP (91). These evidences collectively suggest that heme is transported out of the erythrophagosomes prior to degradation by HMOX1. Indeed, HRG1 is recruited and colocalizes with NRAMP1 on the membrane of erythrophagosomes, surrounding ingested senescent RBCs in bone marrow derived macrophages (BMDMs) (91). HRG1 is strongly expressed in macrophages of the RES and specifically localizes to the phagolysosomal membranes (92). Expression of *Hrg1* mRNA is upregulated during EP and depletion of HRG1 in mouse BMDMs causes defective heme transport from the phagolysosomal compartments and failure to upregulate of *Hmox1* mRNA expression. These results suggest that HRG1 is a heme transporter for heme-iron recycling in macrophages, mobilizing heme from the erythrophagosome into the cytosol. *In vivo* experiments reveal increased level of HRG1 in the spleen and liver of mice injected with phenylhydrazine (PHZ) with acute hemolysis and enhanced heme-iron recycling.

While macrophages promote erythropoietic development by both supporting erythroblast maturation and clearing aged RBCs, RBCs can also affect macrophage differentiation in the RES. It has been recently shown that stressed and senescent erythrocytes can transiently induce differentiation and propagation of monocytes to iron-recycling macrophages on-demand in both liver and spleen (93). The same effects also appear during hemolytic anemia, anemia of inflammation, and sickle cell disease with heme released from damaged RBCs, suggesting that the induction of monocytes to iron-recycling

macrophages is possibly medicated by heme itself. SPI-C, a transcription factor participates in a differentiation circuit for red pulp macrophages (RPMs) and BMDMs. In *Spic*$^{-/-}$ mice, monocytes are unable to develop into RPMs resulting in iron overload in spleen, while other populations of monocytes and macrophages remain unchanged (94). Interestingly, SPI-C expression was activated by heme itself, via release of heme-dependent transcription repressor BACH1 (95). The heme/BACH1/SPI-C axis regulates the differentiation of monocytes into RES macrophages. These evidences further justify the necessity for intercellular heme trafficking during development of RBCs and macrophages.

Zebrafish erythropoiesis resembles those of higher vertebrates

The teleost fish, *Danio rerio*, also known as zebrafish, has been under increasing attention as a model organism for studying vertebrate development owing to its advantage in developmental biology. Adult zebrafish are relatively small and one breeding pair can produce 100-200 progenies per spawning each week, which allows easy maintenance of particular strains with small space and ensures production of numerous embryos for experiments (genetic screening work and building transgenic line). The external fertilization and rapid development *ex utero*, combined with property of transparency, allow direct visualization and manipulation of developmental processes in early embryos, which are not possible in mice. The techniques for transgenesis and gene manipulation are well developed in this model, rendering zebrafish as a genetically-tractable vertebrate animal model (96).

Zebrafish has a similar hematopoietic program compared to higher vertebrates, spanning from developmental waves of hematopoiesis to conservation of producing comparable blood cell components. Two successive waves of hematopoiesis, primitive and definitive, are also found in zebrafish (97, 98). Additionally, crucial regulators have been isolated as orthologues of many essential mammalian hematopoietic regulators and functional conservation of these factors in zebrafish is validated by morpholino mediated knockdown or

identified mutants (99). These conserved properties of zebrafish hematopoiesis make it a good model for hematopoietic study and its application to mammals.

Primitive erythropoiesis in zebrafish occurs in the intermediate cell mass (ICM) of developing embryos, which is functionally equivalent to extra-embryonic yolk sac blood island region in mammals (100). Primitive erythroid lineage arises from ICM previously developed from posterior lateral mesoderm (PLM) region. Primitive erythropoiesis in zebrafish begins at the 4-somite stage with the appearance of expression of erythroid-specific transcription factor Gata1 (101). Gata1, a zinc-finger transcription factor, serves as a determination factor for early primitive erythroid progenitors. The circulating primitive erythroblast cells further proliferate and differentiate into mature erythrocytes through a series of morphological alterations, with elongated nucleus around 4 dpf (days post fertilization), and functionally survive to 10 dpf in blood stream (102). Mature erythrocytes display unique morphological characteristics distinguishable from adult counterparts by less cytoplasm and larger nucleus.

Consistent with hematopoietic program in mammals, definitive hematopoiesis in zebrafish marks its distinctive wave by generating all blood cell lineages throughout the whole lifespan. The initiation site of zebrafish definitive hematopoiesis has been identified by expression pattern of mammalian definitive hematopoietic regulator orthologues, C-MYB and RUNX1. These two transcription factors dictate the formation of definitive HSPCs (hematopoietic stem/progenitor cells) in the AGM (aorta-gonad-mesonephros) region (103). In zebrafish, initial expression of *runx1* and *c-myb* is located in the VDA (ventral wall of dorsal aorta) from 26-48 hpf (hours post fertilization), analogous to the AGM region in mammals, suggesting that definitive HSPCs are generated in the VDA. The initiation of definitive hematopoiesis in VDA happens as early as 36 hpf (104). At around 4-5 dpf , hematopoietic cells are identifiable in pronephros/kidney and thereafter by 13 dpf. The Kidney functions as a counterpart of bone marrow in mammals to sustain definitive

hematopoiesis throughout the lifespan (105). Posterior blood island (PBI) also called caudal hematopoietic tissue (CHT), locates between the caudal artery and the caudal vein at the end of the tail, is recognized as a fetal hematopoietic organ in zebrafish, an intermediate hematopoietic site covering the period between VDA and kidney as a counterpart to fetal liver in mammals (106, 107). Definitive erythrocytes are postulated to populate the circulation at around 5 dpf as RBCs emerge at this stage in *bloodless* mutants with defects in producing primitive erythropoiesis (108). Transfusion experiments reveal that primitive erythrocytes are the major circulating erythroid components for the first 5 days and thereafter they are gradually replaced by presumptive definitive erythrocytes (102). Like mammals, these definitive erythrocytes switch to express adult form of globins and could be discriminated morphologically from their primitive counterparts (109, 110).

The kidney marrow (head kidney) is an adult hematopoietic organ in zebrafish which is functionally equivalent to BM in mammals. Based on forward scatter (cell size) and side scatter (granularity), hematopoietic cells in the kidney marrow could be fractioned into four populations: immature precursors of all lineages, lymphoid cells, mature erythroid cells and myelo-monocytic cells (neutrophils, monocytes, macrophages, and eosinophils) (111). Transplantation rescue experiments by lethal irradiation in zebrafish reveals presence of definitive HSCs in the kidney marrow maintaining lifelong hematopoiesis program (112).

Spleen is postulated to be another hematopoietic tissue in the adult zebrafish, although clear evidence is lacking to define its hematopoietic activity. Compared to the kidney marrow, zebrafish spleen is not well characterized. It was proposed that zebrafish spleen may function as a reservoir for RBCs where erythrocytes are stored and destroyed (113). Splenic macrophages can be found in red pulp and contain phagosomes with erythrocytes and other cellular debris, indicating possible active EP in zebrafish spleen (114, 115). However, the involvement of zebrafish spleen during heme-iron recycling is not well studied since studies with zebrafish are typically confined to embryonic and larval stages.

Zebrafish as a model to study heme and iron metabolism

Beside similar hematopoietic program, zebrafish genome largely resembles the human genome. The complete sequencing of the zebrafish genome makes it a powerful tool for gene discovery research and translates its findings to humans (116). Large-scale forward genetic studies have been carried out in some invertebrate model organisms, particularly in the nematode and fruit fly. However, it is extremely expensive to perform this approach in mice which is a vertebrate model most widely utilized to recapitulate in hematopoietic studies in humans. Zebrafish was the first vertebrate organism established for large-scale forward genetic screening. Chemical mutagenesis is achieved by exposing adult male fish to N-ethyl-N-nitrosourea (ENU) for several days which induces point mutations in the spermatogonia. These male fish are then mated with wild type (WT) female fish to propagate the mutation to F1 progenies (99, 117). Screening methods such as antibody staining, whole mount *in situ* hybridization (WISH) and behavioral analysis can be then used to identify morphological or genetic phenotypes. By contrast, gene-specific knockdown mediated by morpholino-injection serves as an efficient tool for reverse genetic study (118). Mutagenesis and targeted gene disruption have contributed to uncovering the genes involved in heme and iron metabolism in zebrafish. Recent development of gene-editing tools such as TALENs and CRISPR/cas9 for targeted gene disruption complement transient morpholino gene knockdown for reverse genetic studies (119, 120). Several key genes which are involved in heme synthesis and metabolism have been elucidated in zebrafish by both forward and reverse genetic manipulation.

ALAS2

Alas2 is the erythroid-specific enzyme for heme synthesis, while Alas1 is found in all other tissues. Zebrafish mutant *sauternes (sau)* has been identified from ENU mutagenesis

and positional cloning revealed that *sau* contains mutation in *alas2* (121). The *sau* mutants have a microcytic, hypochromic anemia, delayed erythroid maturation, and abnormal globin gene expression, suggesting that defects in heme synthesis can affect globin protein production. Interestingly, *sau* mutants have normal RBC number, and show anemia around 33 hpf. Perhaps maternal heme my permit early RBC development or that the *alas2* mutation is hypomorphic. As mutations in *alas2* cause CSA in humans, *sau* represents the first animal model of this disease in zebrafish (121). Most interestingly, *sau* zebrafish mutants are viable even though it has only one-tenth of overall heme content compared to WT zebrafish. *Sau* mutants can be fully rescued by supplementing developing embryos with ALA, which may further enhanced its value as a model to study the pathology of CSA in humans (122).

ALAD

Unlike ALAS, only one form of ALAD was found in both human and zebrafish. So far, no mutation in *alad* has been identified in zebrafish. However, an *alad* mutant (*who*) was identified in medaka, another teleost fish model (123). *Who* mutants suffer from hypochromic anemia, owing to deficiency in heme synthesis. Initial blood cell number is normal, but it then gradually decreases during the embryonic and larval stages. The RBCs develop an elongated, occasionally curved morphology, possibly caused by accumulated globin protein without heme, representing sickle-cell anemia in humans with globin protein aggregations (124).

UROD

Zebrafish mutant *yqe* embeds a nonsense mutation in the gene encoding UROD, which converts uroporphyrinogen to coproporphyrinogen. Homozygous mutation in *urod* leads to two forms of porphyrias, porphyria cutanea tarda (PCT) and hepatoerythropoietic porphyria

(HEP) in human, similar to the phenotypes in zebrafish with photosensitive porphyria syndrome (125). Excessive amounts of uroporphyrinogens and 7-carboxylate porphyrin accumulate in *yqe* embryos, representing human HEP patients characterized by photosensitive skin and excessive excretion of heme biosynthesis intermediates, uroporphyrin and 7-decarboxylate porphyrin in their urine. The zebrafish *yqe* mutant phenocopies human patients facilitating studying of HEP pathogenesis and development of new therapeutics.

PPOX

Zebrafish porphyria mutant, *montalcino* (*mno*), contains mutation in *ppox*, which catalyzes the oxidation of protoporphyrinogen, representing human variegate porphyria. Initially, at the onset of circulation, *mno* displays normal numbers of RBCs but are *o-dianisidine* negative. A visible decrease in circulating erythrocytes can be observed after 36 hpf and the RBCs in the mutant embryos are epifluorescent. The *mno* mutant zebrafish could survive to approximately 25 dpf. Accordingly, human *PPOX* could partially rescue the hypochromia in homozygous mutants, revealing functional conservation. The zebrafish *mno* mutant will be very useful for further elucidating the pathophysiology of variegate porphyria and identifying chemical modifiers of this disease.

FECH

Two different mutant alleles of *fech* have been identified in zebrafish, *freixenet* (*frx*) and *dracula* (*drc*) (99, 126). Protoporphyrin IX accumulates in *fech* mutant embryos owing to a deficiency in the activity of ferrochelatase, the terminal enzyme in the pathway for heme biosynthesis. The mutants show light-dependent hemolysis and liver diseases, similar to that seen in humans with erythropoietic protoporphyria resulting from a disorder of ferrochelatase.

GRX5

Phenotypic analysis of *shiraz* (*sir*) mutant zebrafish revealed an intimate connection between heme biosynthesis and [4Fe-4S] formation, connecting two main uses for iron in the mitochondria, usually thought to be independent processes (127). In *sir* mutants, hypochromic anemia, in the context of normal mitochondrial iron and oxidative stress levels, was shown to be caused by a deletion in the glutaredoxin 5 (*grx5*) gene. GRX5 is required for the synthesis of Fe-S clusters in mitochondria (128). The zebrafish protein also localizes to the mitochondria and is capable of rescuing *grx5*-deficient yeast strain. Fe-S clusters are known to negatively regulate binding of IRP1 to IREs. Decreased Fe-S cluster assembly in *sir* mutant leads to increased IRP1 activity, which inhibits the expression of IRE-regulated target genes involved in heme biosynthesis like *alas2*. Indeed, *alas2* expression is absent in *sir* mutant. Deletion of IREs in the *alas2* mRNA rescued the anemic phenotype while overexpression of full-length *alas2* mRNA did not, suggesting that the function of GRX5 in regulating ALAS2 expression is through Fe-S clusters and IRP/IRE activity. An evolutionary conserved role for GRX5 in regulating heme synthesis was confirmed in human patients with *GRX5* mutation (129).

MFRN1

Two mitoferrin homologs are found in the zebrafish genome, Mfrn1 and Mfrn2. Positional cloning of *frascati* (*frs*) zebrafish mutants identified a missense mutation in the *mfrn1* (*slc25A37*) gene, an erythroid specific form (31). *Frs* mutants develop hypochromic anemia and arrested erythroid maturation. Mouse *Mfrn1* rescues the phenotypes in zebrafish *frs* mutants. The same anemic phenotype was observed in a mouse model with *Mfrn1*-knockout (32, 130). The MFRN2 (Slc25A28) paralog functions in mitochondrial iron import in non-erythroid tissues.

DMT1

DMT1 was first isolated in the rat duodenum and is upregulated by dietary iron deficiency, while Belgrade rat with mutation in *dmt1* suffer from iron deficient anemia (26, 131). Zebrafish mutants *chardonnay* (*cdy*) carry a nonsense mutation in *dmt1* with reduced hemoglobin levels and delayed erythrocyte maturation (132). The Dmt1 protein localizes to erythroid cells and the intestine, suggesting its role in intestinal and erythropoietic iron absorption. Cells with overexpression of WT zebrafish Dmt1 uptake nearly ten times the amount of iron as non-transfected control cells, whereas the *cdy* mutant form is not functional. However, *cdy* mutant can survive to adulthood irrespective of severe anemia, suggesting alternative pathway for iron absorption in zebrafish. In humans, mutations in *DMT1* cause a phenotype of hypochromic microcytic anemia combined with iron overload, further supporting possible existence of alternative iron absorption mechanisms in the duodenum that bypasses DMT1 (133).

FPN1

The first identified iron exporter Fpn1 (Slc40A1) was found by position cloning of zebrafish *weissherbst* (*weh*) mutant (134). *Weh* mutant embryos suffer from hypochromic anemia, as evidence from decreased hemoglobin levels, blocked erythroid maturation, and reduced numbers of erythrocytes. Erythroid cells of mutant embryos have significantly lower iron concentration compared to WT embryos, suggesting iron deficiency in mutants. Microinjection of iron-dextran rescued the anemic phenotype of *weh* mutants and continuing injection of iron-dextran also rescued embryonic lethality. However, these rescued fish are only normal until six months of age and eventually develop hypochromic anemia by 12 months, suggesting that Fpn1 might be involved in iron-recycling in adult zebrafish.

Compared with iron injected WT fish, the rescued mutants had increased iron staining in kidney macrophages, as well as increased staining in intestinal villi, suggesting that *fpn1* mutation impairs iron export in these tissues. The iron-rescued *weh* mutants also have hepatic iron overload, with particularly high iron levels in the liver küpffer cells (135). FPN1 also localizes to the yolk-syncytial layer (YSL) during embryonic development, suggesting that FPN1 may transport maternal iron from the yolk for embryogenesis. Both mice and humans have homologs of FPN1with high similarities to zebrafish Fpn1. Mammalian *FPN1* is robustly expressed in the placenta, duodenum, and liver. At the protein level, human FPN1 is concentrated on the basal surface of the syncytiotrophoblast in the placenta, an organ that is functionally similar to zebrafish YSL, indicating that human FPN1 plays a role in maternal-fetal iron export. In mice, FPN1 is expressed on the basolateral surface of enterocytes, suggesting a role in intestinal iron transport (136).

TF

The zebrafish mutant *gavi* (*gav*) was shown to have mutations in transferrin-a (Tf-a), which encodes the principal serum iron carrier (137). *Gav* mutant embryos exhibit reduced *tf-a* expression and impaired hemoglobin production with hypochromic anemia and embryonic lethality by 14 dpf. In humans, phenotype of congenital hypotransferrinemia caused by *TF* mutation is highly similar to those of *gav* mutants, including hypochromic anemia and embryonic death (138). The *gav* mutant is thus an ideal whole vertebrate anemia model for studying symptoms corresponding to human pathologies related to Tf.

TFR1

Transferrin-bound iron is taken up into cells by binding to the transferrin receptor 1 (TFR1). Four different zebrafish *chianti* (*cia*) mutants with varying degrees of hypochromic

anemia and defective erythroid differentiation were ascribed to mutations in *tfr1a* gene (139). During early development, *tfr1a* transcripts are expressed specifically in erythrocytes. Importantly, cytoplasmic delivery of iron by microinjection at one-cell stage—but not intravenous iron injections can rescue the hypochromia phenotypes of *cia* mutants, indicating that *tfr1a* mutation prevents erythrocytes from taking up and utilizing circulating iron. Intriguingly, a second *tfr1* gene, *tfr1b* was identified together with *tfr1a*, a typical feature in zebrafish genome which has undergone genome duplication (140, 141). Whereas Tfr1a is expressed in erythrocytes during early development and *cia* mutants are anemic, Tfr1b is expressed ubiquitously throughout embryogenesis and knockdown of *tfr1b* by morpholinos do not affect hemoglobinization. *Tfr1b* morphants have retarded growth and develop brain necrosis, a phenotype that is similar to the neurologic defects observed in the mouse model (142), indicating that *tfr1b* may be involved in iron uptake in non-erythroid tissues. *Tfr1a* (*cia*) and *tfr1b* deficient zebrafish embryos recapitulate the phenotype of $TFR1^{-/-}$ mice (140, 141).

FLVCR

Currently no zebrafish mutants have been reported with perturbation of Flvcr. However, the function of zebrafish Flvcr is related to erythroid differentiation and maturation (143). Two splicing isoforms have been identified: *flvcr1a* and *flvcr1b*. Flvcr1a is required for the expansion of committed erythroid progenitors but cannot drive their terminal differentiation, while Flvcr1b contributes to the expansion phase and is required for differentiation (143). The coordinated expression of Flvcr1a and Flvcr1b contributes to controlling the cytosolic heme pool required to sustain regulation of erythroid progenitors and hemoglobin synthesis for hemoglobinization during terminal maturation. Interestingly, treatment of succinylacetone (SA), an inhibitor of heme synthesis at ALAD enzymatic step, rescues the phenotype of *flvcr1a* morphants while heme supplementation restores

hemoglobinzation of *flvcr1b* morphants, suggesting that intracellular heme pool during erythropoiesis is tightly regulated.

Problem statement

The current tenet dictates that erythroblasts are self-sufficient, *i.e.* they produce large amounts of hemoglobin by simply upregulating endogenous heme synthesis. However, this is puzzling since erythroblasts also express FLVCR1a, a heme exporter. Loss of FLVCR1a expression cause the apoptosis of proerythroblast owing to heme toxicity (144). Why do maturing erythroblasts need to export heme, since they will need large amounts of heme for hemoglobin synthesis? A recent study showed that coordinated expression of heme synthesis and globin protein is essential for effective erythropoiesis (145). Erythropoiesis failure occurs in *flvcr*-null mice at the CFU-E/proerythroblast stage, a point at which the transferrin receptor (CD71) is upregulated to maximize iron import for heme synthesis. However, at this time point, erythroid progenitors contain excess heme over globin production. This excess heme can cause increased cytoplasmic ROS resulting in increased apoptosis in the absence of heme exporter FLVCR1a. By contrast, terminal erythroid maturation includes a coordinated loss of intracellular organelles including the mitochondria, the site for heme synthesis. However, hemoglobin production continues as erythroid cell mature, requiring heme even though the cells lack proper mitochondria function. At this stage, globin synthesis exceeds heme synthesis. We propose that heme uptake at this stage could compensate to reset the stoichiometry between globin and cellular heme levels.

HRG-1 is a heme importer initially identified using *C.elegans* as an animal model, with orthologs in many higher vertebrates (69). Global transcriptome analysis shows that *hrg1* mRNA increases during mouse terminal erythroid maturation (146). This is puzzling because it is unclear why HRG1would be regulated in erythroid precursors. We postulate that during terminal erythroid maturation, erythroid cells import exogenous heme to support hemoglobin

production as intracellular heme synthesis may be insufficient to cope with globin production. In this regard, erythroid precursors likely behave like *C. elegans*, a heme auxotroph, that acquire and utilize exogenous heme. What could be the source of this additional heme? It is possible that a portion of heme and/or iron within maturing RBCs is derived from inter-cellular transport from nurse macrophages in EBIs to support the terminal stages of hemoglobinization, especially under conditions such as stressed erythropoiesis while heme synthesis is insufficient. In support of this hypothesis, heme importers (HRG1) are expressed in both red blood cells and macrophages. While this might be plausible for definitive erythropoiesis, what about primitive erythropoiesis? In situ hybridization reveals clear expression of mouse *hrg1* in placenta and trophoblast cells, primitive and definitive erythroid cells [since they make up the vast majority of the cells in yolk sac blood islands/ blood vessels (E7.5-E8.5/E9.5; primitive lineage)], E12.5 fetal liver (definitive lineage), and developing neural tissues. These results support a model in which inter-tissue and inter-cellular heme transport must occur during development and maternal HRG1 may be essential for mobilizing pre-existing heme stores in oocytes for early embryonic development and primitive erythropoiesis. To elucidate the heme trafficking during erythropoiesis, I exploited zebrafish as a whole vertebrate animal model to uncover the possible mechanisms of erythropoietic regulation by heme transporters.

Chapter 2: Materials and Methods

Zebrafish methods

Zebrafish husbandry

All zebrafish procedures were approved by University of Maryland Animal Care and Use Committee. All used zebrafish embryos and lines were kept within the zebrafish facility (Aquatic Habitats, USA) in Department of Animal and Avian Sciences, University of Maryland College Park. The fish water is kept at 28 °C, conductivity ~1000**,** stable pH value between 7.3~7.4. The light providing cycle is maintained around 10 h light off (9:30 pm ~ 7:30 am) and 14 h light on.

To generate embryos, male fish was bred to female fish by putting them together in a tank with an inner nested mesh overnight and embryos were collected next morning. To make fish spawning for a controlled time point (e.g. micro-injection or collecting embryos of relatively synchronized developmental stages), a transparent divider was placed in the middle of tank to separate male and female. Embryos were obtained once the divider was removed at the following morning. Embryos were kept in embryo medium prepared as described in *The zebrafish book* (4th) (147). To keep the embryos transparent at early stages, 0.003 % PTU was added around 18-24 hpf. Zebrafish strain Tü were used as WT throughout this study.

Microinjection of zebrafish embryos

The injection needles were made from capillaries with internal filaments (BF100-58-10, Sutter Instrument, Novato, CA) on needle puller (P-97, Sutter Instrument, Novato, CA). The pulling parameter was empirically determined. A commonly used set of parameter was as follows: Heat (574) Pull (110) Velocity (50) Time (140). The needles were further broken with a clean sharp forcep in order to make fine wedge-shaped tips.

To carry out the microinjection, embryos were held in wedge-shaped mold made by 1.5 % Agarose in Petri dish. For injection of DNA constructs or mRNA, embryos were oriented with animal poles of embryos opposite to injection needle. Injection solutions were backfilled into needle with microloader (Eppendorf, Hamburg, Germany). Injections were performed on the stage of Nikon stereomicroscope equipped with manipulator (Harvard Apparatus, Holliston, MA) and injector (World Precision Instrument, Sarasota, FL). Usually, around 1.4 nL solution was injected into a single embryo without affecting normal development.

Morpholino-mediated gene knockdown

Morpholinos were designed and synthesized by GeneTools (Philomath, OR). Translation- and splice-blocking morpholinos were designed to block mRNA translation and pre-mRNA splicing, respectively. Morpholinos were delivered to one-cell staged embryos by microinjection as described above. The sequences of morpholinos were listed in **Appendix I**.

In vitro transcription

The in vitro transcription was used to generate digoxigenin (DIG)-labeled RNA probe for WISH and cRNA (capped RNA) for microinjection to fish embryos.

For WISH, fragments were PCR amplified and then subcloned into distinct plasmids. To make DIG labeled anti-sense RNA probe, plasmid DNA was first linearized by appropriate restriction enzyme and purified using DNA purification kit (Machinery-Nagel, Germany). The purified linearized DNA was then used as a template for in vitro transcription with DIG RNA Labeling Kit (SP6/T7) (Roche).

For generation of cRNA for injection, plasmid DNA with the specific fragments of interest was linearized, gel-purified and used for in-vitro transcription according to the manuals of mMESSAGE mMACHINE T7/T3/SP6 Transcription Kit (Thermo Fisher).

Whole-amount in situ hybridization

Whole amount in situ hybridization was perform as described (148). Briefly, embryos were dechorinated either manually or by 1 μg/ml pronase (Roche, Mannheim, Germany). The dechorinated embryos were then fixed in 4 % paraformaldehyde (PFA) in PBS at 4 °C overnight or room temperature (RT) for 2 h. Following fixation, embryos were rinsed with PBST (PBS plus 0.1 % Tween 20) for 2 × 5 min. Embryos were then dehydrated in 50 % methanol (MeOH)/PBST for 5 min and 100 % MeOH for 5 min before storage in fresh MeOH at RT. Embryos were sequentially rehydrated with 75 % MeOH/PBST for 5 min, 50 % MeOH/PBST for 5 min, 25 % MeOH/PBST for 5 min, and PBST, 4 × 3 min. Embryos were treated with 10 μg/mL proteinase K in PBS for permeabilization as periods described (148). After permeabilization, embryos were re-fixed with 4 % PFA for at least 20 min followed by PBST wash for 4 × 3 min. Subsequently embryos were incubated with hybridization buffer (HB) buffer for 5 min at 65 °C before changing to new HB buffer for prehybridization for 1 h at 65 °C. Following prehybridization, embryos were hybridized with denatured DIG-labeled anti-sense RNA probe at 65 °C for overnight. The following day, embryos were sequentially washed with HB/2 × SSCT (1:1) at 65 °C for 2 × 30 min, 2 × SSCT, 0.2 × SSCT at 65 °C for 2 × 30 min and PBST at RT for 4 × 3 min. After extensive wash, embryos were pre-incubated with blocking solution made with 2 % lamb serum + 2 % BSA in PBST for 1 h followed by incubation in antibody solution (Anti-Dig alkaline phosphatase (AP) (Roche) 1:4000 diluted in blocking solution) at RT for 2 h or 4 °C overnight. Afterwards, embryos were washed with PBST for 6 × 20 min in order to remove excessive antibody. Before staining, embryos were equilibrated in buffer 9.5T (100 mM Tris,

50 mM $MgCl_2$, 100 mM NaCl, 0.1 % Tween20, pH 9.5) for 2 × 10 min. The signals were developed by incubating embryos with NBT/BCIP (nitroblue tetrazolium / 5-bromo-3-chloro-3-indolyl phosphate) tablet (Roche).

Zebrafish tissue dissection

Dissection of various adult zebrafish tissue was performed as previously described (149). For RT-PCR experiments, dissected tissues were immediately placed in TRIzol (Invitrogen) and flash frozen in liquid nitrogen before RNA extraction. For membrane fractionation, tissues were directly flash frozen before fractionation.

Generating of zebrafish mutants by TALEN and CRISPR/Cas9 gene-editing

TALEN targeting vectors were cloned and generated by Golden Gate serial ligation as described (150). The TALEN target sites were selected *in silico* at TAL Effector Nucleotide Targeter 2.0 (https://tale-nt.cac.cornell.edu/) with *hrg1a* ORF sequence (NCBI accession No.: NM_200006.1). The pcGoldy-TALEN targeting constructs were generated according to the selected sequence. The plasmids were linearized by restriction enzyme digestion and then gel-purified. Linearized plasmid (1 μg) was used for *in-vitro* transcription to produce capped TALEN mRNA. Equimolar of TALEN mRNA (300 ng) pair was used for microinjection.

The CRISPR gRNA was designed using Optimized CRISPR Design (http://crispr.mit.edu/). The gRNA target sequences were *in silico* predicted using *hrg1a* (NM_200006.1) and *hrg1b* (NM_001002424.2) ORFs as inputs. The gRNA constructs were cloned using pT7-gRNA as backbone (120). pCS2-Cas9 was used to produce Cas9 cRNA after linearization and *in-vitro* transcription. Cas9 cRNA (300ng) and gRNA (100ng) was co-injected into embryos at the one-cell stage.

Both TLAEN and CRIPSR-injected embryos were raised to adulthood as F0 founders. The founders were subjected to tail-clip genotyping to confirm indels at target sites. Positive chimeric F0 founders were them crossed to WT zebrafish to generate F1 offsprings. The F1 embryos with indels at target sites were raised to adulthood for genotyping and screening for stable mutant lines.

Zebrafish mutant genotyping

For genotyping of adult zebrafish, a small piece of tail was clipped and placed in 50 µl 50 mM NaOH at 95 °C for 30 min. For genotyping of embryos, either whole embryos or clipped small piece of tail from 3 dpf embryos were dissolved in 10 ul of 50 mM NaOH at 95 °C for 30 min (151). The solution was vortexed to completely dissolve the tail. One tenth volume of 1 M Tris-HCl at pH 8.0 was added to neutralize the solution. One microliter of crude lysate was used for PCR genotyping. Primers used for genotyping were listed in **Appendix VII**.

RNA Extraction

Total RNA was extracted from whole zebrafish embryos or from dissected tissues using TRIzol. Pooled embryos (20~30 for each) were placed in TRIzol and RNA was extracted accordingly. After resuspension in RNase-free water, total RNA was further digested by RNAase-free DNase (Ambion), to get rid of genomic DNA, followed by isopropanol/sodium acetate precipitation.

RT-PCR

Total RNA (1 µg) was used for reverse transcription by iScript cDNA synthesis kit (Bio-Rad). The reaction without reverse transcriptase was used for negative control. The

cDNA was diluted 2-5 times for following PCR reaction. To relatively quantify gene expression, RT-PCR of cDNA samples was performed by limited 25 PCR amplification cycles. Quantitative RT-PCR (qRT-PCR) was done with SsoAdvanced Universal SYBR Green Supermix (Bio-Rad). Each reaction was technically triplicated.

O-dianisidine staining

O-dianisidine staining was performed to detect hemoglobin in RBCs of whole embryos as previously described (152). The principle for this assay is that heme in hemoglobin catalyzes oxidation of *o*-dianisidine in the presence of H_2O_2, producing a dark brown color in hemoglobin-positive cells. Briefly, collected embryos were placed in 1 ml staining solution (0.06 % (w/v) *o*-dianisidine, 25 % ethanol, 10 mM Sodium Acetate and 0.02 % H_2O_2) for 20 min in the dark. Staining was stopped by rinsing embryos with 70 % ethanol. Embryos were post-fixed in 4 % formaldehyde in PBS and stored in 50 % glycerol in PBS for microscopy.

DAB enhanced Perl's iron staining in zebrafish

Perl's Prussian blue stain was performed to detect ferric iron in whole zebrafish embryos and zebrafish sections (153). Embryos were fixed by 4 % PFA at RT for 2 h and were immersed in a freshly prepared staining solution (2.5 % potassium ferrocyanide, 0.25 M HCl) for 30 min at RT, then rinsed three times in PBST. To prepare stain enhancement, endogenous peroxidase activity was quenched by incubating embryos in 0.3 % H_2O_2 (in methanol) for 20 min at RT. Following rinse in PBST, embryos were incubated for 7 min in SigmaFast DAB tablet (Sigma-Aldrich) dissolved in distilled water. Ferric ferrocyanide catalyzes the H_2O_2-mediated oxidation of DAB, producing a reddish brown color. Embryos were rinsed in PBST, and stored in glycerol: PBS (1:1) for microscopy.

FACS cell sorting

The embryos from globinLCR: GFP line (crossed with *hrg1a* or *hrg1b* mutant line or morpholino-injected embryos) were pooled and harvested. The cells were disaggregated with 0.25 % trypsin (154), and were then sequentially filtered through 70 μm and 40 μm cell strainers. The percentage of GFP-positive cells in transgenic embryos were analyzed by FACSCanto II machine (BD Biosciences) (155).

Membrane fractionation

Dechorinated zebrafish embryos or dissected adult tissues were homogenized by Dounce Homogenizer in appropriate volume of homogenization buffer (10 mM Tris-HCl, mM EDTA, 1 mM PMSF, protease inhibitor cocktail (Roche)). The homogenized solution was then centrifuged at 800 g 4 °C for 5 min. Then the supernatant was ultra-centrifuged at 100, 000 g 4 °C for 90 min with XL90 ultracentrifuge (Beckman, Germany). The supernatant was considered as the cytosolic fraction and the pellet was treated as the total membrane fraction. The pellet was collected and dissolved in lysis buffer (2 % triton-x100, 150 mM NaCl, 50 mM Tris-HCl, 20 mM HEPES, 1 mM PMSF, 1 mM EDTA, 1X protease inhibitor cocktail). The membrane lysate was used for the following immunoblotting experiments.

Immunblotting

HRG1 antibody serum was generated in rabbits using the 17 amino acid peptide sequence (YAHRYRADFADIILSDF) from c-terminus of human HRG1 as the immunogen (Thermo Fisher). Since the C-terminal 17 amino acid sequence of human HRG1 is highly conserved with zebrafish Hrg1a and Hrg1b (15/17), it cross-reacts well with both Hrg1a and Hrg1b.

For zebrafish Hrg1 immunoblotting, total protein concentration in membrane fraction

lysate was measured using the Pierce BCA assay kit (Thermo Scientific). Equal amount of total protein was mixed with Laemmli sample buffer and were separated on 12 % SDS-PAGE and transferred to a 45 µM nitrocellulose membrane using the semi-dry transfer apparatus (Bio-Rad). The affinity purified Hrg1 primary antibody was used at a concentration of 1:1000; goat anti-rabbit HRP-conjugated secondary was used at 1:30,000, and blots were developed with the SuperWest Femto Chemiluminescent Substrate (Thermo Scientific).

Collection of Embryonic RBCs

Zebrafish were firstly anesthetized in few drops of tricaine solution: 0.02 % tricaine (Sigma-Aldrich), 1 % bovine serum albumin (BSA) in calcium- and magnesium-free PBS (pH 7.4). For each sample, tails of approximate ten zebrafsih were cut by either a blade or surgical scissor to allow RBCs to flow into the tricaine solution. The tricaine solution containing RBCs was loaded into Shandon EZ Single Cytofunnels (Thermal scientific) and RBCs were concentrated onto a superfrost slide (Thermal scientific) by centrifugation at 450 rpm for 3 min using a Shandon Cytospin® 4 cytocentrifuge (Thermal scientific) according to the manufactory's instruction. Slides were air-dried prior to May-Grünwald Giemsa staining.

Collection of adult circulating blood

Adult fish were placed in fish water with 0.02 % tricaine for anesthesia. Under a stereoscope, use a micro-capillary was used to punctuate in caudal vein around the fish tail. The blood was allowed to back-fill into the heparinized capillary. A maximum 1-2 µl of blood could be collected from each adult zebrafish. The collected blood was placed in PBS and centrifuged, then smeared on charged slides for further staining.

May-Grünwald Giemsa Staining

May-Grünwald staining solution (May-Grünwald solution (MG500, sigma-aldrich) : methanol= 1:3) was gently added onto slides containing RBCs covering area and incubated at RT for 5 min and then gently washed off with double distilled water. Subsequently, the slides were incubated with 1 ml Giemsa staining solution (Giemsa Stain (GS500, Sigma-Aldrich) : water = 1:20) for 15-30 min. The Giemsa staining solution was then washed off with water and slides were air-dried before examining under microscope.

Phenylhydrazine (PHZ) treatment

To induce acute hemolysis at the embryonic stages, 4 dpf embryos were put in embryo medium with 1 µg/ml PHZ (pH 7.4) for 1 h. PHZ was then removed and embryos were rinsed three times with fresh embryo medium. For PHZ treatment in adult fish, 2.5 µg/ml PHZ was prepared in system fish water. The adult fish was placed in fish water with PHZ for 25 min at 28°C. PHZ was removed by three time rinse with fresh fish water. After 1 or 3 days post PHZ-treatment, the fish was used for dissection and histological sectioning.

Succinylacetone (SA), ALA, PBG and heme treatment of zebrafish embryos

To potentially block endogenous heme synthesis, zebrafish embryos were dechorinated at 24 hpf manually and placed in embryo medium with 1mM SA (Sigma). PTU was added to block pigmentation in embryos. ALA (1 mM), PBG (250 µM) or heme (10 µM) were added to embryos medium for treatment.

Fixation of adult zebrafish for histological section

Adult zebrafish (5-6 months old) were anesthetized with 0.02 % tricaine in fish water. Adult fish was slitting along the ventral abdominal wall from anus opening, allowing the fixative to immerse the gastrointestinal organs. The volume of fixative should be at least 10

times of fish volume. Adult fish was first fixed by modified davidson's fixative (to make 1L, mix 220 ml Formaldehyde (37-40 %), 115 ml Glacial acetic acid, 330 ml 95 % Ethyl alcohol and 335 ml Distilled water) for 24-48 h. The carcasses are then rinsed in 70 % ethanol and then stored in 10 % Neutral buffered formalin (NBF). Each specimen is paraffin-embedded and sectioned along the sagittal plane. Slides were used for histological staining by H&E and Perl's.

RNAseq

The kidneys and spleens from 5-6 months old adult zebrafish (four genotypes: *hrg1a*$^{+/iq261}$*; hrg1b*$^{+/iq361}$, *hrg1a*$^{iq261/iq261}$*; hrg1b*$^{+/+}$, *hrg1a*$^{+/+}$*; hrg1b*$^{iq361/iq361}$ and *hrg1a*$^{iq261/iq261}$*; hrg1b*$^{iq361/iq361}$) were dissected out and flash-frozen in TRIzol before RNA extraction (3 fish as a cohort, 3 cohorts per genotype).

Total RNA was extracted following TRIzol manual (Invitrogen). Extracted RNA was then digested with RNase free-DNase to remove remaining genomic DNA and cleaned up using Qiagen RNA mini column (Qiagen, Germany). Quality and quantity of total RNA were checked by Agilent Bioanalyzer 2100 (**Appendix IX**). Spleen (100 ng) or Kidney (1 µg) of total RNA were used for RNAseq library construction. Purified mRNA was prepared from total RNA following the manufactory's manual of NEBNext® Poly-A) mRNA Magnetic Isolation Module (E7490S, New England Biolabs). RNAseq libraries was constructed with NEBNext® Ultra™ RNA Library Prep Kit for Illumina® (E7530L, New England Biolabs). The RNAseq libraries and fragment size was roughly qualified by Agilent Bioanalyzer 2100 (**Appendix X, XI**). RNAseq libraries were quantified using NEBNext® Library Quant Kit for Illumina® (E7630S, New England Biolabs).

RNAseq was performed using STAR-DESeq2 pipeline. Total of 24 samples with single-end 50 base reads were sequenced with HiSeq 2500 (Illumina); with triplicate libraries of spleens and kidneys for the four phenotypes. Bioinformatics quality control was done

using FastQC, version 0.11.5. The reads were aligned to zebrafish GRCz10reference genome using STAR, version 2.5.2b. The numbers of reads mapped to genes were counted using htseq, version 0.6.1p1. Finally, differentially expressed genes were identified via DESeq2, version 1.12.3 with the cutoff of 0.05 on False Discovery Rate (FDR). R version 3.3.2 (2016-10-31) was used, and Bioconductor version 3.4 with BioInstaller version 1.24.0 were used. For gene annotation, we used Ensembl GRCz10, release 87. False Discovery Rate (FDR) by Benjamini-Hochberg was used to determine the statistical significance with the cutoff value of 0.05.

Yeast Methods

Strains and Growth

S. cerevisiae strains W303 contained the *hem1Δ* mutation has been described previously (156, 157). The mutant yeast cells were maintained at 30°C in yeast peptone dextrose (YPD) media supplemented with 250 μM ALA (Frontier Scientific).

Cloning and Transformation

To generate yeast expression plasmids, zebrafish *hrg1a* and *hrg1b* ORF were cloned into the pYES-DEST52 plasmid (Invitrogen). The mutant alleles of *hrg1a* and *hrg1b* were amplified from cDNA of zebrafish mutants (with and without a C-terminal HA tag) and cloned into pYES-DEST52 plasmid.

Yeast Growth Assays

The dilution spot assays were performed as described previously (156, 157). Plasmids containing potential heme transporters were transformed into *hem1Δ* yeast using the lithium method (158) and transformant yeast was selected on 2 % w/v glucose synthetic complete

(SC) (-Ura) plates supplemented with 250 μM ALA. Several colonies with appropriate similar size were streaked onto 2 % w/v raffinose SC (-Ura) plates supplemented with 250 μM ALA for 48-72 h. The transformant yeast cells were then grown in 2 % w/v raffinose SC (-Ura) liquid medium without heme or ALA for at least 12 h to depleting endogenous heme. The concentrations of yeast were determined by OD 600 measurement. Yeast cells were 10-fold serially diluted with OD 600 from 0.2 to 0.00002. The diluted yeast solutions were then spotted in 10 μl aliquots onto 2 % w/v raffinose SC (-Ura) plates supplemented with varying concentrations of heme or ALA (positive control) and 0.4 % w/v galactose to induce gene expression from the GAL1 promoter. Plates only supplement with ALA and Glucose were treated as negative control. Plates were incubated for 3 days before imaging.

To assay aerobic growth exclusively, yeast were induced with 2 % galactose in the absence of ALA, and then spotted onto plates containing indicated heme or ALA concentrations as well as 2 % glycerol and 2 % lactate as carbon sources.

Yeast Cell Immunoblotting

The immunoblotting experiments were performed as previously reported (159). Briefly, yeasts were growing in YPD medium with 0.4 % w/v galactose to induce gene expression from the GAL1 promoter. Cells were centrifuged at 5,000 x g and lysed with SUTEB buffer (1 % SDS, 8 M Urea, 10 mM tris-HCl, pH 7.4, 10 mM EDTA) in the presence of protease inhibitors (Roche). Following cell lysis, the lysates were centrifuged at 14,000 x g, 5 min and the supernatant was collected in clean 1.7ml Eppendorf tubes. Total protein concentrations were quantified using the BCA method (Thermo Scientific). Equal amount of total protein of each sample was loaded on 12 % SDS-PAGE and transferred to 45 μM nitrocellulose membrane with semi-dry transfer apparatus (Bio-Rad). The membranes were blocked overnight and incubated with either Hrg1 antibody or rabbit anti-HA (Sigma) as primary antibody at a 1:1,000 dilution for 2 h at room temperature, followed by HRP-

conjugated goat anti-rabbit antibody at a 1:30,000 dilution for 1 h at RT. For loading control, the membranes were re-probed with anti-PGK1 at 1:5,000 (Invitrogen). Signal was detected by using SuperSignal Chemiluminescence reagents (Thermo Scientific) in the Gel documentation system (Bio-Rad).

Chapter 3: Hrg1 is dispensable for primitive erythrocytes maturation in zebrafish

Summary

HRG1 was identified as the first *bona fide* eukaryotic heme importer conserved across metazoans. We have previously shown that knockdown of zebrafish Hrg1 impaired primitive erythroid cell maturation, but not specification, resulting in severe anemia in addition to developmental defects such as hydrocephalus, body axis curvature, and a shortened yolk tube extension. Subsequent genome annotation identifies two *hrg1* paralogs in the zebrafish genome, *hrg1a* (*slc48a1b*) and *hrg1b* (*slc48a1a*) with 73% identical at the amino acid level. We now show that both *hrg1a* and *hrg1b* are ubiquitously expressed in embryonic and adult zebrafish. Yeast growth assays reveal that zebrafish Hrg1a and Hrg1b are capable of mediating heme transport. However, knockdown of *hrg1a* by morpholinos targeting different region of RNA causes divergent phenotypes in zebrafish embryos, while knockdown of *hrg1b* does not have any visible anemic or morphological phenotypes. To investigate the physiological role of Hrg1a and Hrg1b, we generated *hrg1a* and *hrg1b* double mutants using CRISPR/Cas9 gene-editing. Immunoblotting revealed that Hrg1 proteins are absent in the $hrg1a^{iq261/iq261}$; $hrg1b^{iq361/iq361}$ double mutants. Intriguingly, $hrg1a^{iq261/iq261}$; $hrg1b^{iq361/iq361}$ double mutants do not show overt defects in RBCs development and hemoglobinization, as observed in the *hrg1a* morphants. Morpholino knockdown of *hrg1a* either in $hrg1a^{iq261/iq261}$ or $hrg1b^{iq361/iq361}$ mutants caused anemia. These results suggest that Hrg1 is not required for maturation and hemoglobinization of primitive erythroid cells in zebrafish and that the anemic phenotype of *hrg1a* morphants might be due to a dominant negative or off-target effect.

Results

Hrg1 genes are duplicated in zebrafish genome

The zebrafish genome is extensively duplicated owing to developmental gene duplication events in teleost (141). There are two *hrg1* paralogs in the zebrafish genome – *hrg1a* (*slc48a1b*) and *hrg1b* (*slc48a1a*), located on chromosome 6 and chromosome 23 respectively (**Fig. 3.1A**). Phylogenetic analysis shows that both Hrg1a and Hrg1b are HRG1 orthologs (**Fig. 3.1B**). Sequence alignment shows that the protein sequences of Hrg1a and Hrg1b are 73 % identity and 84 % similar (**Fig. 3.1C**). TMHMM prediction suggests that Hrg1a and Hrg1b proteins have similar transmembrane topology as *C. elegans* HRG-1 (CeHRG-1), mouse HRG1 (mHRG1) and human HRG1 (hHRG1), comprising four transmembrane domains, cytoplasmic N- and C-terminus (**Fig. 3.1C**). Zebrafish Hrg1a and Hrg1b also contain highly conserved histidine residue which can potentially bind heme, as site-directed mutagenesis of this residue in *C.elegans* and human HRG1 causes loss of heme transport activity when expressed in yeast (**Fig. 3.1C**, asterisk) (159). In summary, the topological similarity of Hrg1 suggests conserved function of HRG1s in metazoans.

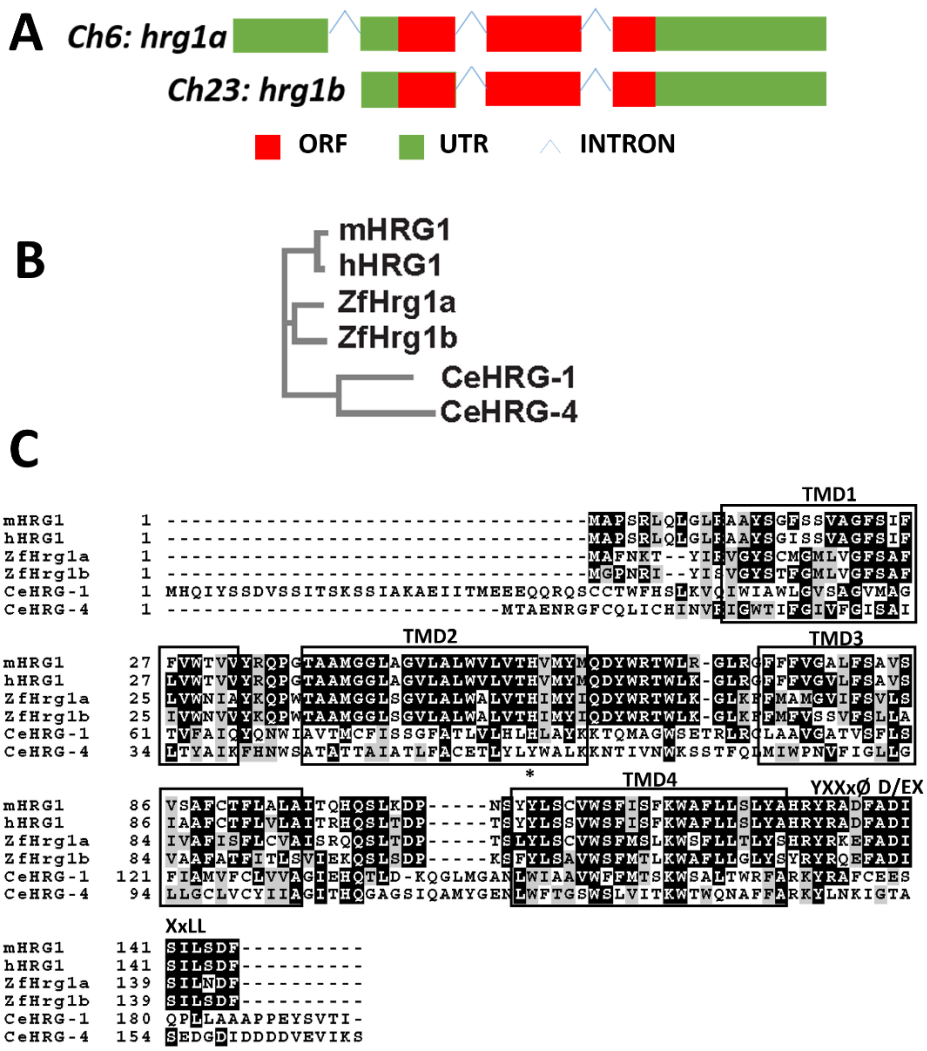

Figure 3.1 *Hrg1* is duplicated in the zebrafish genome

A). Loci of two *hrg1* paralogs in the zebrafish genome. *Hrg1a* (*slc48a1b*) is located on chromosome 6 and *hrg1b* (*slc48a1a*) is on chromosome 23.

B). Phylogenetic analysis of zebrafish *hrg1a* and *hrg1b* with CeHRG-1, CeHRG-4, mHRG1, and hHRG1. Sequences were aligned using ClustalW2 and a phylogenetic tree was generated using the Neighbor-Joining method in MEGA5.

C). Multiple sequence alignment of zebrafish Hrg1a and Hrg1b with CeHRG-1, CeHRG-4, mHRG1, and hHRG1. Asterisk, conserved histidine; black box, putative transmembrane domains; YXXxØ, C-terminal tyrosine sorting motif; D/EXXxLL, di-leucine sorting motif.

Expression of *hrg1a* and *hrg1b* in embryonic stage and adult tissues

We have previously shown that *hrg1* mRNA is expressed throughout the embryo, including the central nervous system at the 15-somite stage and 24 hpf with WISH (69). However, at that time, the zebrafish genome was not fully annotated and *hrg1b* had not been identified. Since the ORFs of *hrg1a* and *hrg1b* are 84 % sequence similar, we were unable to differentiate the temporospatial expression of *hrg1a* and *hrg1b* by using full-length ORF as RNA probes for WISH. To determine the temporospatial expression of *hrg1a* and *hrg1b* mRNA, we exploited sequence difference in the 3'UTR region of *hrg1a* and *hrg1b* mRNA to synthesize the probes for WISH. Expressions of *hrg1a* and *hrg1b* mRNA are very similar with ubiquitous expression throughout the developing embryo and strong expression in the central nervous system **(Fig. 3.2A and B)**. Both *hrg1a* and *hrg1b* mRNA can be detected by WISH at one-cell stage, suggesting that the *hrg1a* and *hrg1b* mRNA detected before 3 hpf are maternally deposited during oogenesis, as zygotic mRNA expression is occurred after 3 hpf in the zebrafish embryo (160).

Total mRNA was extracted from embryos at different stages, from one-cell to 4 dpf (day post fertilization). RT-PCR analysis shows that the temporal expression patterns of *hrg1a* and *hrg1b* are similar and both *hrg1a* and *hrg1b* mRNA are maternally deposited in the developing embryos (**Fig. 3.2C**). Quantitative RT-PCR (qRT-PCR) shows embryonic expression of *hrg1a* is relatively greater than *hrg1b* **(Fig. 3.2D)**, with maternal *hrg1a* and *hrg1b* mRNA being highly expressed during early embryonic stages compared to zygotic expression.

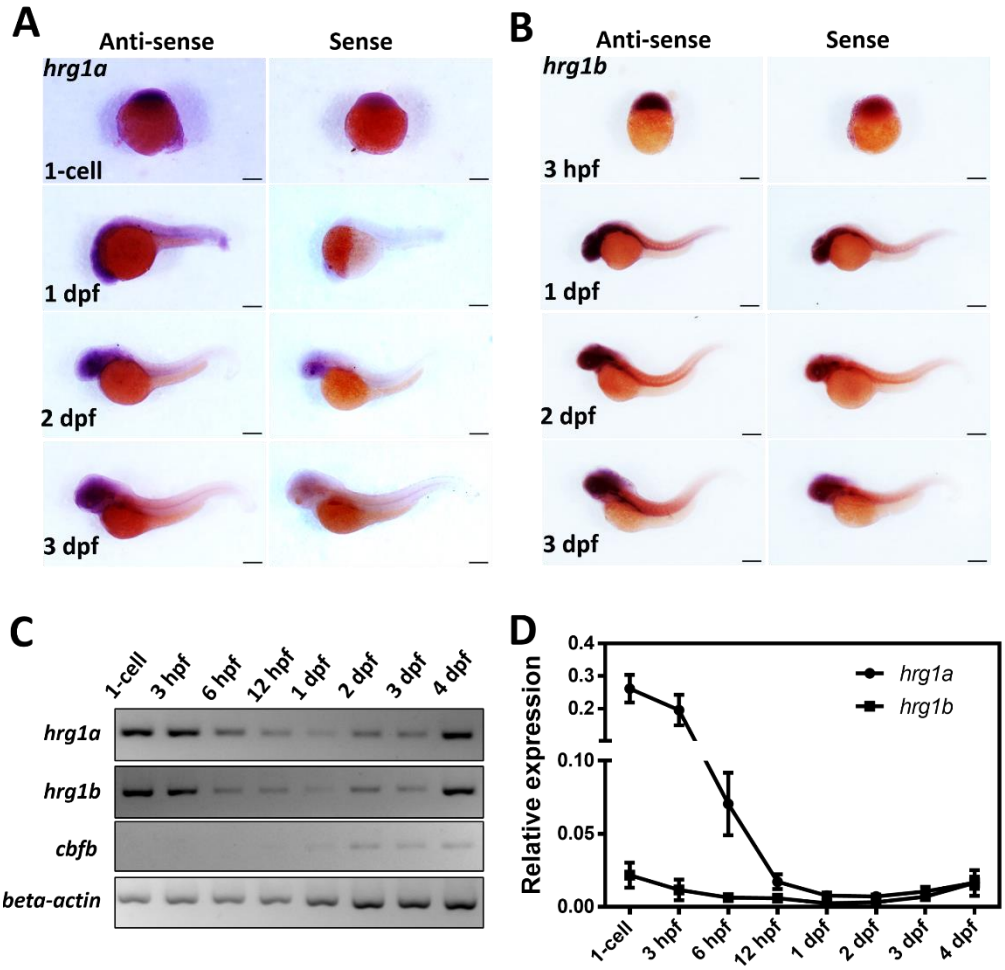

Figure 3.2 *Hrg1a* and *hrg1b* mRNA expression in zebrafish embryos

A) and B). WISH of *hrg1a* and *hrg1b* expression in embryos at different developmental stages. Anterior is to the left. Anti-sense probe is used to detect mRNA expression; sense probe is shown to indicate background staining. Scale bar: 200 μm.

C). RT-PCR of *hrg1a* and *hrg1b* mRNA in zebrafish embryos at different developmental stages. *ß-actin* is the control for house-keeping gene; *cbfb* is a transcription factor which is expressed around 18 hpf.

D). qRT-PCR of *hrg1a* and *hrg1b* mRNA in zebrafish embryos at different developmental stages. Fifty embryos before 24 hpf were pooled as one cohort. Thirty embryos at stages on or later than 24 hpf were pooled as one cohort. Three cohorts of pooled embryos at each stage were harvested for biological replicates. Expression level was normalized to *ß-actin*.

To determine the expression of *hrg1a* and *hrg1b* in adult zebrafish, both female and male zebrafish were dissected and tissues were collected for total RNA extraction. qRT-PCR was preformed to determine expression of *hrg1a* and *hrg1b* in various adult zebrafish tissues. *hrg1a* and *hrg1b* are widely expressed in adult zebrafish, however, with different expression intensity (**Fig. 3.3A and B)**. Both *hrg1a* and *hrg1b* are highly expressed in the brain, which is consistent with the WISH results. Surprisingly, expression level of *hrg1b* mRNA is higher than *hrg1a* in peripheral blood in both male and female. *hrg1a* and *hrg1b* is also expressed in the kidney, the major hematopoietic tissue in adult zebrafish, suggesting a potential role of Hrg1a and Hrg1b in adult erythropoiesis. Additionally, both *hrg1a* and *hrg1b* are expressed in spleen, an organ which clears senescent or damaged RBCs and recycles heme-iron. Consistent with the high expression levels of *hrg1a* mRNA in embryos at one-cell stage, *hrg1a* mRNA is abundant in the ovary.

Confocal microscopy studies in HEK293 cells expressing fluorescently tagged proteins show that Hrg1a and Hrg1b are distributed in intracellular compartments, co-localizing with LAMP1, a lysosomal marker, consistent with previous studies for worm and human HRG1 (**Fig. 3.4**) (69). Co-expression of fluorescent protein tagged Hrg1a and Hrg1b resulted in both proteins co-localizing to the same intracellular vesicles. These results suggest that zebrafish Hrg1a and Hrg1b are located primarily in the endosomes and lysosomes-related organelles, consistent with the presence of sorting motifs in the C-terminus (**Fig. 3.1C, Fig. 3.4**).

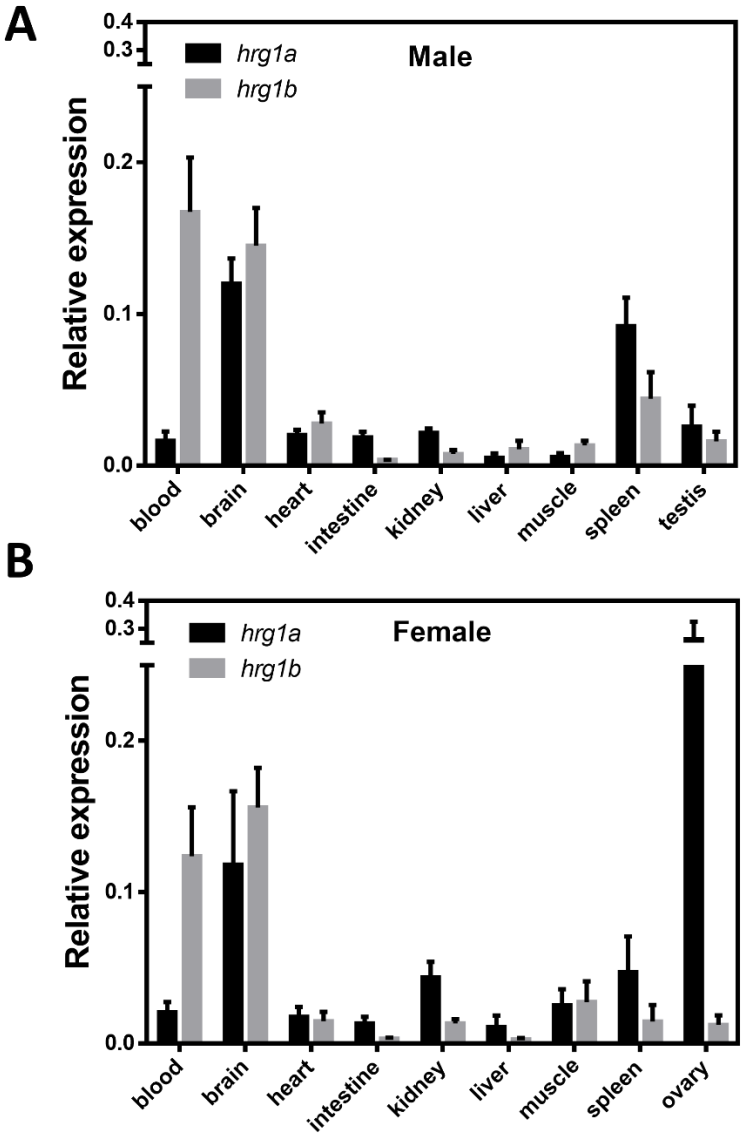

Figure 3.3 Expression of *hrg1a* and *hrg1b* mRNA in adult zebrafish tissues

A). qRT-PCR of *hrg1a* and *hrg1b* mRNA in dissected tissues from adult male.

B). qRT-PCR of *hrg1a* and *hrg1b* mRNA in dissected tissues from adult female

Two male or female fish were dissected as one cohort, and each gender had three cohorts as biological replicates. Expression level was normalized to *ef1α*.

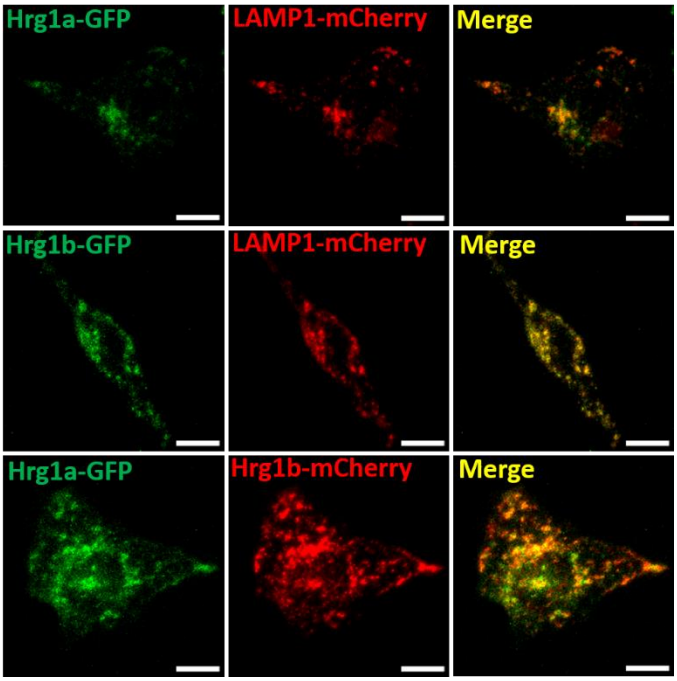

Figure 3.4 Subcellular localization of fluorescent tagged Hrg1a and Hrg1b when expressing in HEK293 cells

Confocal microscopy of subcellular localization of Hrg1a and Hrg1b with C-terminus tagged fluorescent proteins in transfected HEK-293 cells. LAMP1 is a marker for lysosomal compartments. Scale bar: 10 µm.

Expression of Hrg1 in a heterologous system improves utilization of exogenous heme

To determine whether zebrafish Hrg1 is able to transport heme, we utilized previously established growth assays in yeast. The heme biosynthetic pathway is conserved among eukaryotes, with the first step catalyzed by ALAS. In yeast, mutation in *hem1* (*hem1Δ*), which encodes ALAS, causes failure in production of δ-aminolevulinic acid (ALA), an intermediate of heme synthesis. The growth of *hem1Δ* mutants can be rescued by supplementation with ALA or by providing excess of exogenous heme in the growth medium (156, 157)**.** Expression of a heme importer can greatly ameliorate growth defects of *hem1Δ* in low concentrations of exogenous heme (159).

We previously showed that the expression of CeHRG-1 or CeHRG-4 greatly improves *hem1Δ* yeast growth in the presence of low heme concentration (69). Expression of zebrafish Hrg1a and Hrg1b also showed the same rescued growth of *hem1Δ* yeast in the presence of exogenous heme (0.25 μM and 10 μM), suggesting that Hrg1a and Hrg1b can mediate heme transport comparable to established *C.elegans* heme transporters (**Fig. 3.5**).

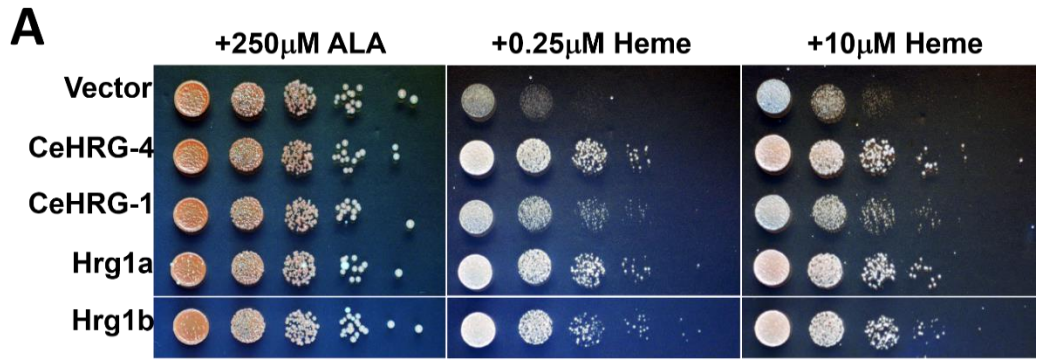

Figure 3.5 Hrg1a and Hrg1b are capable of heme transport upon expression in yeast

A). Yeast growth assay showing zebrafish Hrg1a and Hrg1b are able to mediate heme transport in yeast. The *hem1Δ* strains transformed with empty vector pYes-DEST52, CeHRG-4, CeHRG-1, Hrg1a and Hrg1b were cultivated overnight and spotted in serial dilutions on SC plates supplemented with 250 μM ALA and different concentrations of heme.

Transient knockdown of *hrg1a* or *hrg1b* by morpholinos in zebrafish embryos

The yeast growth assays showed that Hrg1a and Hrg1b are both capable of rescuing the growth of *hem1Δ yeast*, suggesting that zebrafish Hrg1a and Hrg1b are functionally interchangeable heme transporters. To elucidate Hrg1a and Hrg1b function in zebrafish embryonic development and erythropoiesis, gene knockdowns by antisense morpholino were utilized to transiently block the expression of *hrg1a* and *hrg1b* in zebrafish embryos. Both translation-blocking and pre-mRNA splice-blocking morpholinos were designed to knockdown the gene expression of *hrg1a* and *hrg1b* (**Fig. 3.6A**). The translation-blocking morpholino is designed to target the ATG start codon and can inhibit protein translation initiation by preventing ribosome binding to the mature mRNA. The pre-mRNA splice-blocking morpholino is designed to target the exon-intron boundaries and can selectively induce mRNA mis-splicing with either retained introns or deleted exons. The morpholinos were delivered by microinjection into zebrafish embryos at the one-cell stage. Hemoglobinization was determined by *o*-dianisidine staining of RBCs (99). *hrg1a* knockdown by pre-mRNA splice-blocking morpholino, which targeted the boundary of *hrg1a* intron 2 and exon 3 (*Hrg1a_I2E3_MO2*), caused body curvature defects and severe anemia, consistent with previously published results (**Fig. 3.6B**) (69). However, *hrg1a* translation-blocking morpholino (*Hrg1a_ATG_MO*) and another splicing-blocking morpholino targeting *hrg1a* exon 2 and intron 2 (*Hrg1a_E2I2_MO1)* boundaries did not cause comparable phenotypes as *Hrg1a_I2E3_MO2*. In contrast, knockdown of *hrg1b* by either translation-blocking (*Hrg1b_ATG_MO*) or splice-blocking morpholino (*Hrg1b_E2I2_MO*) did not cause anemic phenotype (**Fig. 3.6B**).

To evaluate the efficiency of *hrg1a* or *hrg1b* knockdown by splice-blocking morpholino, RT-PCR analysis was performed on total mRNA extracted from these morphants. *hrg1a* mRNA expression was efficiently blocked by *Hrg1a_E2I2_MO1* resulting in use of cryptic splicing site, 25 nt downstream of the morpholino targeting sequence

(**Appendix II)**. *Hrg1b* expression was also efficiently disrupted by *Hrg1b_E2I2_MO* knockdown causing a deletion of *hrg1b* exon 2 and mRNA degradation, probably through nonsense mediated decay (**Appendix IV**). Knockdown of either *hrg1a* or *hrg1b* by splice-blocking morpholinos did not affect the expression of the other paralog (**Fig. 3.7A**). Although causing severe anemia, knockdown of *hrg1a* by *Hrg1a_I2E3_MO2* showed partially defective splicing of *hrg1a* mRNA (**Appendix III**), with majority of *hrg1a* mRNA intact (**Fig. 3.7A**).

The efficiency of translation-blocking morpholinos was determined by immunoblotting with Hrg1 antibody. As *Hrg1a_ATG_MO* and *Hrg1b_ATG_MO* decreased Hrg1 protein individually, co-injection of *Hrg1a_ATG_MO* and *Hrg1b_ATG_MO* together greatly reduced Hrg1 protein abundance (**Fig. 3.7B and C**).

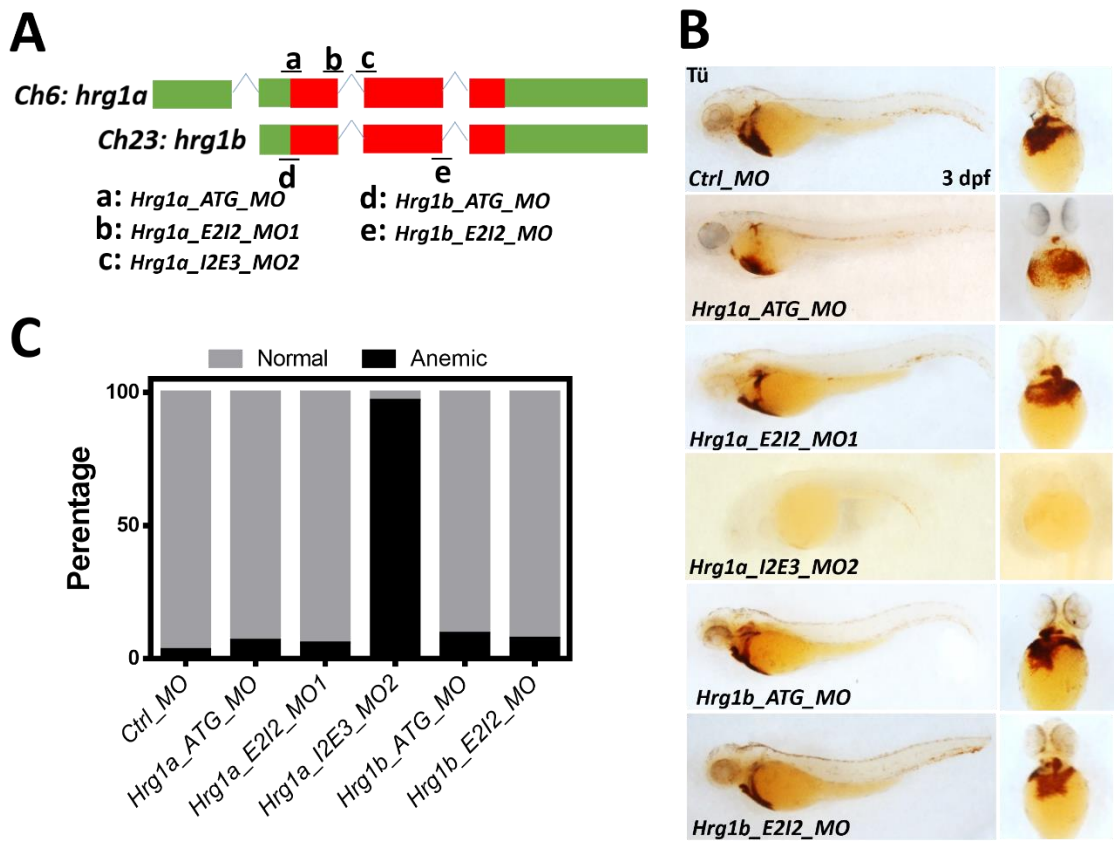

Figure 3.6 Knockdown of *hrg1a* and *hrg1b* by multiple morpholinos

A). Targeting sites of morpholinos for *hrg1a* and *hrg1b*. Two splice-blocking and one translation-blocking morpholinos for *hrg1a*, one splice-blocking and one translation-blocking morpholino for *hrg1b* were designed. The control morpholino (*Ctrl_MO*) was injected as a random scramble control in these knockdown experiments. Each morpholino is 25 nt in length.

B). *O*-dianisidine staining of 3 dpf embryos after injection of indicated morpholinos at the one-cell stage. Knockdown of zebrafish *hrg1a* by *Hrg1a_I2E3_MO2* results in body curvature and severe anemia, as indicated by reduced *o*-dianisidine-positive RBCs.

C). Quantification of anemic embryos shown as a percentage of overall injected populations.

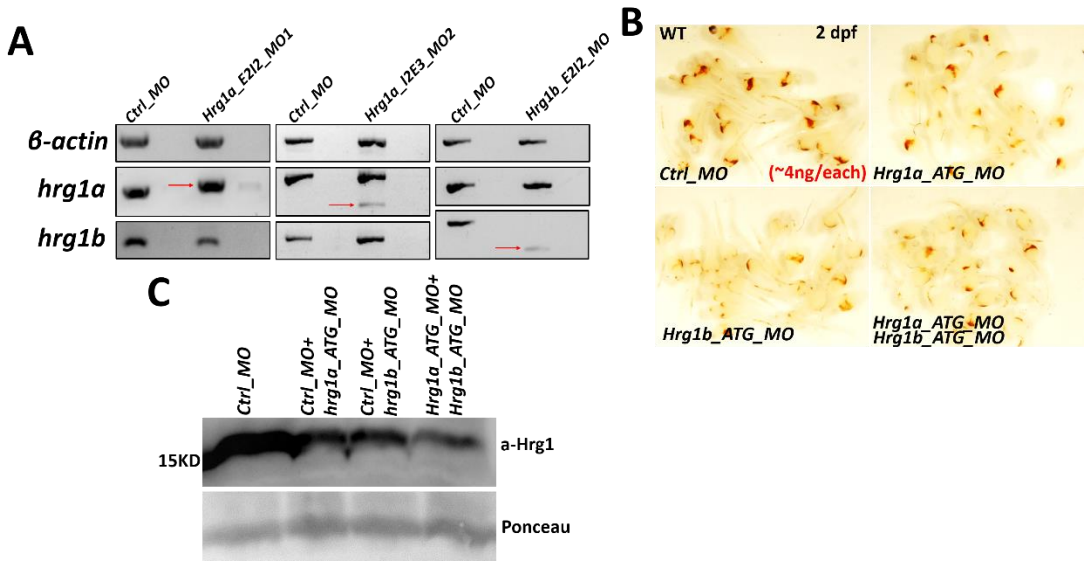

Figure 3.7 Knockdown efficiency by morpholinos

A). Knockdown efficiency of *Hrg1a_E2I2_MO1*, *Hrg1a_I2E3_MO2*, *Hrg1b_E2I2_MO* by RT-PCR. *Hrg1a_E2I2_MO1* blocks original splicing acceptor site and utilizes 25 nt downstream splicing acceptor, causing 25 nt longer ORF with frameshift (red arrow). *Hrg1a_I2E3_MO2* partially blocks the splicing on intron 2 and exon 3 junction, resulting in small-sized cDNA with deletion of exon 3 (red arrow), however, majority of *hrg1a* mRNA is normal. *Hrg1b_E2I2_MO* causes deletion of exon 2, resulting in small sized *hrg1b* cDNA (red arrow). Knockdown *hrg1a* or *hrg1b* did not affect cDNA of the other paralog. Red arrows show the PCR products of cDNA affected by morpholino knockdown.

B). Co-injection of *Hrg1a_ATG_MO* and *Hrg1b_ATG_MO* did not cause severe anemic phenotypes as shown by *o*-dianisidine staining at 3 dpf embryos.

C). Hrg1 Western blot showed Hrg1 protein was decreased by co-injection of *Hrg1a_ATG_MO* and *Hrg1b_ATG_MO*. 100 µg membrane fraction lysates were used for each lane. Ponceau was used as a loading control.

Generating *hrg1a* and *hrg1b* mutants by TALEN and CRISPR/Cas9 gene editing

Antisense morpholinos are useful for transient gene knockdown due to convenience and high efficiency of delivery throughout the zebrafish embryos. However, several caveats still exist for morpholinos, including the transient nature of knockdown, dose optimization, toxicity, off-target effects, and loss of knockdown efficacy in embryos that are past 50 hpf. To better delineate the function of Hrg1 in zebrafish, we utilized TALEN (transcription-activator like effector nuclease) and CRISPR/Cas9 (clustered regularly interspaced short palindromic repeats) gene-editing to generate *hrg1a* and *hrg1b* zebrafish mutants (119, 161).

TALEN and CRISPR-Cas9 gene editing has been shown to be capable of generating double strand breaks (DSB) in targeted sites with high efficiency in zebrafish (119, 161). DSBs are repaired by inaccurate non-homologous end joining (NHEJ), causing either an insertion or deletion (indel) at the targeting sites. We used both TALEN and CRISPR for gene editing in our studies. Two pairs of TALEN for *hrg1a*, and two CRISPRs for *hrg1a* and *hrg1b* were used in this study. All these sites were chosen from *in silico* optimization to minimize off-target effects for each TALEN pair and CRISPR.

To check the efficiency of each TALEN for *hrg1a*, TALEN mRNA was obtained by in-vitro transcription and two mRNAs for one TALEN pair were co-injected in equimolar concentration into zebrafish embryos at the one-cell stage. The efficiency and specificity of TALEN induced indels on target site was determined by single embryo PCR. Genotyping on injected embryos was performed next day after microinjection to determine the efficiency of TALEN and whether the embryos contained mutation in the expected target site. The indels in the target sites resulted in loss of restriction sites within the two TALEN recognition sites, AvaII for *hrg1a* exon2 and Sau96I for *hrg1a* exon 3 **(Fig. 3.8A and B)**. DNA fragments were amplified using primers on both sides of TALEN targeting sites. Embryos injected with mRNA encoding TALENs revealed undigested PCR products when treated with AvaII or Sau96I **(Fig. 3.8A and B)**. The undigested fragments were further purified and sequenced.

Sequencing results on the purified undigested PCR products confirmed that indels were induced at the target sites **(Fig. 3.8A and B)**. These results demonstrated that TALENs induce DSBs and random indels occur due to NHEJ.

To generate null mutants for *hrg1a* with large-size deletion, two pairs of verified *hrg1a* TALENs were co-injected into zebrafish embryos at one-cell stage. If both TALEN pairs successfully make DSBs on exon 2 and exon 3 at the same allele, it may take out a large fragment of DNA sequence between two TALEN targeting sites and lead to a larger deletion of up to ~2.5 kb in the *hrg1a* gene locus between exon 2 and exon 3 (**Fig. 3.9A**). The deletion of ~2.5 kb can be detected using primers flanking these two TALEN cutting sites, resulting in a smaller size PCR product after deletion. Seven out of twenty-five F0 chimeric founders were identified to carry large-size deletion at *hrg1a* locus, with various lengths of deletions (**Fig. 3.9B**). Subsequent sequencing results confirmed the large-sized deletion at *hrg1a* locus (**Fig. 3.9C**). One founder (No.5) carried an entire deletion of ~2.5 kb sequence between two TALEN targeting sites, whereas No. 1, No. 2, No. 7 founders had insertions of different DNA sequences after the ~2.5kb deletion.

TALEN is efficient in gene-editing and generating mutants in zebrafish, however, the assembly of each TALEN pair is tedious and time-consuming. While my project was coming along, CRISPR/Cas9 technology was established and demonstrated to have a much higher efficiency in term of inducing DSB in DNA sequence, together with easier assembly (120). A functional unit of CRISPR/Cas9 contains two elements, gRNA and Cas9 nuclease. The gRNA can be specifically designed to target 20 nt sequence and recruit Cas9 nuclease to its target sequence to induce DSBs. Co-injection of multiple gRNAs together with Cas9 mRNA was used to generate multiple mutations or large-size deletions in zebrafish embryos (162). To generate large-sized deletion mutants for *hrg1a* and *hrg1b*, two different gRNAs targeting exon 2 and exon 4 in *hrg1a* locus, and two different gRNAs targeting exon 1 and exon 3 in *hrg1b* were co-injected into zebrafish embryos at the one-cell stage (**Fig. 3.10A and Fig.**

3.11A). Twenty-four F0 chimeric founders were raised to adult for genotyping; four among these carried deletions in *hrg1a* and two for *hrg1b* (**Fig. 3.10B and Fig. 3.11B**). Sequencing results confirmed the disruption of *hrg1a* and *hrg1b* loci in these F0 founders (**Fig. 3.10C, Fig. 3.11C**).

F0 chimeric founders with large-sized deletion of *hrg1a* or *hrg1b* were further crossed to WT to generate F1 offsprings. If the large-size deletion is heritable via the germline, we can generate stable F1 heterozygote of *hrg1a* or *hrg1b* mutants. However, we were unable to obtain *hrg1a* or *hrg1b* mutants with the large deletion even after screening over 300 F1 fish (**Table 3.1**). This was unexpected since we obtained high efficiency gene-editing by TALEN or CRISPR in our pilot screening of individual injected embryos and chimeric F0 founders. It is possible that large-size deletion may cause genome instability which will result in embryonic lethality.

Instead of screening for large-size deletion, we decided to screen for smaller indels (**Fig. 3.12**). Several *hrg1a* mutant alleles carrying different indels were retrieved from TALEN gene-editing. *hrg1a*^{iq210} has a deletion of 10 nt in exon 2, while *hrg1a*^{iq305} carries a 5 nt deletion in exon 3, resulting in a frameshift of *hrg1a* ORF (**Fig 3.12A**). We also obtained *hrg1* mutants with two indels in the same allele. *hrg1a*^{iq1001} mutant allele carries two indels in *hrg1a* locus: 10 nt deletion in exon 2, and 1nt deletion in exon 3 (**Fig. 3.12A**). We also selectively retrieved several mutants for *hrg1a* and *hrg1b* by CRISPR/Cas9. *hrg1a*^{iq261} carries a 61 nt deletion and 7nt insertion resulting in deletion of the ATG translation start site (**Fig. 3.12B**). Computational analysis reveals that *hrg1b*^{iq306} has a 6 nt substitution in exon 3, causing a pre-mature stop codon with a deletion of 17 aa in the C-terminus of the mature protein, while *Hrg1b*^{iq361} has a 61nt deletion which causes a truncation and removal of 28 aa in C-terminus (**Fig. 3.12C**)

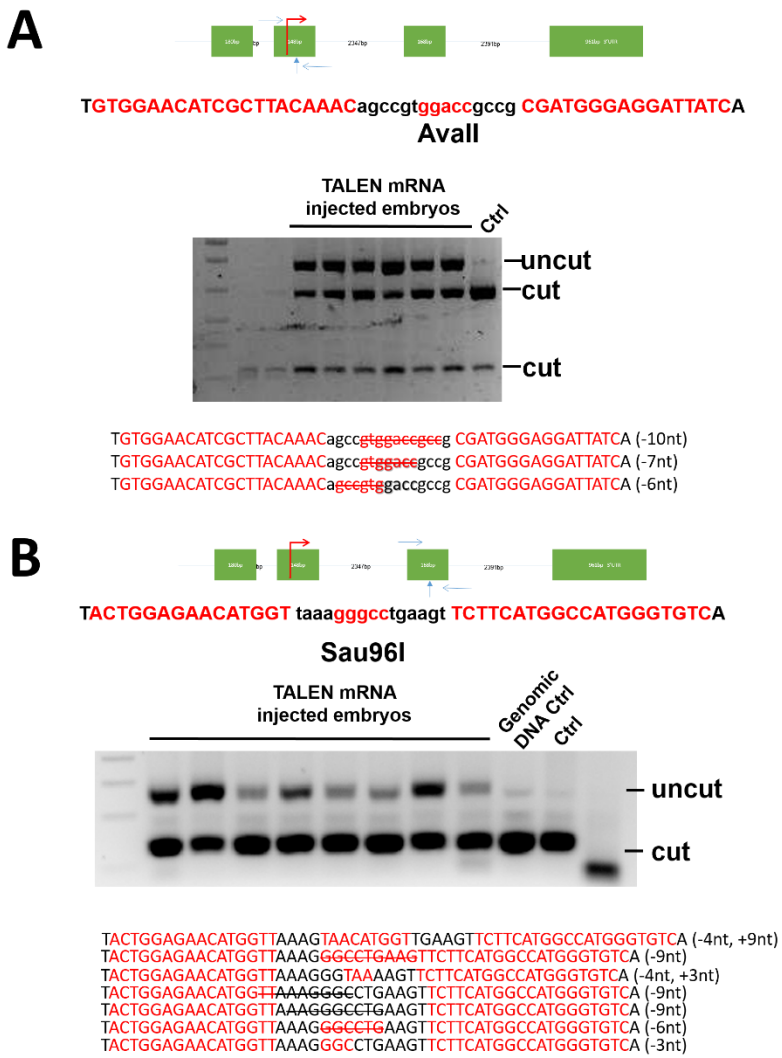

Figure 3.8 Targeted disruption of *hrg1a* in zebrafish by TALENs

A). TALEN targeting site on *hrg1a* exon 2.

B). TALEN targeting site on *hrg1a* exon 3.

The binding sites of TALEN pair are shown as red bold uppercase. The space region is shown as lowercase with restriction site (red text). Detection of mutations in injected embryos was performed by AvaII (exon 2) or Sau96I (exon 3) digestion. PCR product with potential indels at the AvaII or Sau96I site cannot be cut (uncut band). Complete digestion of PCR products with AvaII or Sau96I can be detected using genomic DNA as a control. Sequences of *hrg1a* indel in exon2 or exon 3 mutations were showed as strikethrough text.

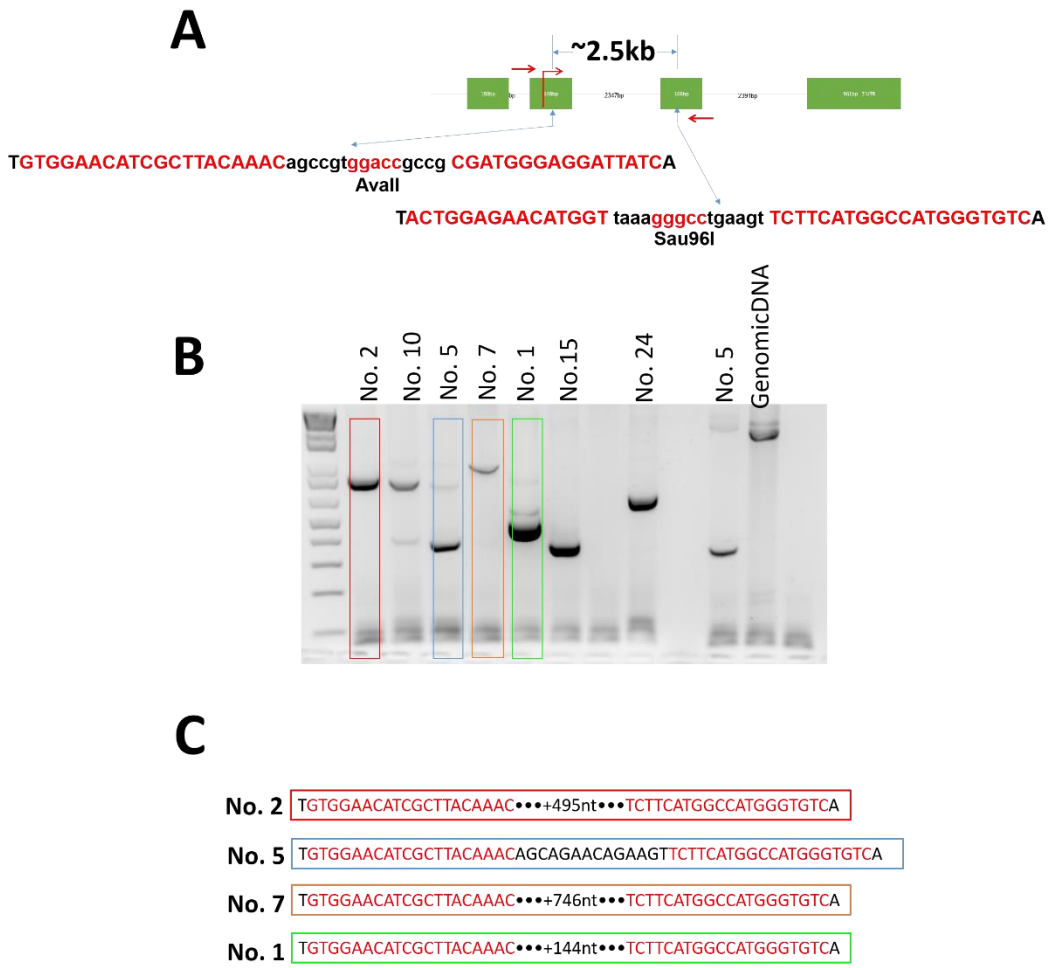

Figure 3.9 Targeted deletion of large-size fragment between exon 2 and exon 3 in *hrg1a* by using two TALEN pairs

A). Structure and sequence of *hrg1a* TALEN targeting sites, showing the binding sites (red bold uppercase) of TALENs. The space region is shown as lowercase with restriction site (red).

B). Detection of large-sized deletion in F0 founders by PCR and DNA gel electrophoresis. If both TALENs cut, the PCR product will be smaller than that amplified from genomic DNA (gDNA).

C). Sequences of PCR products from F0 chimeric founders with large-size deletion in *hrg1a* locus.

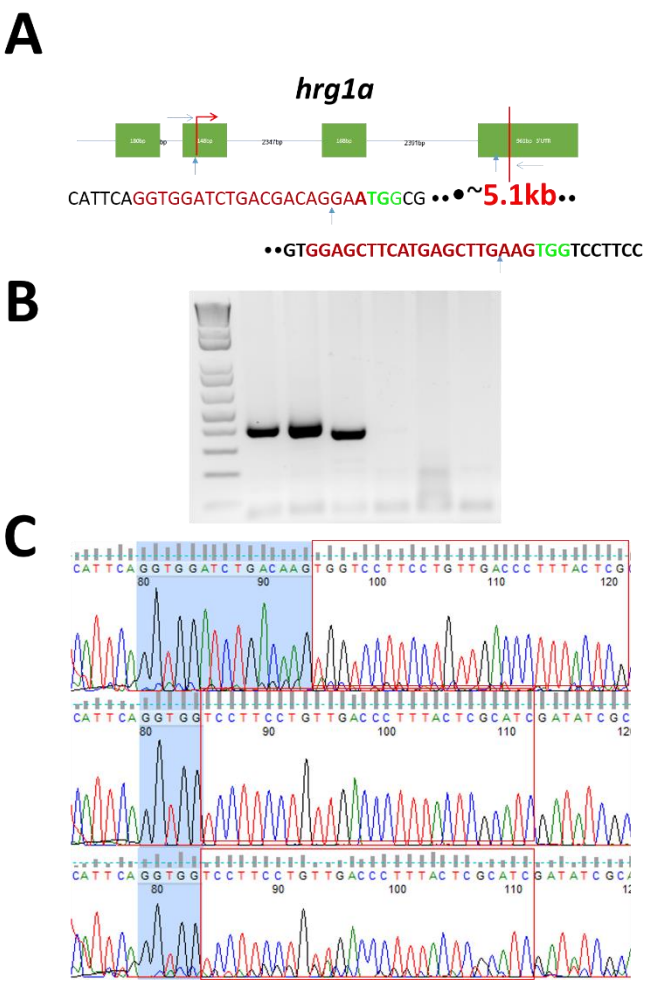

Figure 3.10 Targeted deletion of *hrg1a* by CRISPR /Cas9.

A). Target sites in *Hrg1a* for CRISPR. The vertical arrows show the location of Cas9 cutting sites. The horizontal arrows indicate the primers for PCR.

B). Detection of deletion in injected embryos by PCR and DNA gel electrophoresis.

C). Sequencing results of PCR products from embryos with positive targeted deletion caused by CRISPR.

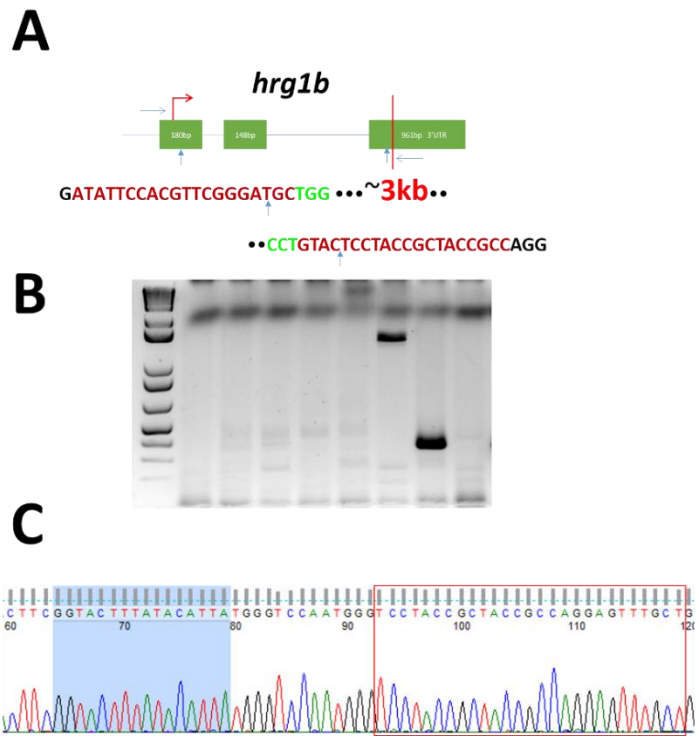

Figure 3.11 Targeted deletion of *hrg1b* by CRISPR /Cas9.

A). Target sites in *Hrg1a* for CRISPR. The vertical arrows showed the location of Cas9 cutting sites. The horizontal arrows indicate the primers for PCR

B). Detection of deletion in injected embryos by PCR and DNA gel electrophoresis.

C). Sequencing result of PCR products from embryos with positive targeted deletion.

Gene editing	Screened F0	Screened F1
Hrg1a TALEN	7/25	340
Hrg1a CRISPR	4/24	376
Hrg1b CRISPR	2/24	363

Table 3.1 Screening of *hrg1a* and *hrg1b* mutants with large-size deletion

Seven out of twenty-five F0 founders generated by TALENs were shown to carry large-size deletion in *hrg1a* locus. Four out of twenty-four F0 founders generated by CRISPR/Cas9 were shown to carry large-size deletion in *hrg1a* locus. For *hrg1b*, two F0 founders generated by CRISPR/Cas9 were shown to carry large-size deletion. The positive F0 founders were further crossed with WT to generate F1 progenies. Indicated numbers of F1 offsprings were screened, however no heritable germline transmission was found in F1 offsprings with large-size deletion for *hrg1a* or *hrg1b*.

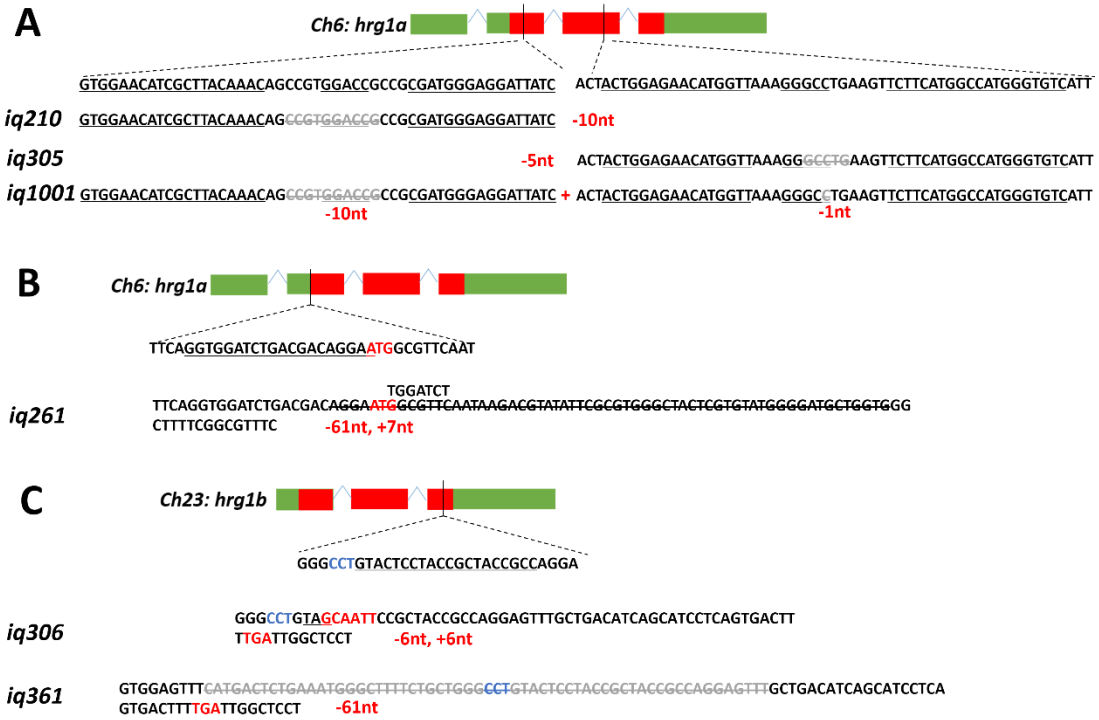

Figure 3.12 *Hrg1a* and *hrg1b* mutant alleles generated by TALEN or CRISPR/Cas9 gene-editing.

A). *Hrg1a* mutant alleles generated by TALEN.

B). *Hrg1a* mutant allele generated by CRISPR.

C). *Hrg1b* mutant alleles generated by CRISPR.

The underline texts show the TALEN or CRISPR targeting sequences. The deleted nucleotides are shown with strikethrough texts. Red texts show the deletion of each mutant allele.

Mutant forms of Hrg1a and Hrg1b cannot rescue the growth of heme-deficient yeast

To evaluate whether mutant forms of Hrg1a and Hrg1b created by TALEN and CRISPR/Cas9 are functional, we determined whether the putative proteins encoded by these mutants can rescue the growth of *hem1Δ* yeast. For *hrg1a*^{iq210} and *hrg1a*^{iq261} mutant alleles, the putative ORF with the downstream potential alternate translation start site was cloned, with the truncation of 34 aa in the N-terminus. Compared to wild type Hrg1a and Hrg1b, none of the mutant constructs rescued *hem1Δ* growth in the presence of exogenous heme (**Fig. 3.13A**). RT-PCR on total RNA extracted from transformed yeast revealed that the WT and mutant forms of *hrg1a* and *hrg1b* were transcribed in the transformed yeast (**Fig. 3.13B**). Immunoblotting showed that some mutant forms of Hrg1a and Hrg1b protein were expressed in yeast transformants (**Fig. 3.13C and D**). Collectively, these results suggest that the mutant forms of Hrg1a and Hrg1b either does not transport heme or are poorly translated into functional protein.

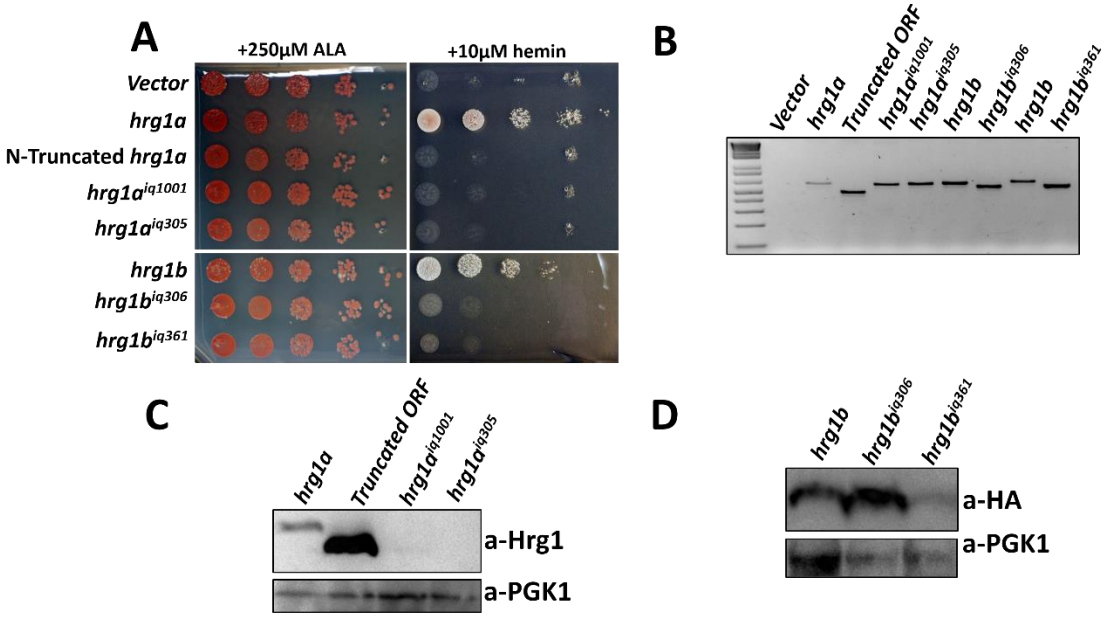

Figure 3.13 Mutant forms of Hrg1a and Hrg1b cannot rescue *hem1Δ* growth in the presence of exogenous heme

A). Yeast growth assay with mutant forms of Hrg1a and Hrg1b. The *hem1Δ* strain transformed with empty vector pYes-DEST52, Hrg1a, Hrg1b, mutant forms of Hrg1a and Hrg1b were cultivated overnight and spotted in serial dilutions on SC plates supplemented with 250 μM ALA and indicated concentration of heme.

B). RT-PCR showing both WT and mutant forms of *hrg1a* and *hrg1b* ORFs are transcribed in transformed yeast.

C). Mutant forms of Hrg1a are expressing in yeast revealed by immunoblotting. Hrg1a truncated ORF is generated by using downstream alternative ATG translation start site, with deletion of 38aa at N-terminus. The other *hrg1a* mutant alleles *hrg1a*^{iq1001} and *hrg1a*^{iq305} caused frameshift, expressed proteins cannot be recognized by Hrg1 antibody.

D). Western blot showing mutant forms of HA-tagged Hrg1b are expressing in yeast. *Hrg1b*^{iq361} and *hrg1b*^{iq306} mutant alleles caused frameshift, thus c-terminus HA-tag version was used for yeast growth assay. Imuunoblotting on HA showed both *Hrg1b*^{iq361} and *hrg1b*^{iq306} were expressed in yeast. Expression level of *Hrg1b*^{iq306}-HA was low.

Hrg1 knockout zebrafish are viable despite no detectable Hrg1 proteins

We next crossed *hrg1a*^{iq261} and *hrg1b*^{iq361} zebrafish mutants to obtain double heterozygous, which were then intercrossed to generate *hrg1a*$^{iq261/iq261}$*; hrg1b*$^{iq361/iq361}$ double mutants. Genotyping of *hrg1a*$^{iq261/iq261}$, *hrg1b*$^{iq361/iq361}$ and *hrg1a*$^{iq261/iq261}$*; hrg1b*$^{iq361/iq361}$ revealed that *hrg1* mutants can survive to 3 dpf (**Fig. 3.14A**). Immunoblotting with Hrg1 antibody on genotyped 3 dpf embryos confirmed no detectable Hrg1 protein in *hrg1a*$^{iq261/iq261}$*; hrg1b*$^{iq361/iq361}$ double mutants (**Fig. 3.14B**). Intercrossing of *hrg1a*$^{+/iq261}$*; hrg1b*$^{+/iq361}$ produced expected Mendelian segregation of *hrg1a*$^{iq261/iq261}$*; hrg1b*$^{iq361/iq361}$ double mutants (**Table 3.2**) (Chi-square test, $p > 0.05$). *hrg1a*$^{iq261/iq261}$*; hrg1b*$^{iq361/iq361}$ can survive to adulthood with no visible differences compared to WT or single mutants.

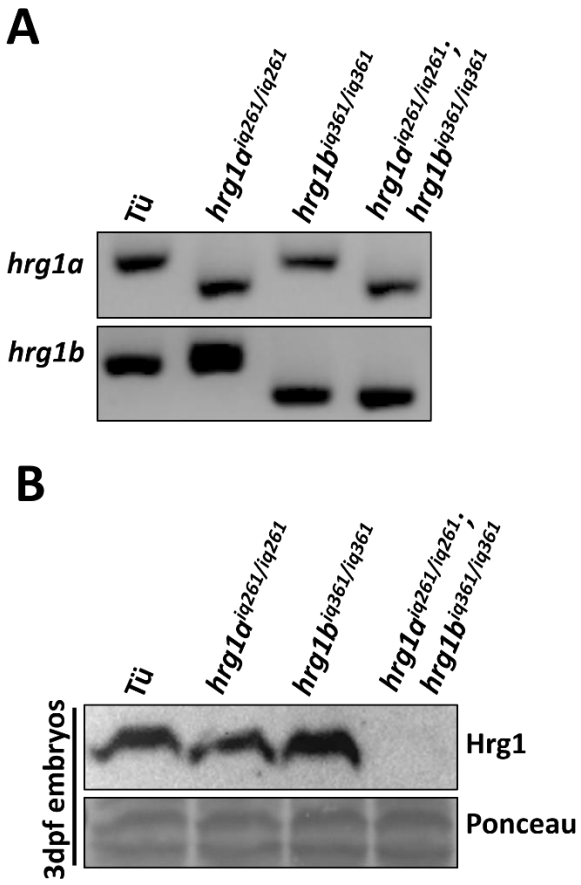

Figure 3.14 Genotyping and immunoblotting of *hrg1a*$^{iq261/iq261}$; *hrg1b* $^{iq361/iq361}$, and *hrg1a*$^{iq261/iq261}$; *hrg1b*$^{iq361/iq361}$.

A). Genotyping of *hrg1a*$^{iq261/iq261}$; *hrg1b* $^{iq361/iq361}$, and *hrg1a*$^{iq261/iq261}$; *hrg1b*$^{iq361/iq361}$ 3 dpf zebrafish embryos. *Hrg1a*$^{iq261/iq261}$ has an indel of -61 nt, and +7 nt in exon 2; and *hrg1b* $^{iq361/iq361}$ carries -61nt deletion in exon 3, causing small-sized PCR products.

B). Immunoblotting on Hrg1 of membrane fraction lysates from wild-type WT, *hrg1a*$^{iq261/iq261}$, *hrg1b*$^{iq361/iq361}$ and double mutant *hrg1a*$^{iq261/iq261}$; *hrg1b*$^{iq361/iq361}$. Each crude membrane fraction lysate was from pooled ~30 embryos. Each lane represented 100 µg protein. Ponceau is used as a loading control.

hrg1a$^{+/iq261}$; *hrg1b*$^{+/iq361}$ intercross				Expected
Other	119	82	183	9
hrg1a$^{iq261/iq261}$	41	28	85	3
hrg1b$^{iq361/iq361}$	39	31	79	3
hrg1a$^{iq261/iq261}$; *hrg1b*$^{iq361/iq361}$	18	7	24	1

Table 3.2 Intercross of *hrg1a*$^{+/iq261}$; *hrg1b*$^{+/iq361}$ shows progenies with expected mendelian ratio

Screening of progenies from intercross of *hrg1a*$^{+/iq261}$; *hrg1b*$^{+/iq361}$ at the stage of 3 dpf with expected Mendelian ratio. No significant difference (Chi-square test, $p>0.05$).

Hrg1a$^{iq261/iq261}$; hrg1b$^{iq361/iq361}$ double mutants do not show defects in embryonic erythropoietic differentiation and RBC hemoglobinization

To characterize whether *hrg1a$^{iq261/iq261}$*, *hrg1b$^{iq361/iq361}$* or *hrg1a$^{iq261/iq261}$; hrg1b$^{iq361/iq361}$* double mutant embryos have overt defects in primitive erythropoiesis, WT and mutant embryos were collected for WISH. No alteration for *gata1*, a transcription factor required for primitive erythropoiesis lineage, and *ae1*, a marker for developing RBCs in intermediate cell mass was observed at 1 dpf. These results indicate that there are no defects in erythropoietic differentiation in *hrg1a$^{iq261/iq261}$*, *hrg1b$^{iq361/iq361}$* or *hrg1a$^{iq261/iq261}$; hrg1b$^{iq361/iq361}$* mutant embryos (**Fig. 3.15**) (n = 30). To characterize whether *hrg1a$^{iq261/iq261}$*, *hrg1b$^{iq361/iq361}$* or *hrg1a$^{iq261/iq261}$; hrg1b$^{iq361/iq361}$* double mutant embryos have deficiency in RBC maturation and hemoglobinization, we performed *o*-dianisidine staining for embryos at 3 dpf. We did not detect defects in RBC hemoglobinization in any of these three mutants at 3 dpf compared to WT (n = 50) (**Fig. 3.16A**). We next examined whether there are any hematological phenotypes at the cellular level by withdrawing circulating peripheral blood from 3 dpf zebrafish embryos; *O*-dianisidine staining of isolated primitive RBCs showed no obvious differences in hemoglobinization with the RBCs in the peripheral blood of *hrg1a$^{iq261/iq261}$*, *hrg1b$^{iq361/iq361}$* or *hrg1a$^{iq261/iq261}$; hrg1b$^{iq361/iq361}$* (**Fig. 3.16B**). We also crossed the *hrg1a$^{iq261/iq261}$*, *hrg1b$^{iq361/iq361}$* or *hrg1a$^{iq261/iq261}$; hrg1b$^{iq361/iq361}$* mutants into the globinLCR: GFP transgenic zebrafish. FACS quantification further confirmed that there were no differences in GFP^{+} cells between WT and mutant zebrafish embryos (**Fig. 3.17**) (Two way ANOVA, $p>0.05$). In addition, May-Grünwald-Giemsa staining on isolated primitive erythrocytes showed no alternations in RBC morphology from 3 dpf embryos (**Fig. 3.18**). Collectively, these results suggest that no measurable defects were detected in the erythropoietic lineage for *hrg1a$^{iq261/iq261}$*, *hrg1b$^{iq361/iq361}$* or *hrg1a$^{iq261/iq261}$; hrg1b$^{iq361/iq361}$* mutants. Furthermore, ICP-MS from collected 3 dpf embryos also showed no significant

differences in iron or heme content in *hrg1a*$^{iq261/iq261}$, *hrg1b*$^{iq361/iq361}$ or *hrg1a*$^{iq261/iq261}$*;* *hrg1b*$^{iq361/iq361}$ mutants (**Fig. 3.19**) (Two-way ANOVA, $p>0.05$).

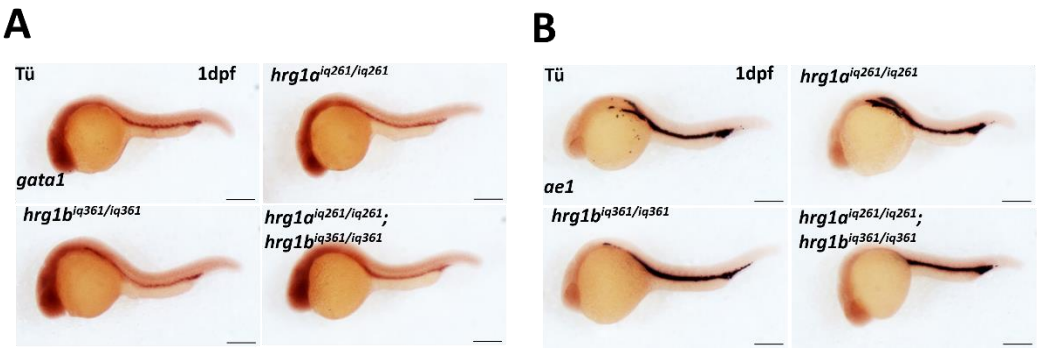

Figure 3.15 Expression of *ae1* and *gata1* in *hrg1a*$^{iq261/iq261}$, *hrg1b*$^{iq361/iq361}$ and *hrg1a*$^{iq261/iq261}$; *hrg1b*$^{iq361/iq361}$ mutants

Lateral view of *ae1* and *gata1* expression by WISH at 1 dpf embryos from WT, *hrg1a*$^{iq261/iq261}$, *hrg1b*$^{iq361/iq361}$ and *hrg1a*$^{iq261/iq261}$; *hrg1b*$^{iq361/iq361}$. Anterior is to the left. N=50 for each genotype. Scale bar: 200 µm.

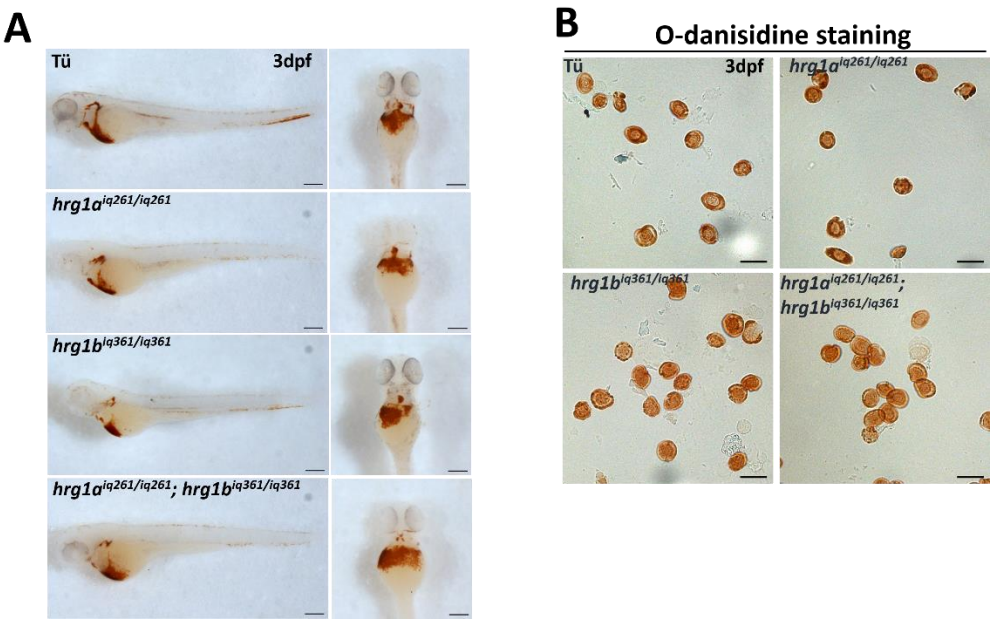

Figure 3.16 No defects in RBC hemoglobinization in *hrg1a*$^{iq261/iq261}$, *hrg1b*$^{iq361/iq361}$ and *hrg1a*$^{iq261/iq261}$; *hrg1b*$^{iq361/iq361}$ mutants

A). *O*-dianisidine staining of RBCs in 3 dpf embryos from WT, *hrg1a*$^{iq261/iq261}$, *hrg1b*$^{iq361/iq361}$ and *hrg1a*$^{iq261/iq261}$; *hrg1b*$^{iq361/iq361}$ (n=50 for each genotype). Scale bar: 200 μm.

B). *O*-dianisidine staining of isolated RBCs from peripheral blood of 3 dpf embryos. Scale bar: 20 μm.

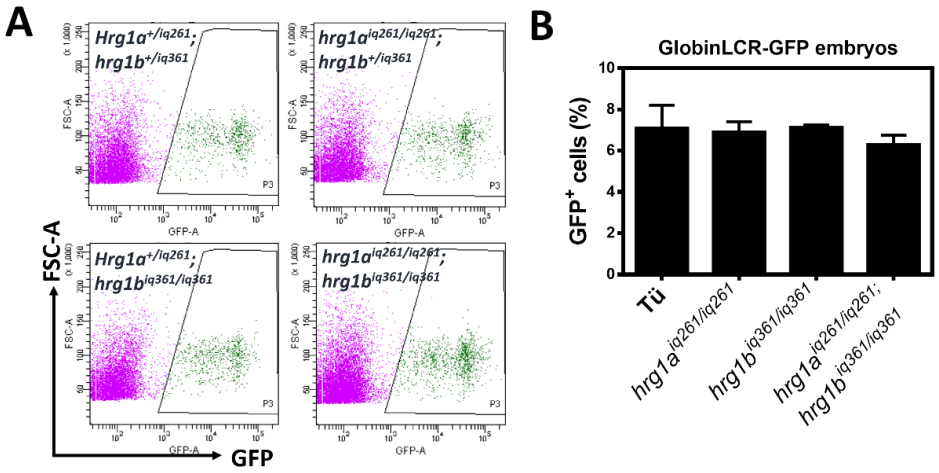

Figure 3.17 Quantification of GFP+ cells of *hrg1a*$^{iq261/iq261}$, *hrg1b*$^{iq361/iq361}$ and *hrg1a*$^{iq261/iq261}$; *hrg1b*$^{iq361/iq361}$ in globinLCR: GFP transgenic background

A). Representative FACS analysis to show percentages of GFP^{+} cells in globinLCR: GFP embryos.

B). Quantitative percentages of GFP^{+} cells in WT, *hrg1a*$^{iq261/iq261}$, *hrg1b*$^{iq361/iq361}$ and *hrg1a*$^{iq261/iq261}$; *hrg1b*$^{iq361/iq361}$ mutants in globinLCR: GFP transgenic background. GlobinLCR: GFP; *hrg1a*$^{+/iq261}$; *hrg1b*$^{+/iq361}$ were crossed with *hrg1a*$^{iq261/iq261}$; *hrg1b*$^{iq361/iq361}$ to produce progenies with *hrg1a*$^{+/iq261}$; *hrg1b*$^{+/iq361}$, *hrg1a*$^{iq261/iq261}$; *hrg1b*$^{+/iq361}$, *hrg1a*$^{+/iq261}$*hrg1b*$^{iq361/iq361}$ and *hrg1a*$^{iq261/iq261}$; *hrg1b*$^{iq361/iq361}$ in globinLCR: GFP transgenic background. Progenies were genotyped at 3 dpf by tail-clip. Thirty embryos of each genotype were pooled and disaggregated to single cell suspension for FACS analysis. Error bars indicate SEM of 3 independent experiments (two-way ANOVA, p >0.05).

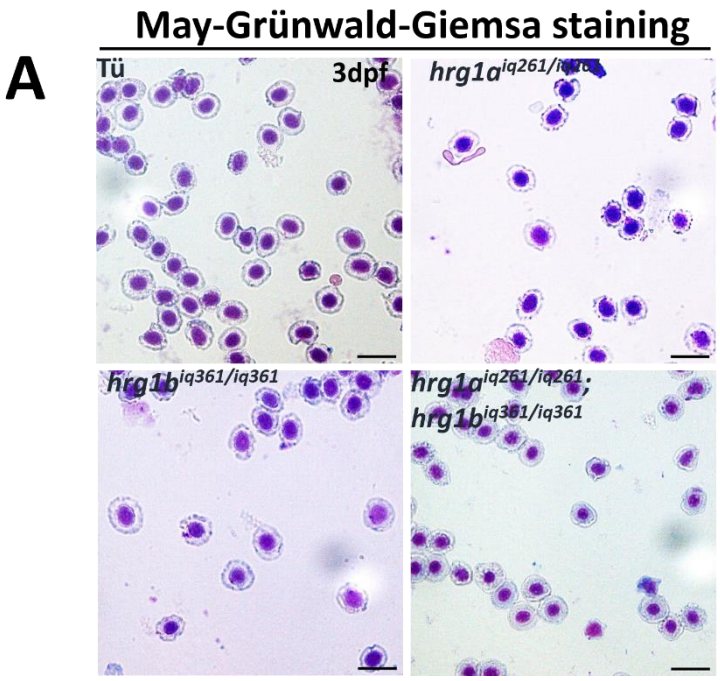

Figure 3.18 Morphology of RBCs from 3 dpf embryos of *hrg1a*$^{iq261/iq261}$, *hrg1b*$^{iq361/iq361}$ and *hrg1a*$^{iq261/iq261}$; *hrg1b*$^{iq361/iq361}$

A). May-Grünwald-Giemsa staining of isolated peripheral RBCs at 3 dpf embryos from WT, *hrg1a*$^{iq261/iq261}$, *hrg1b*$^{iq361/iq361}$ and *hrg1a*$^{iq261/iq261}$; *hrg1b*$^{iq361/iq361}$. Circulated RBCs were isolated by cleaving the vein around CHT and collected in PBS. N=30. Scale bar: 20 µm.

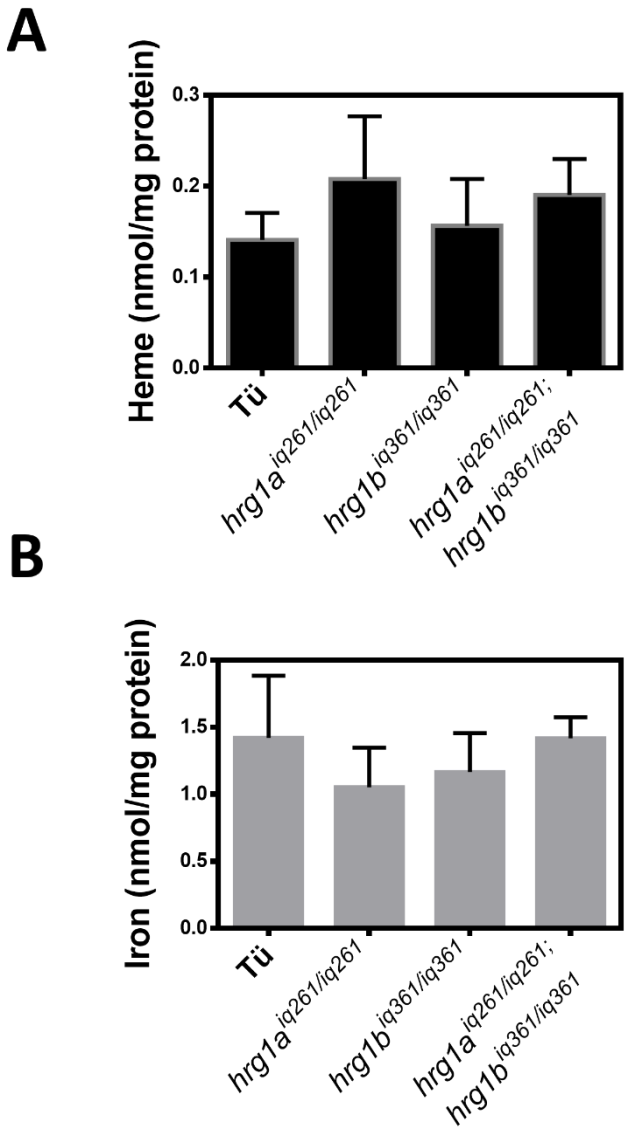

Figure 3.19 ICP-MS of 3 dpf embryos from WT, *hrg1a*$^{iq261/iq261}$, *hrg1b*$^{iq361/iq361}$ and *hrg1a*$^{iq261/iq261}$*; hrg1b*$^{iq361/iq361}$

Around sixty embryos were pooled and flash-frozen for ICP-MS analysis. Error bars indicate SEM of 3 independent experiments (two-way ANOVA, $p>0.05$).

Knockdown of *hrg1b* in *hrg1a* mutant embryos or *vice versa* depletes Hrg1 protein but lacks anemic phenotypes

One explanation for the discrepancy between morpholino knockdown and gene knockout is that morpholinos have an acute effect, while effects in gene knockout mutants are chronic and long-lasting permitting genetic compensation to occur. We therefore knocked down *hrg1b* in the *hrg1a* mutant background and *vice versa*. *Hrg1a*$^{iq210/iq210}$ has a 10nt deletion in exon 2 after ATG translation start codon causing a +1 frameshift in the ORF. Although *hrg1a*^{iq210} may utilize an alternative downstream ATG *in silico*, the predicted truncated protein with loss of 34aa in N-terminus is not functional based our yeast growth assay (**Fig. 3.13**). Knockdown of *hrg1b* by translation-blocking *Hrg1b_ATG_MO* or splice-blocking *Hrg1b_E2I2_MO* in *hrg1a*$^{iq210/iq210}$ did not show any significant anemic phenotype (**Fig. 3.20A**). RT-PCR revealed that *hrg1b* mRNA was decreased by *Hrg1b_E2I2_MO* in both WT and *hrg1a*$^{iq210/iq210}$ mutants(**Fig. 3.20B**). Since *hrg1a* and *hrg1b* gene sequences have relatively high similarity, we also checked whether knockdown of *hrg1b* altered the expression of *hrg1a*. Knockdown of *hrg1b* by *Hrg1b_E2I2_MO* did not affect *hrg1a* mRNA expression (**Fig. 3.20B**). In *hrg1a*$^{iq210/iq210}$ embryos, knockdown of *hrg1b* by either *Hrg1b_ATG_MO* or *Hrg1b_E2I2_MO* showed little or no detectable Hrg1 proteins (**Fig. 3.20A, 3.20C)**. These results show that knockdown of *hrg1b* in the *hrg1a* mutants does not cause anemia in early zebrafish embryos.

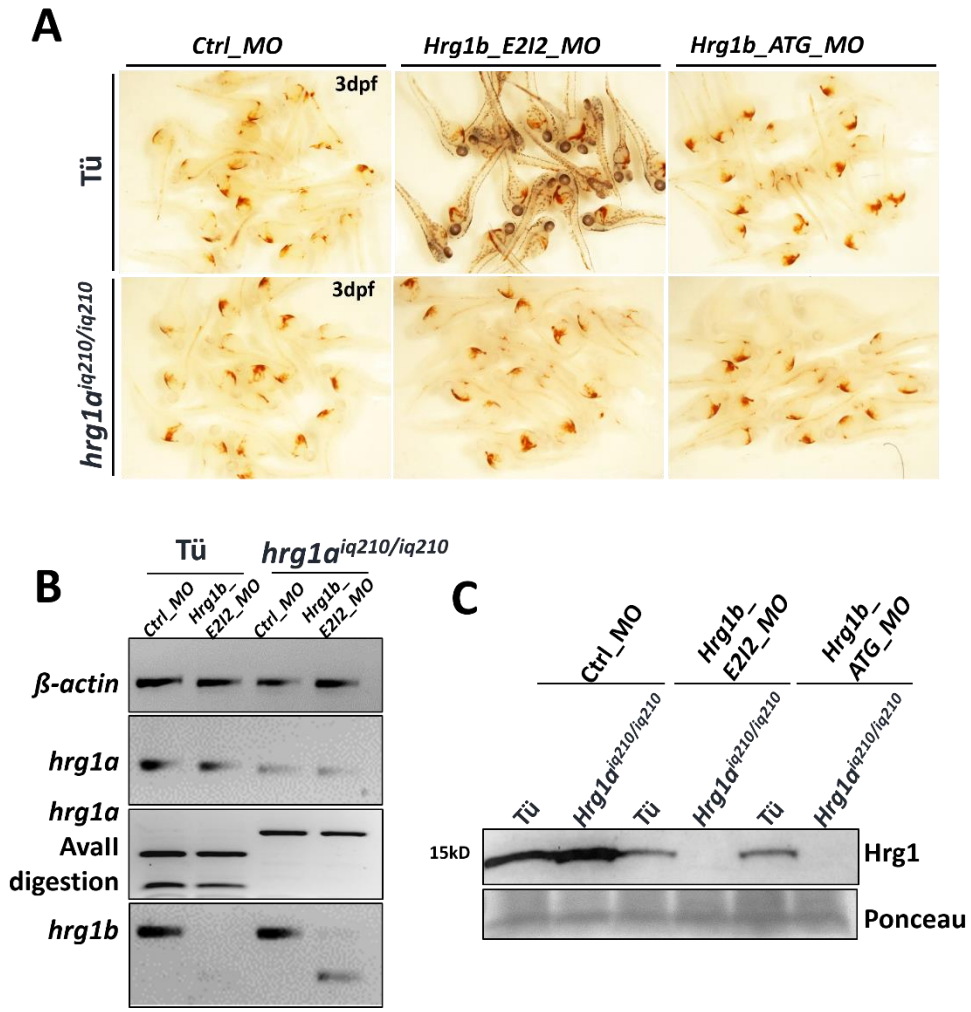

Figure 3.20 Knockdown of *hrg1b* in *hrg1a*$^{iq210/iq210}$ causes loss of Hrg1 protein without anemic phenotypes

A). *O*-dianisidiane staining of embryos injected with indicated morpholinos.

B). RT-PCR on morphants from *control_MO* and *Hrg1b_E2I2_MO*. *Hrg1a*^{iq210} mutant allele has a 10 nt deletion causing loss of AvaII restriction sites. PCR product from *hrg1a*$^{iq21/iq210\ 0}$ has a slightly smaller size and cannot be digested by AvaII. *Hrg1b* mRNA is tremendously decreased by *Hrg1b_E2I2_MO* morpholino knockdown.

C). Immunoblotting of Hrg1 proteins in membrane fraction of embryos injected with indicated morpholinos in WT or *hrg1a*$^{iq210/iq210}$ mutants.

It is important to note that the *hrg1a* morpholino binding site is still intact in the TALEN induced *hrg1a*^{iq210} mutant. We therefore injected *Hrg1a_I2E3_MO2* into *hrg1a*$^{iq210/iq210}$ mutant embryos to check whether the phenotypes brought by *Hrg1a_I2E3_MO2* injection still persists. Knockdown of *hrg1a* by *Hrg1a_I2E3_MO2* resulted in profound anemia together with morphological defects, even though *hrg1a*$^{iq210/iq210}$ mutants do not show detectable Hrg1a protein (**Fig. 3.21A**). RT-PCR revealed that a small percentage of *hrg1a* mRNA expression was mis-spliced in the *Hrg1a_I2E3_MO2* injected morphants (**Fig. 3.21B**).

We next knocked down *hrg1a* by injecting *Hrg1a_ATG_MO*, *Hrg1a_E2I2_MO1*, or *Hrg1a_I2E3_MO2* morpholinos into either WT or *hrg1b*$^{iq361/iq361}$ mutant background. Injection of *Hrg1a_ATG_MO* and *Hrg1a_E2I2_MO1* to either WT or *hrg1b*$^{iq361/iq361}$ mutant did not result in severe anemia, but injection of *Hrg1a_I2E3_MO2* morpholino knockdown again caused developmental defects with anemic phenotypes (**Fig. 3.22A and B**). If *hrg1a* morpholinos can efficiently decrease *hrg1a* expression, we should not detect Hrg1 protein in the *hrg1b*$^{iq361/iq361}$ mutant background. Injection of all these morpholino significantly reduced Hrg1 protein levels in the *hrg1b*$^{iq361/iq361}$ mutant. These results suggest that *Hrg1a_I2E3_MO2* effects may be independent of depleting Hrg1 protein levels.

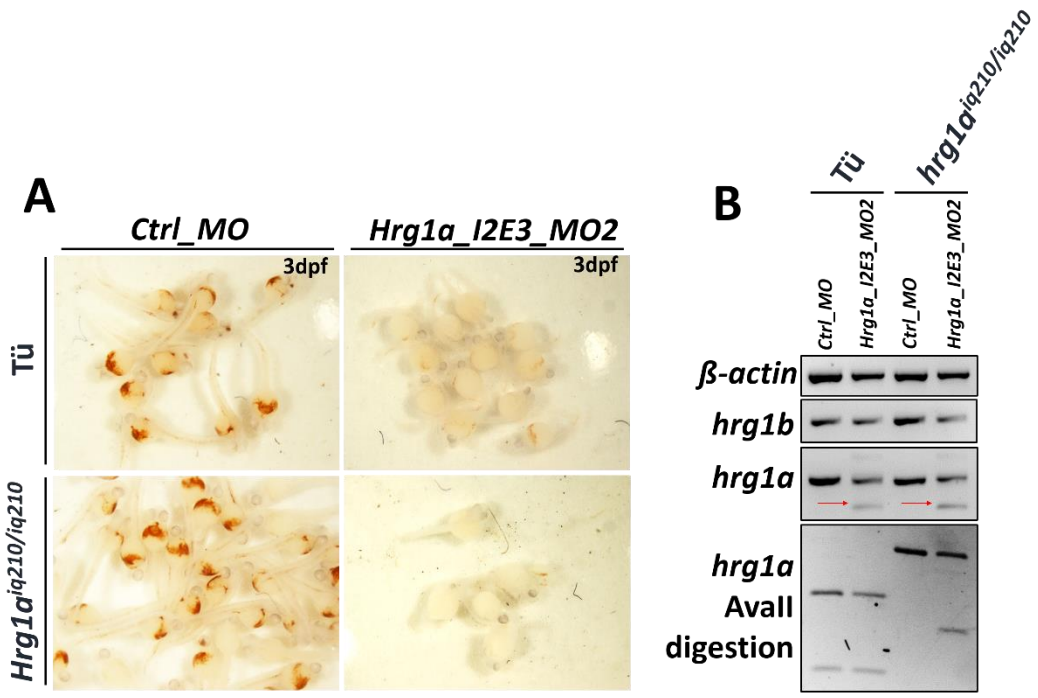

Figure 3.21 Morpholino knockdown of *hrg1a* by *Hrg1a_I2E3_MO2* in *hrg1a*$^{iq210/iq210}$ still causes profound anemia

A). Injection of *Hrg1a_I2E3_MO2* causes anemic phenotypes in both WT and *Hrg1a*$^{iq210/iq210}$ mutant embryos.

B). RT-PCR of *hrg1a* and *hrg1b* in *Hrg1a_I2E3_MO2* morphants. *Hrg1a* is only partially affected by *Hrg1a_I2E3_MO2* in both WT and *Hrg1a*$^{iq210/iq210}$ mutants, as the mis-spliced mRNA shown by red arrows. AvaII digestion is shown as RFLP genotyping of WT and *Hrg1a*^{iq210} mutant embryos and PCR product from *Hrg1a*^{iq210} cannot be digested by AvaII. *Hrg1b* is not changed by *Hrg1a* knockdown. ß-actin is a house-keeping gene control.

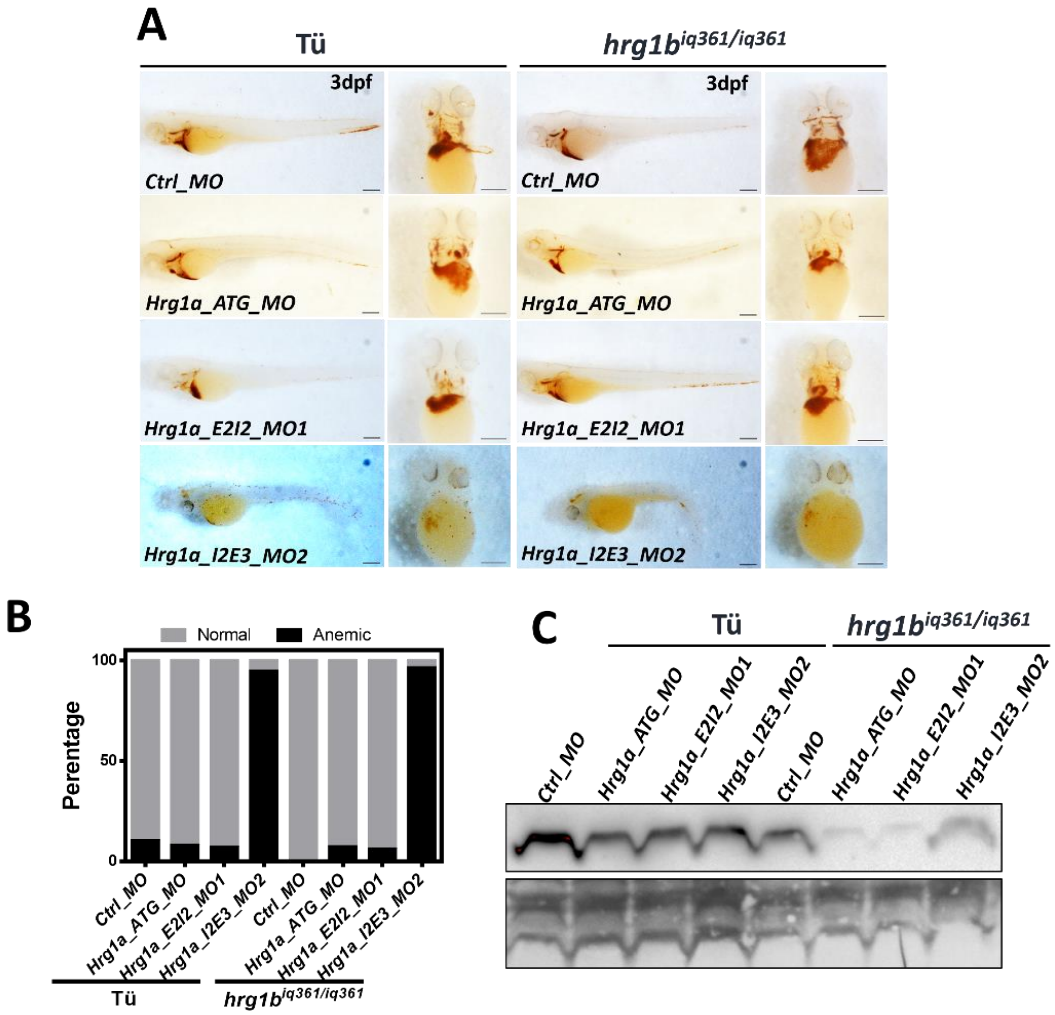

Figure 3.22 Knockdown *hrg1a* by *Hrg1a_I2E3_MO2* results in anemia without depleting Hrg1 protein

A). *O*-dianisidine staining of 3 dpf embryos after injection indicated morpholinos at one-cell stage in WT and *hrg1b*$^{iq361/iq361}$ mutant. Scale bar: 200 µm.

B). Quantification of anemic embryos shown as a percentage of overall injected embryos.

C). Immunoblotting of Hrg1 protein from membrane fractionation lysates of 3 dpf morphants with injection of indicated morpholinos. Each lane represented 100 µg protein lysates. Ponceau is used as loading control.

P53 inhibition does not ameliorate *Hrg1a_I2E3_MO2* morphants

One possible explanation for the discrepancies in phenotypes between morpholinos and deletion mutants is *p53* upregulation due to morpholino injections (163). Consequently, knockdown of *p53* by morpholino alleviates off target effects without affecting phenotypes associated with gene-specific morpholino knockdown. To test whether the phenotypes of *Hrg1a_I2E3_MO2* morphants are ascribed to *p53* activation, we co-injected *Hrg1a_I2E3_MO2* and *p53_MO* into one-cell stage zebrafish embryos and evaluated the hemoglobinization of 3 dpf embryos. Injection of *p53_MO* did not ameliorate the anemic phenotypes of *Hrg1a_I2E3_MO2* morphants (**Fig. 3.23A and B**).

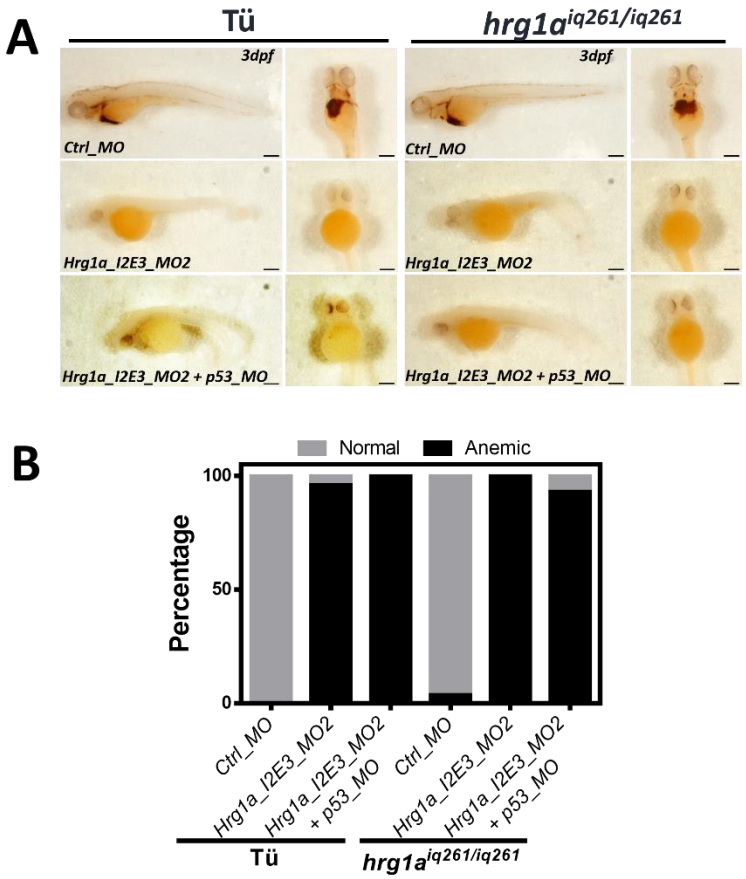

Figure 3.23 Co-injection of *Hrg1a_I2E3_MO2* and *p53_MO* does not ameliorate the phenotypes in *Hrg1a_I2E3_MO2* morphants

A). *O*-dianisidine staining of 3 dpf embryos after injection of indicated morpholinos at one-cell stage in t WT and *hrg1a*$^{iq261/iq261}$ mutant. Scale bar: 200 µm.

B). Quantification of anemic embryos shown as percentages of injected embryos.

Inhibiting heme synthesis in zebrafish embryos results in anemia but cannot be rescued by heme supplementation

Zebrafish, like most metazoans, synthesis the heme through a highly conserved eight-step biosynthetic pathway. The majority of heme in zebrafish embryos comes from endogenous heme synthesis. Thus, zebrafish embryos may not require a heme importer such as Hrg1 to maintain heme levels. However, given that single-cell embryos contain *hrg1a* and *hrg1b* mRNA and that *hrg1a* is highly expressed in the ovaries, we decided to establish a condition for heme synthesis deficiency in the embryos to tease out a potential role for Hrg1 in the absence of heme synthesis. Therefore, we inhibited mitochondrial heme synthesis by supplementing the embryos medium with SA which inhibits heme biosynthesis by binding to ALAD, the second enzyme of the heme synthesis pathway (164) (165). Incubation of zebrafish embryos in embryo medium buffered to pH 7.4 with 2 mM SA did not cause any significant defects in RBC hemoglobinization of 3 dpf WT embryos. However, when the pH of embryo medium was allowed to drop to around 3.5, 2 mM SA caused severe anemia in comparison to embryos without SA (**Fig. 3.24A**). Removal of low pH embryo medium with 2 mM SA and addition of buffered embryo medium with 2 mM SA (pH 7.4) recovered the hemoglobinization after 24 hr (**Fig. 3.24B**). The anemia in zebrafish embryos in the acidic embryonic medium with 2 mM SA could not be rescued by supplementation of exogenous heme, as heme precipitates in acidic condition.

Since the effects of SA on heme synthesis of zebrafish embryos seems to be a pH-dependent phenomenon, we sought to genetically block endogenous heme synthesis by inhibiting ALAS, the rate-limited enzyme responsible for ALA synthesis. In mammals, two enzymes exist for ALAS: ALAS1 is ubiquitously expressed and ALAS2 is erythroid-specific. Zebrafish *alas2* was identified by positional cloning of the mutant *sauternes* (*sau*) from a large-scale mutagenesis screen (121). We used morpholino to knockdown *alas2* in zebrafish

embryos by injecting *Alas2_MO* into one-cell embryos from WT and *hrg1a*$^{iq261/iq261}$*; hrg1b*$^{iq361/iq361}$ double mutants. As expected, *Alas2_MO* caused severe hemoglobinization defects as assessed by *o*-dianisidine staining of 3 dpf embryos (**Fig. 3.25**). Surprisingly, supplementation of ALA or PBG, the product of ALAS2 in the embryo medium failed to rescue the *alas2* knockdown. Additionally, supplementation of 10 μM heme in the embryo medium also did not rescue the anemic phenotypes in *Alas2_MO* morphants in both WT and *hrg1a*$^{iq261/iq261}$*; hrg1b*$^{iq361/iq361}$ double mutants (**Fig. 3.25**). Together, these results show that neither exogenous ALA, PBG or heme rescued heme synthesis defects in zebrafish embryos causing by acidic SA treatment.

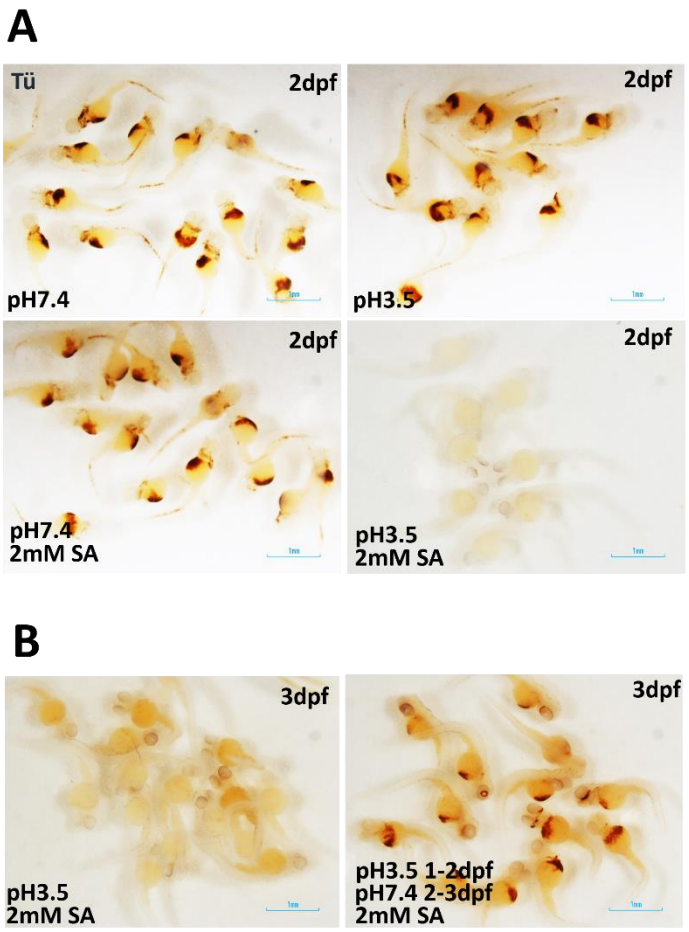

Figure 3.24 SA causes anemia in zebrafish embryos in acidic condition

A). *O*-dianisidine staining of 2 dpf embryos incubated in 2 mM SA for 24 hr in buffered (pH7.4) and acidic (pH 3.5) conditions. Scale bar: 200 µm.

B). *O*-dainisidine staining of 3dpf embryos in normal and acidic conditions with 2 mM SA. Scale bar: 200 µm.

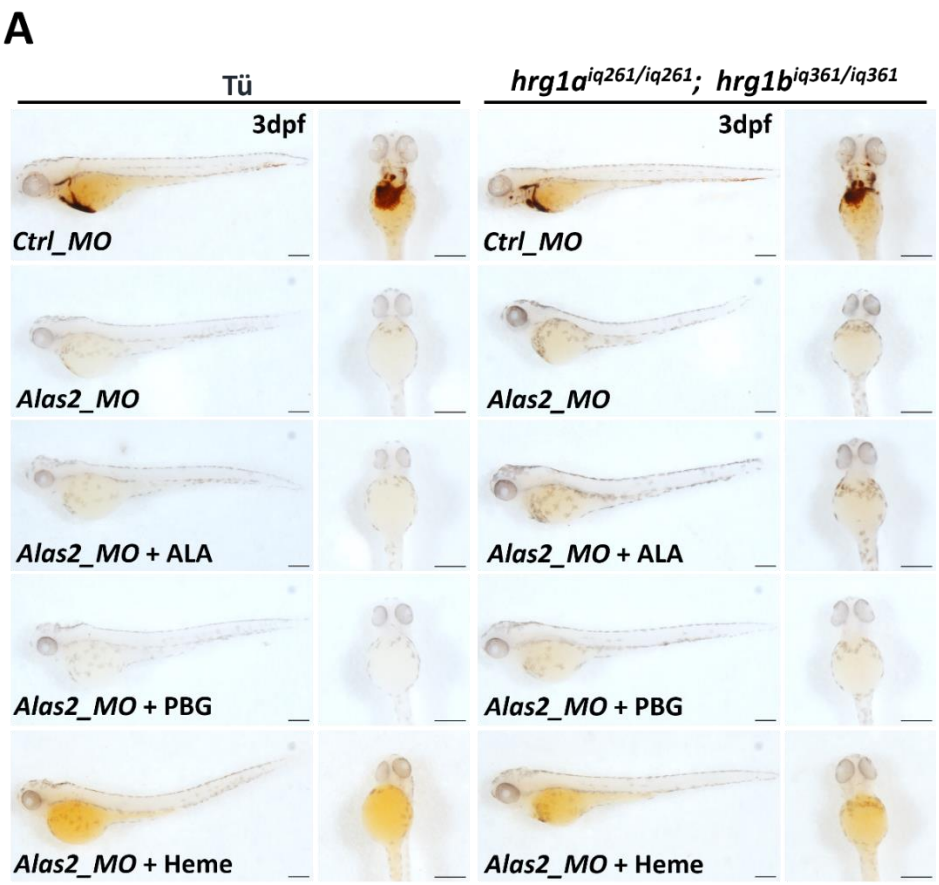

Figure 3.25 Morpholino knockdown of *alas2* causes anemia and cannot be rescued by supplementation of heme or its biosynthetic intermediates

A). *O*-dianisidine staining of 3 dpf zebrafish embryos from both WT and *hrg1a*$^{iq261/iq261}$; *hrg1b*$^{iq361/iq361}$ mutants. Scale Bar: 200 µm.

Discussion

In this chapter, we characterized two *hrg1* homologs in zebrafish. Hrg1a and Hrg1b are ubiquitously expressed throughout developing embryos with high expression levels in nervous system. Both *hrg1a* and *hrg1b* mRNA can be detected in the one-cell stage embryos, and *hrg1a* is highly expressed in the ovary, suggesting that *hrg1* may transport maternal heme to the developing oocytes to support early embryogenesis before zygotic heme synthesis is turned on. This is possible since zebrafish *fpn1* mutant embryos *weissherbst* (*weh*) have defects in utilizing maternal iron (134). However, progenies from *hrg1a*$^{iq261/iq261}$, *hrg1b*$^{iq361/iq361}$ or *hrg1a*$^{iq261/iq261}$; *hrg1b*$^{iq361/iq361}$ intercrosses have no obvious anemia and survive through adulthood without functional Hrg1. Although the zebrafish genome is almost fully sequenced, functional annotation is still ongoing and at least 26% of all genes are duplicated due to genome duplication, a process called ohnologues (116). It is possible that Hrg1 may not be the sole pathway for maternal heme delivery to embryos and other genes might compensate for the loss of Hrg1 function in early embryos. Previous studies in *C.elegans* have shown that a small peptide HRG-3 is secreted and functions as a heme chaperone for maternal heme delivery to the embryos (166). Similar mechanisms may exist to support early embryogenesis in zebrafish. Another possibility is that additional Hrg1 ohnologues may exist in as in C. *elegans* which possesses four paralogs, *hrg-1*, *-4*, *-5* and *-6*.

We have previously identified HRG-1 as a membrane-bound permease that can bind and translocate heme across membranes (69). Knockdown of zebrafish *hrg1a* by *Hrg1a_I2E3_MO2* causes severe anemia with failure in maturation of primitive erythroid cells in addition to developmental defects such as hydrocephalus, body axis curvature and shortened yolk tube extension. Our genetic characterizations of *hrg1* mutants reveal that these phenotypes are only specific to the *Hrg1a_I2E3_MO2* based on the following results: a). only a small proportion of *hrg1a* mRNA is perturbed by *Hrg1a_I2E3_MO2* morpholino; b). injection of *Hrg1a_I2E3_MO2* into *hrg1a*$^{iq261/iq261}$ and *hrg1a*$^{iq210/iq210}$ genetic mutants

causes anemia; c) injection of *Hrg1a_ATG_MO* or *Hrg1a_E2I2_MO1* which showed significant reduction in Hrg1 proteins in *hrg1b*$^{iq361/iq361}$ mutants, did not cause anemia or morphological defects. We also ruled-out that the phenotypes in *Hrg1a_I2E3_MO2* morphants are due to *p53* activation by co-injecting *p53_MO* (163). Morpholinos are great tools for transient knockdown in animal models such as zebrafish and chick embryos, however, off-target effects and chemical toxicity of morpholino can complicate interpretation of results from studies using mopholinos (118, 167, 168). Kok *et al* reported that morpholino-induced phenotypes cannot be recapitulated by mutants generated by gene-editing tools (169). They also state that this is consistent with previously published results showing that approximately 80 % of morpholino phenotypes cannot be recapitulated in mutant embryos from large-scale mutagenesis (170). It is possible that compensatory pathways can buffer against deleterious mutations, an effect typically not observed in morpholino knockdown. Indeed, Rossi *et al* showed that *egfl7* mutants do not show any obvious phenotypes compared to morphants because Emilin2 and Emilin3 can compensate for loss of Egfl7 (171). Another study showed that *tmem88a*$^{-/-}$ mutant embryos partially recapitulated but had a much milder phenotype compared to *tmem88a* morphants (172). In our study, we show that phenotypes associated with *hrg1a* knockdown by *Hrg1a_I2E3_MO2* cannot be simply attributed to knockdown of *hrg1a* since other *hrg1a* specific morpholinos and the *hrg1a* mutant embryos do not show the same phenotypes. Short sequence BLAST showed that *Hrg1a_I2E3_MO2* is specific to its targeting site with low homology to other sequences. It is possible that *Hrg1a_I2E3_MO2* produce a mis-spliced mRNA which may perturb other pathways. One way to conclusively address this possibility is to delete the target site of *Hrg1a_I2E3_MO2*. Although we did detect several F0 chimeric founders with entire *hrg1* gene locus deleted, we were unable to successfully obtain F1 mutants with heritable germline transmission even after screening large number of F1 embryos

Since the majority of heme is synthesized endogenously, we tried to inhibit heme synthesis to recapitulate the heme auxotrophy found in *C. elegans*, where Hrg1 was discovered. Although SA is widely used to inhibit heme synthesis in cell culture models, it is not capable of inhibiting heme synthesis in zebrafish embryos in normal embryonic medium unless acidic conditions below pH 4 is used.

We also tried to inhibit erythropoietic heme synthesis by morpholino knockdown of *alas2* in WT and *hrg1a*$^{iq261/iq261}$; *hrg1b*$^{iq361/iq361}$ embryos. However, anemia in *alas2* morphants could not be rescued by either ALA, PBG or heme supplementation, even though ALA has been reported to be capable of rescuing ALAS2 mutant embryos with defects in heme synthesis (122). However, it was also reported that ALA fails to rescue ALAS2 morphants, and high concentration of ALA (1 mM) is toxic to developing embryos (44).

In summary, our results reveal that Hrg1 is dispensable for maturation and hemoglobinization of primitive erythroid cells in zebrafish embryos and genetic studies solely based on morpholinos should be carefully interpreted.

Chapter 4: Hrg1 is involved in heme-iron recycling in adult zebrafish

Summary

In mouse BMDMs, HRG1 localizes to the erythrophagosome membrane and transports heme derived from recycled RBCs into the cytosol. Depletion of HRG1 by siRNA prevents heme-induced upregulation of HMOX1 and FPN1, indicating that HRG1 is upstream from these two genes in the heme-iron recycling pathway. To study the function of Hrg1 in a vertebrate animal model, we generated *hrg1a*$^{iq261/iq261}$; *hrg1b*$^{iq361/iq361}$ mutant zebrafish by CRISPR/cas9 gene editing. Although *hrg1* mutants are apparently normal in definitive erythropoiesis, whole transcriptome sequencing of RNA extracted from the adult spleen and kidney revealed large numbers of genes involved in macrophages homeostasis, immune response, lipid transport, oxidation-reduction process, and hypoxia are aberrantly expressed in the *hrg1* mutants. PHZ induces acute hemolysis in zebrafish with accumulation of iron in the spleen and kidney as assessed by DAB-enhanced Perl's staining. Both *hrg1a* and *hrg1b* mRNA were upregulated in zebrafish spleen and kidney upon acute hemolysis concomitant with induction of *hmox1* and iron accumulation in the spleen, implying that spleen might be the predominant site for heme-iron recycling in zebrafish. Despite a trend of low *hmox1* level in *hrg1a*$^{iq261/iq261}$; *hrg1b*$^{iq361/iq361}$ double mutants during PHZ-induced hemolysis, the double mutant fish did not show significant reduction in *hmox1* induction. Although iron staining patterns in the spleen from *hrg1* mutants were similar to WT, macrophages from the kidney in *hrg1* mutants showed aberrant accumulation of iron. These studies support a model in which heme iron recycling might be mediated by Hrg1 in zebrafish as observed in mammals.

Results

Gene expression profile in adult *hrg1* mutants revealed by whole transcriptome sequencing

We hypothesized that if Hrg1 is involved in heme-iron recycling in adults, then there might be significant changes in the RNA profile in the RES. We therefore performed RNAseq of RNA from spleens and kidneys of *hrg1a*$^{iq261/iq261}$, *hrg1b*$^{iq361/iq361}$ and *hrg1a*$^{iq261/iq261}$*; hrg1b*$^{iq361/iq361}$. WT fish were crossed to *hrg1a*$^{iq261/iq261}$*; hrg1b*$^{iq361/iq361}$ to generate heterozygote *hrg1a*$^{+/iq261}$*; hrg1b*$^{+/iq361}$ which were used as control. To minimize variations from individual fish, spleens and kidneys from 3 adult zebrafish were dissected and pooled for each biological replicate. Thus, samples from control heterozygotes, *hrg1a*$^{iq261/iq261}$, *hrg1b*$^{iq361/iq361}$ and *hrg1a*$^{iq261/iq261}$; *hrg1b*$^{iq361/iq361}$ were sequenced in three biological replicates. False Discovery Rate (FDR) was determined by Benjamini-Hochberg with a cutoff of 0.05.

hrg1 DKO adult zebrafish had no detectable Hrg1 protein by immunoblotting of brain samples (**Fig. 4.1A**). *O*-dianisidine and May-Grünwals-Giemsa staining revealed no hemoglobinization or morphological defects in circulating RBCs (**Fig. 4.1B and C**).

The RNAseq analyzed 24, 220 genes in the zebrafish genome GRCz10 (173). Overall, we found 355 genes in the spleen and 422 genes in the kidney that were differentially expressed in *hrg1a*$^{iq261/iq261}$; *hrg1b*$^{iq361/iq361}$ double mutants compared to control. We also compared the transcriptomes of *hrg1a*$^{iq261/iq261}$ and *hrg1b*$^{iq361/iq361}$ which showed 77 genes in *hrg1a*$^{iq261/iq261}$, and 617 genes in *hrg1b*$^{iq361/iq361}$ spleen; and 247 genes in *hrg1a*$^{iq261/iq261}$, and 114 genes in *hrg1b*$^{iq361/iq361}$ kidney that were differentially expressed (**Fig. 4.2A**). Clustering of the top 30 mis-regulated genes with the greatest statistical significance in *hrg1a*$^{iq261/iq261}$, *hrg1b*$^{iq361/iq361}$ and *hrg1a*$^{iq261/iq261}$; *hrg1b*$^{iq361/iq361}$ for both spleen and kidney revealed different gene expression patterns of each genotype (**Fig. 4.2B**).

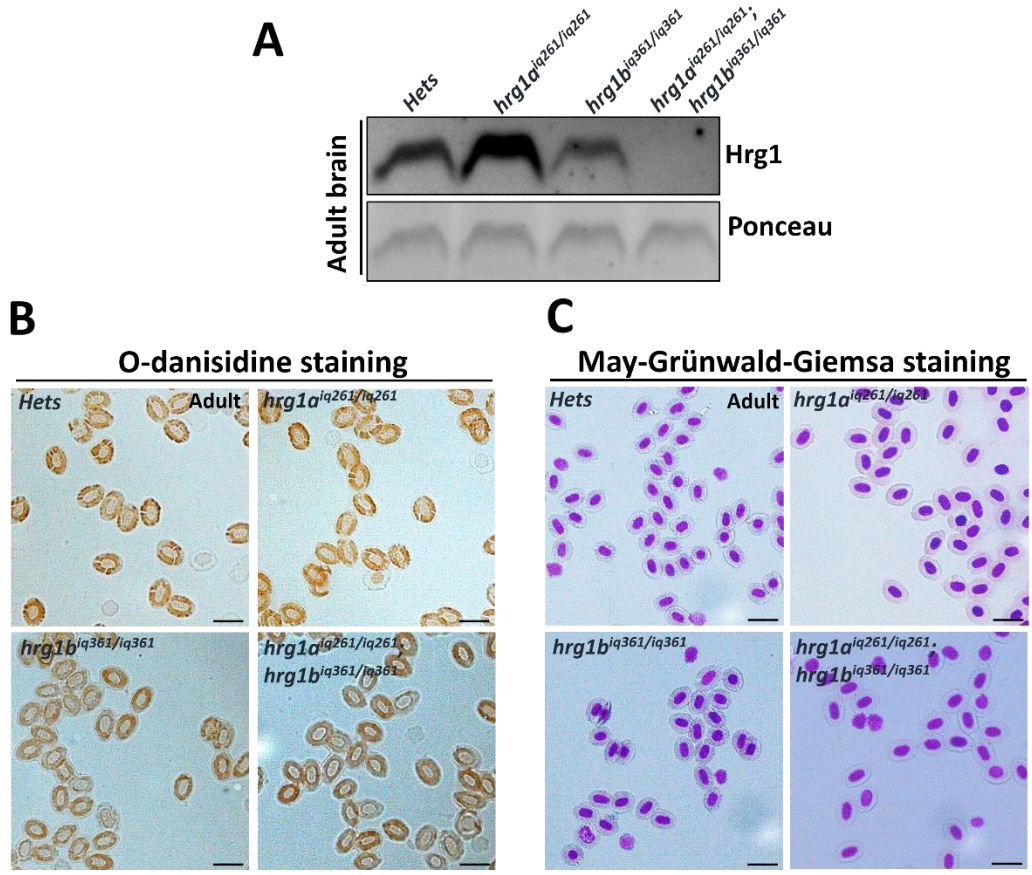

Figure 4.1 Hrg1 proteins are absent in *hrg1* mutants without defects in definitive erythropoiesis

A). Hrg1 immunoblot of membrane fraction lysates from brains of *Hets*, *hrg1a*$^{iq261/iq261}$, *hrg1b*$^{iq361/iq361}$ and *hrg1a*$^{iq261/iq261}$*; hrg1b*$^{iq361/iq361}$. Each lane represented 100 µg protein. Ponceau is used as a loading control.

B). *O*-dianisidine staining of isolated RBCs from adult zebrafish peripheral blood. Scale bar: 20 µm.

C). May-Grünwald-Giemsa staining of isolated peripheral RBCs from adult zebrafish peripheral blood. Scale bar: 20 µm.

A

Spleen	Up	Down	Total
hrg1a$^{iq261/iq261}$	34	43	77
hrg1b$^{iq361/iq361}$	509	108	617
hrg1a$^{iq261/iq261}$; *hrg1b*$^{iq361/iq361}$	217	138	355

Kidney	Up	Down	Total
hrg1a$^{iq261/iq261}$	123	124	247
hrg1b$^{iq361/iq361}$	39	75	114
hrg1a$^{iq261/iq261}$; *hrg1b*$^{iq361/iq361}$	225	197	422

B

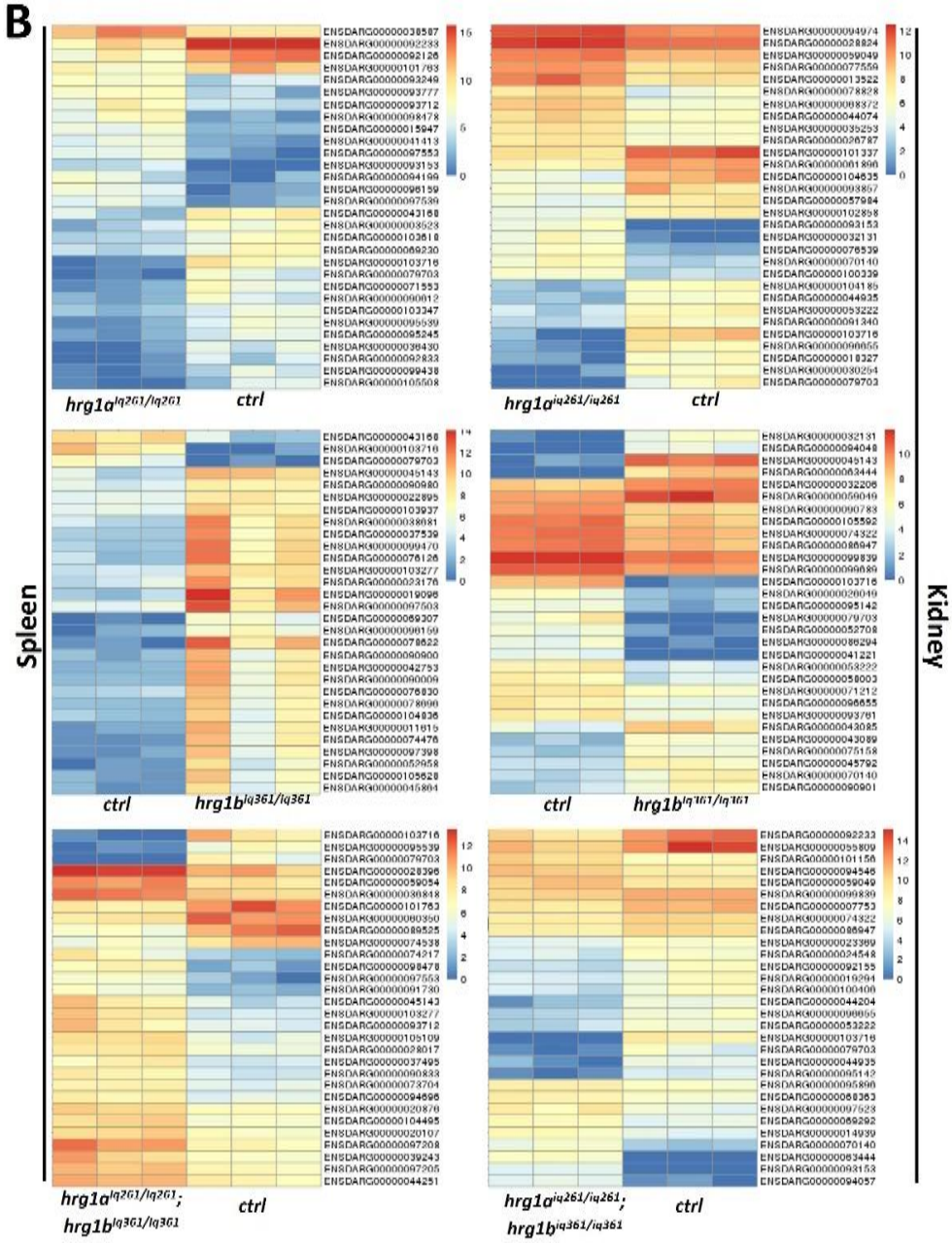

Figure 4.2 Overview of differentially expressed genes revealed by RNAseq

A). The numbers of differentially regulated genes in spleens and kidneys of *hrg1a*$^{iq261/iq261}$, *hrg1b*$^{iq361/iq361}$ and double mutant *hrg1a*$^{iq261/iq261}$*; hrg1b*$^{iq361/iq361}$.

B). The heat-map clustering of top differentially regulated genes in spleens and kidneys of *hrg1a*$^{iq261/iq261}$, *hrg1b*$^{iq361/iq361}$ and *hrg1a*$^{iq261/iq261}$*; hrg1b*$^{iq361/iq361}$. The genes were selected based on the significant levels with lowest p-value.

Detailed examination of RNAseq datasets revealed that expression of 22 genes in spleen and 28 genes in kidney were altered in all three mutants (**Fig. 4.3A**). Only 4 genes were common for the kidney and spleen datasets in all three mutants (**Fig. 4.3B**). Interestingly, among these 4 genes, 2 were downregulated and 2 were upregulated across *hrg1a*$^{iq261/iq261}$, *hrg1b*$^{iq361/iq361}$ and *hrg1a*$^{iq261/iq261}$; *hrg1b*$^{iq361/iq361}$ (**Fig. 4.3C**). ENSDARG00000103716 (annotated as MHC II alpha subunit) is the top gene which was downregulated across all genotypes. In mammals, MHC II is highly expressed in neutrophils as well as macrophages, including red pulp macrophages (RPMs) which are involved in EP (174). In zebrafish, MHC II is expressed in dendritic cells and T cells with phagocytosis and antigen-presentation. However, whether MHC II is expressed on the surface of macrophages in zebrafish is not clear (175, 176). ENSDARG00000079703 is not well annotated in the zebrafish genome. By sequence alignment, ENSDARG00000079703 encodes an E3 ubiquitin-protein ligase TRIM38-like protein, which may be important for proteasome function. The INTERPRO protein domain analyses show that it has a SPla/RYanodine receptor (SPRY) and butyrophylin-like domain, however, its function is unknown. ENSDARG00000090901 encodes a protein which is predicted to be NACHT, LRR and PYD domains-containing protein 12 (NALP12). NALPs are highly expressed in macrophages and implicated in the activation of pro-inflammatory caspases within inflammasomes (177). Lastly, ENSDARG00000093153 transcribes a 651 nt RNA with no known translated protein , as revealed by ENSEMBL database. Considering that Hrg1 is involved in heme-iron recycling by macrophages, the extensive upregulation of NALP12 and downregulation of MHC-II may suggest a defect in macrophage function and heme-iron recycling in adult zebrafish.

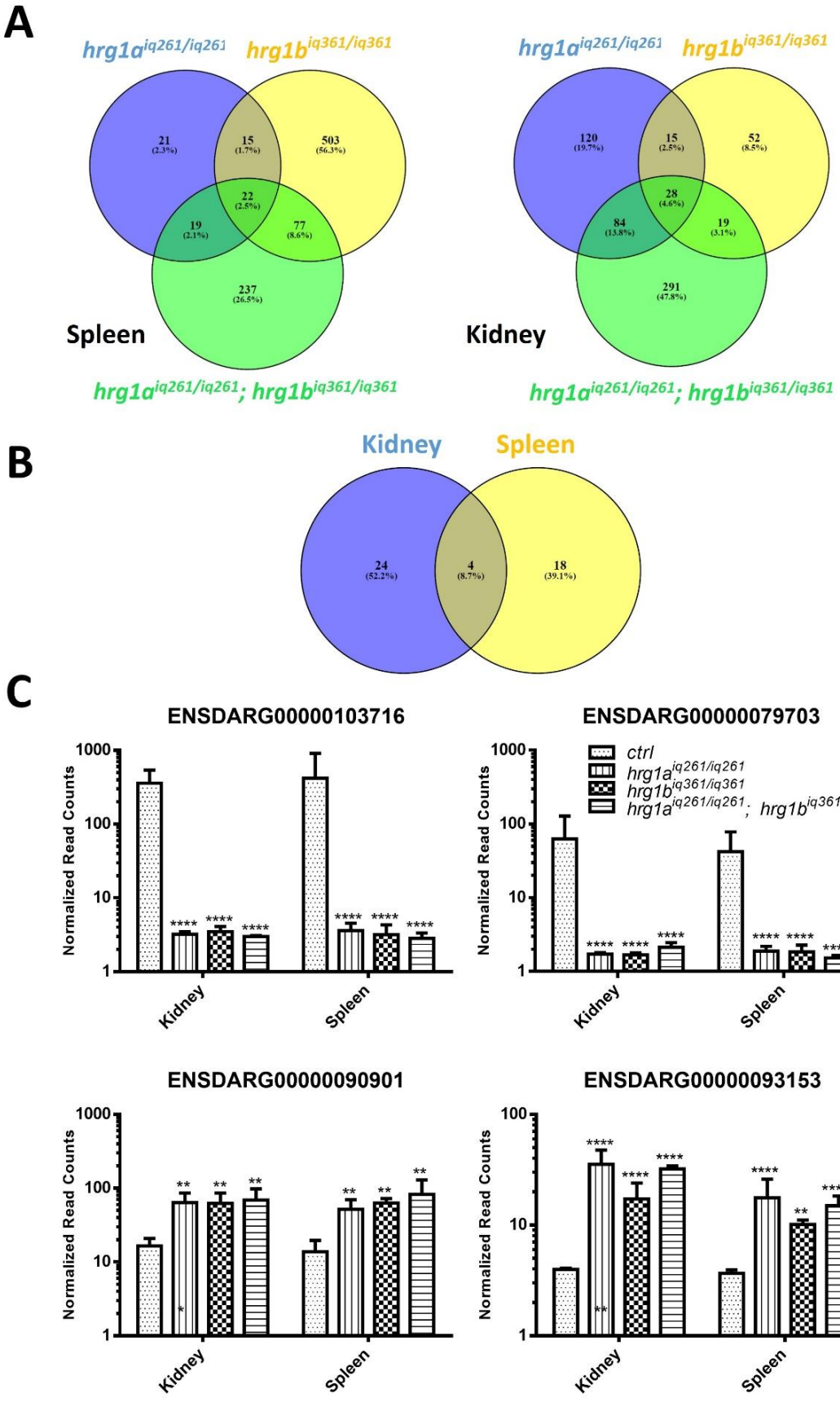
A
hrg1a iq261/iq261
hrg1b iq361/iq361
21 (2.3%)
15 (1.7%)
503 (56.3%)
22 (2.5%)
19 (2.1%)
77 (8.6%)
237 (26.5%)
Spleen
hrg1a iq261/iq261; hrg1b iq361/iq361
hrg1a iq261/iq261
hrg1b iq361/iq361
120 (19.7%)
15 (2.5%)
52 (8.5%)
28 (4.6%)
84 (13.8%)
19 (3.1%)
291 (47.8%)
Kidney
hrg1a iq261/iq261; hrg1b iq361/iq361
B
Kidney
Spleen
24 (52.2%)
4 (8.7%)
18 (39.1%)
C
ENSDARG00000103716
ENSDARG00000079703
ctrl
hrg1a iq261/iq261
hrg1b iq361/iq361
hrg1a iq261/iq261; hrg1b iq361/iq361
Normalized Read Counts
1000
100
10
1
Kidney
Spleen
ENSDARG00000090901
ENSDARG00000093153

Figure 4.3 Common differentially regulated genes in *hrg1* mutants

A). Venn diagram of overlapping differentially regulated genes from *hrg1a*$^{iq261/iq261}$, *hrg1b*$^{iq361/iq361}$ and *hrg1a*$^{iq261/iq261}$; *hrg1b*$^{iq361/iq361}$ mutants. The individual mutants are showed with corresponding colors as in the diagram.

B). Venn diagram of common differentially regulated genes in both spleens and kidneys of *hrg1a*$^{iq261/iq261}$, *hrg1b*$^{iq361/iq361}$ and *hrg1a*$^{iq261/iq261}$; *hrg1b*$^{iq361/iq361}$.

C). Expression level of 4 common differentially regulated genes in spleens and kidneys across control, *hrg1a*$^{iq261/iq261}$, *hrg1b*$^{iq361/iq361}$ and *hrg1a*$^{iq261/iq261}$; *hrg1b*$^{iq361/iq361}$.

Enrichment analysis of biological processes

We next determined the gene ontology (GO) of the differentially regulated genes in spleens and kidneys from *hrg1a*$^{iq261/iq261}$, *hrg1b*$^{iq361/iq361}$ and *hrg1a*$^{iq261/iq261}$; *hrg1b*$^{iq361/iq361}$ mutants. We imported all the differentially regulated genes to DAVID database and analyzed the genes with their assigned GO terms (**Table 4.1**). Interestingly, the GO term "immune response" was the common highly enriched GO term in all six RNAseq datasets. In the kidney datasets for *hrg1a*$^{iq261/iq261}$ and *hrg1a*$^{iq261/iq261}$; *hrg1b*$^{iq361/iq361}$, the GO term "transport activity" was the most common. In terms of *hrg1a*$^{iq261/iq261}$; *hrg1b*$^{iq361/iq361}$ double mutants, the GO terms oxidation-reduction process, proteolysis, and lipid metabolism were the most enriched. For spleen datasets, lipid transport, oxidation-reduction process together with response to hypoxia were highly enriched. Hrg1 is reported to be upregulated as one of hematopoietic targeted genes mediated by NRF2 transcriptional factor during oxidative and hypoxic stresses (178). The enrichment of oxidation-reduction process and response to hypoxia implies that Hrg1 may be involved in response to oxidative and hypoxic stress in zebrafish. If HRG1 is highly expressed in macrophages and transports heme out of erythrophagosome for heme-iron recycling and the lysis of senescent RBCs involves degradation of large amount of proteins and lipids from RBC debris, genes involved in immune response, lipid transport and proteolysis may be aberrantly regulated when *hrg1* function is negatively affected.

We next examined the RNAseq results with KEGG pathways (179). In the kidney, the "metabolic pathways" was the most common term for *hrg1a*$^{iq261/iq261}$ and *hrg1a*$^{iq261/iq261}$; *hrg1b*$^{iq361/iq361}$. We did not retrieve a significant KEGG pathway with the RNAseq results of kidney from *hrg1b*$^{iq361/iq361}$. For the KEGG analysis in regulated genes from spleens, no KEGG pathways was highly enriched (**Table 4.2**).

Table 4. 1 Gene ontology enrichment analysis of differentially regulated genes in spleens and kidneys of *hrg1* mutants

Gene Ontology Term	Number of genes	P Value	Fold Enrichment
Kidney			
Differentially regulated genes in *hrg1a*$^{iq261/iq261}$			
transport	18	2.15E-02	1.79
immune response	15	3.53E-07	5.70
defense response to virus	6	2.36E-05	17.12
neurotransmitter transport	5	1.09E-03	10.91
organelle fission	4	2.37E-05	63.59
gamma-aminobutyric acid transport	4	1.09E-04	40.47
antigen processing and presentation	4	2.11E-02	6.74
chemical synaptic transmission	4	9.04E-02	3.74
amino acid transmembrane transport	3	3.68E-02	9.82
one-carbon metabolic process	3	3.88E-02	9.54
biosynthetic process	3	8.37E-02	6.18
eukocyte migration	2	6.08E-02	31.80
positive regulation of leukocyte chemotaxis	2	6.08E-02	31.80
purine nucleobase metabolic process	2	6.92E-02	27.82
epithelial to mesenchymal transition	2	7.75E-02	24.73
collagen fibril organization	2	9.39E-02	20.23
Differentially regulated genes in *hrg1b*$^{iq361/iq361}$			
immune response	4	7.49E-02	3.99
organelle fission	3	2.29E-04	125.31
defense response to virus	3	7.54E-03	22.49
cell chemotaxis	3	1.13E-02	18.27
inflammatory response	3	8.11E-02	6.22
innate immune response	3	9.52E-02	5.66
neutrophil migration	2	1.67E-02	116.96
Differentially regulated genes in *hrg1a*$^{iq261/iq261}$; *hrg1b*$^{iq361/iq361}$			
transport	30	8.36E-03	1.64
oxidation-reduction process	26	2.39E-05	2.59
immune response	16	9.05E-05	3.35
proteolysis	16	2.59E-02	1.86
lipid transport	13	1.18E-09	11.40
lipid metabolic process	8	3.55E-02	2.58

neurotransmitter transport	6	1.38E-03	7.22
cellular response to estrogen stimulus	5	7.64E-04	11.80
purine nucleobase metabolic process	4	2.23E-04	30.68
lipoprotein metabolic process	4	5.88E-03	10.67
heterophilic cell-cell adhesion via plasma membrane cell adhesion molecules	4	2.19E-02	6.63
gamma-aminobutyric acid transport	3	1.31E-02	16.74
aromatic amino acid family metabolic process	3	1.56E-02	15.34
triglyceride catabolic process	3	1.56E-02	15.34
arachidonic acid metabolic process	3	1.82E-02	14.16
cell recognition	3	7.06E-02	6.82
chemokine-mediated signaling pathway	3	9.47E-02	5.75
negative regulation of macrophage activation	2	3.22E-02	61.37
lipoprotein catabolic process	2	4.79E-02	40.91
complement activation	2	7.86E-02	24.55
response to estradiol	2	7.86E-02	24.55
response to retinoic acid	2	7.86E-02	24.55
regulation of immune response	2	7.86E-02	24.55
hyaluronan metabolic process	2	7.86E-02	24.55
hydrogen ion transmembrane transport	2	9.35E-02	20.46

Spleen

Differentially regulated genes in *hrg1a*$^{iq261/iq261}$			
lipid transport	6	1.47E-07	45.65
immune response	6	1.60E-04	10.91
cellular response to estrogen stimulus	2	4.61E-02	40.97
cell recognition	2	4.78E-02	39.45
heterophilic cell-cell adhesion via plasma membrane cell adhesion molecules	2	6.49E-02	28.79

Differentially regulated genes in *hrg1b*$^{iq361/iq361}$			
transport	38	2.85E-02	1.41
oxidation-reduction process	29	8.95E-04	1.96
immune response	17	1.91E-03	2.42
cell adhesion	13	8.14E-02	1.70
heart development	11	1.11E-02	2.56
heart looping	10	1.38E-03	3.75
cellular response to estrogen stimulus	9	1.07E-07	14.42
heart contraction	9	1.09E-04	6.05
sarcomere organization	8	6.81E-06	10.75

inflammatory response	8	5.30E-02	2.36
skeletal muscle tissue development	7	9.48E-04	6.07
regulation of cell proliferation	7	6.85E-02	2.43
embryonic heart tube development	6	1.78E-03	6.75
antigen processing and presentation	6	2.08E-02	3.79
gluconeogenesis	5	9.42E-04	10.96
myofibril assembly	5	9.42E-03	5.95
hindbrain development	5	2.07E-02	4.73
single organismal cell-cell adhesion	5	2.94E-02	4.25
response to lipopolysaccharide	5	3.14E-02	4.17
striated muscle contraction	4	5.35E-05	41.65
blood coagulation, fibrin clot formation	4	1.31E-04	33.32
cardiac muscle contraction	4	9.92E-03	8.77
skeletal muscle contraction	4	1.15E-02	8.33
regulation of heart contraction	4	2.60E-02	6.17
glycolytic process	4	5.07E-02	4.76
blood coagulation	4	8.79E-02	3.79
protein polymerization	3	1.69E-03	41.65
ventricular cardiac myofibril assembly	3	3.32E-03	31.24
cardiac muscle fiber development	3	5.45E-03	24.99
cardiac myofibril assembly	3	8.04E-03	20.83
positive regulation of leukocyte chemotaxis	3	1.11E-02	17.85
platelet activation	3	2.27E-02	12.50
cardiac muscle tissue development	3	2.73E-02	11.36
multicellular organismal response to stress	3	2.73E-02	11.36
aromatic amino acid family metabolic process	3	3.22E-02	10.41
response to xenobiotic stimulus	3	3.75E-02	9.61
cardiac muscle cell proliferation	3	4.30E-02	8.93
muscle contraction	3	7.48E-02	6.58
oxygen transport	3	7.48E-02	6.58
atrial cardiac myofibril assembly	2	4.73E-02	41.65
fibrinolysis	2	4.73E-02	41.65
tryptophan catabolic process to acetyl-CoA	2	4.73E-02	41.65
bile acid biosynthetic process	2	4.73E-02	41.65
tryptophan catabolic process to kynurenine	2	7.01E-02	27.77
cornea development in camera-type eye	2	7.01E-02	27.77
ventricular cardiac muscle tissue morphogenesis	2	7.01E-02	27.77
cell proliferation in hindbrain	2	9.24E-02	20.83
L-phenylalanine catabolic process	2	9.24E-02	20.83

Differentially regulated genes in *hrg1a*$^{iq261/iq261}$; *hrg1b*$^{iq361/iq361}$			
immune response	8	7.45E-02	2.18
dorsal/ventral pattern formation	7	2.55E-03	5.07
defense response to virus	6	1.17E-04	12.27
response to hypoxia	5	4.26E-03	7.52
response to virus	3	1.66E-02	14.95
insulin receptor signaling pathway	3	2.78E-02	11.39
growth	3	8.12E-02	6.30
positive regulation of pathway-restricted SMAD protein phosphorylation	3	8.87E-02	5.98
SMAD protein signal transduction	3	9.64E-02	5.70
intrinsic apoptotic signaling pathway in response to endoplasmic reticulum stress	2	4.90E-02	39.87
regulation of lipid metabolic process	2	8.41E-02	22.78
organelle fission	2	8.41E-02	22.78

Table 4. 2 Enrichment of KEGG pathways of differentially regulated genes in spleens and kidneys of *hrg1* mutants

KEGG Pathways	Numbers of genes	P Value	Fold Enrichment
Kidney			
Differentially regulated genes in *hrg1a*$^{iq261/iq261}$			
Metabolic pathways	16	1.39E-02	1.81
Cysteine and methionine metabolism	3	3.57E-02	9.75
Differentially regulated genes in *hrg1a*$^{iq261/iq261}$; *hrg1b*$^{iq361/iq361}$			
Metabolic pathways	29	7.51E-05	2.01
Purine metabolism	6	6.10E-02	2.77
Arachidonic acid metabolism	4	1.91E-02	6.87
Steroid hormone biosynthesis	4	7.97E-03	9.48
Cysteine and methionine metabolism	4	1.29E-02	7.97
Ubiquinone and other terpenoid-quinone biosynthesis	3	5.26E-03	26.29
Linoleic acid metabolism	3	2.27E-02	12.52
Tyrosine metabolism	3	5.24E-02	7.97
Phenylalanine metabolism	3	1.34E-02	16.43
Intestinal immune network for IgA production	3	7.37E-02	6.57
Glycine, serine and threonine metabolism	3	9.03E-02	5.84
Spleen			
Differentially regulated genes in *hrg1a*$^{iq261/iq261}$			
Intestinal immune network for IgA production	2	4.34E-02	38.81
Differentially regulated genes in *hrg1b*$^{iq361/iq361}$			
Adrenergic signaling in cardiomyocytes	10	3.08E-02	2.26
Tight junction	9	4.30E-02	2.26
Cardiac muscle contraction	8	5.29E-03	3.71
Glycolysis / Gluconeogenesis	7	5.43E-03	4.27
Insulin resistance	7	7.54E-02	2.34
PPAR signaling pathway	6	1.72E-02	3.93
Biosynthesis of amino acids	6	4.03E-02	3.14
Drug metabolism - other enzymes	5	7.95E-03	6.19
Pentose phosphate pathway	4	3.08E-02	5.75
Steroid hormone biosynthesis	4	4.83E-02	4.82

Phenylalanine metabolism	3	4.81E-02	8.35
Differentially regulated genes in *hrg1a*$^{iq261/iq261}$; *hrg1b*$^{iq361/iq361}$			
Insulin signaling pathway	6	3.12E-02	3.33
TGF-beta signaling pathway	5	1.85E-02	4.81
Insulin resistance	5	4.74E-02	3.58
FoxO signaling pathway	5	9.70E-02	2.80
Phenylalanine metabolism	3	1.14E-02	17.88
Tyrosine metabolism	3	4.49E-02	8.67
ABC transporters	3	5.26E-02	7.94
Intestinal immune network for IgA production	3	6.34E-02	7.15
Phenylalanine, tyrosine and tryptophan biosynthesis	2	6.03E-02	31.78
Ubiquinone and other terpenoid-quinone biosynthesis	2	9.85E-02	19.07

PHZ causes acute hemolysis in zebrafish embryos

Hrg1 localizes to the membrane of erythrophagosomes during heme-iron recycling by EP and mediates heme transport from the erythrophagosome to the cytosol for heme degradation in primary mouse BMDMs (92). Zebrafish Hrg1a and Hrg1b are close homologs to mouse and human HRG1 with ~80% homology and similar topology. Therefore, we postulated that Hrg1 may have a similar role in heme-iron recycling in the reticuloendothelial organs of the zebrafish. PHZ is a strong hemolytic chemical toxicant, causing acute hemolysis in embryonic and adult zebrafish (137, 180).

We first determined the function of Hrg1 in possible heme-iron recycling during definitive erythropoiesis at the larval stage by exposing 4 dpf embryos to PHZ because at this stage definitive erythrocytes appear in the circulation. *O*-dianisidine staining found no overt deficiencies in staining levels among WT, *hrg1a*$^{iq261/iq261}$, *hrg1b*$^{iq361/iq361}$ and *hrg1a*$^{iq261/iq261}$; *hrg1b*$^{iq361/iq361}$. Exposure to PHZ caused depletion of *o*-dianisidine positive RBCs in the circulation (**Fig. 4.4A**). We then removed the PHZ from the embryo medium to assess the recovery of definitive RBCs in the circulation. At 3 days post-PHZ treatment, *o*-dianisidine positive RBCs started to repopulate the circulation; however, no significant differences in the recovery of definitive RBCs were observed among WT, *hrg1a*$^{iq261/iq261}$, *hrg1b*$^{iq361/iq361}$ and *hrg1a*$^{iq261/iq261}$; *hrg1b*$^{iq361/iq361}$ (**Fig. 4.5A**).

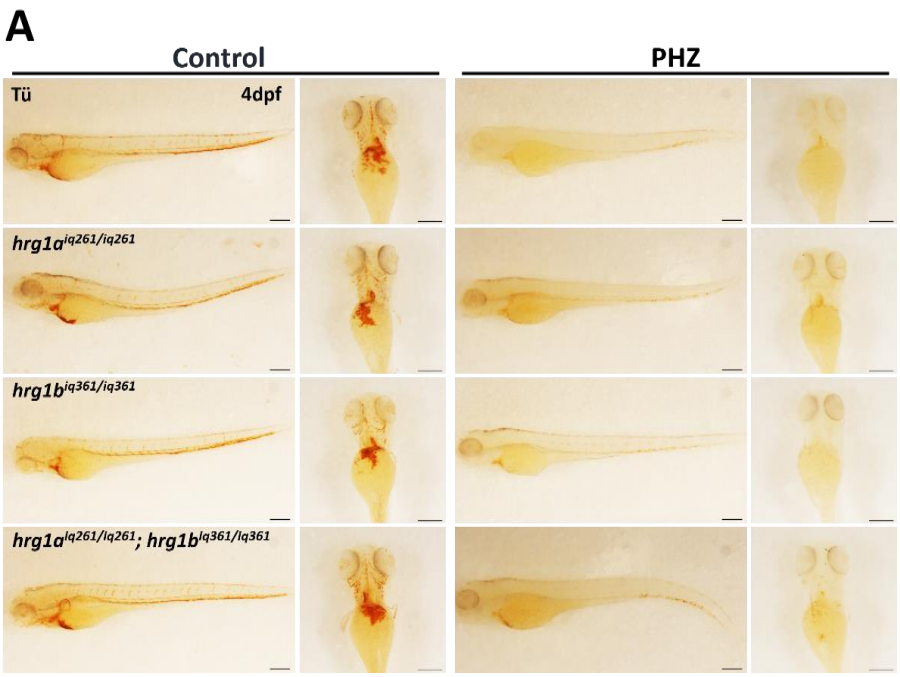

Figure 4.4 PHZ causes depletion of *o*-dianisidine positive RBCs in 4 dpf zebrafish embryos

A). *O*-dianisidine staining of 4 dpf embryos from WT, *hrg1a*$^{iq261/iq261}$, *hrg1b*$^{iq361/iq361}$ and *hrg1a*$^{iq261/iq261}$*; hrg1b*$^{iq361/iq361}$ Scale bar: 200 µm.

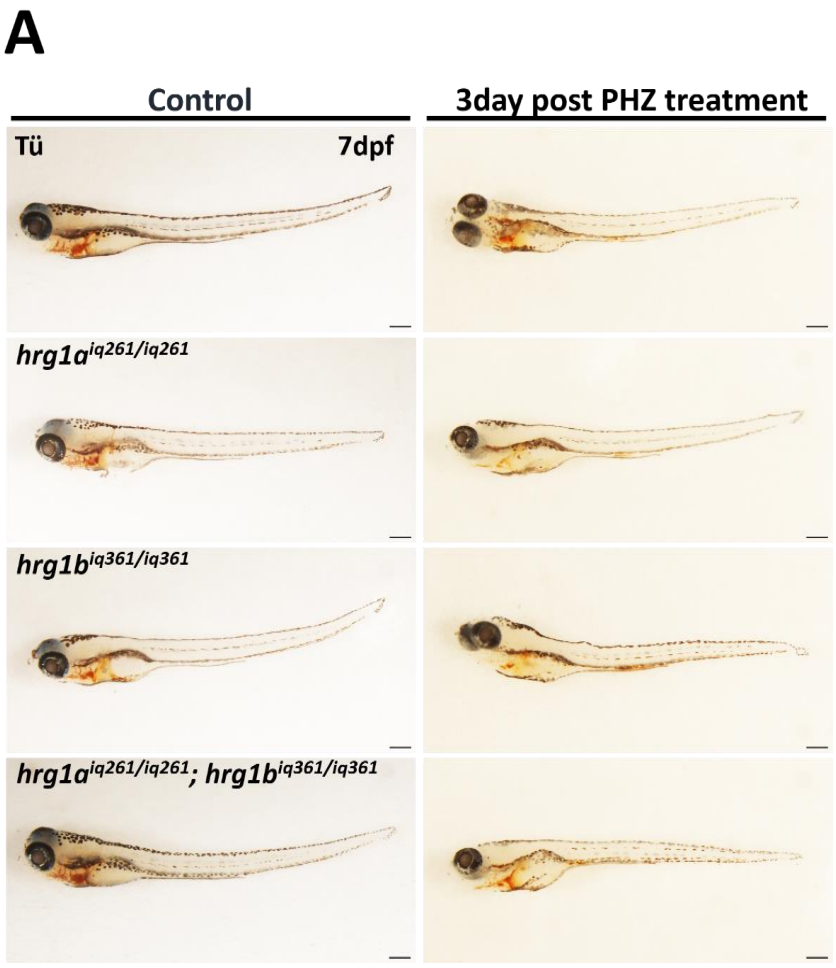

Figure 4.5 Recovery of definitive erythrocytes at 3 days post-PHZ treatment

A). *O*-dianisidine staining of 7 dpf embryos from WT, *hrg1a*$^{iq261/iq261}$, *hrg1b*$^{iq361/iq361}$ and *hrg1a*$^{iq261/iq261}$*; hrg1b*$^{iq361/iq361}$ Scale bar: 200 µm.

Zebrafish *hrg1a* and *hrg1b* are upregulated during acute hemolysis induced by PHZ

To study heme-iron recycling in adult zebrafish, we used PHZ to cause acute hemolysis and induce EP in the adult zebrafish RES. Adult zebrafish (5-6 months) were treated with 2 µg/ml PHZ directly in fish water for 30 min. At 1 day post-PHZ treatment, we isolated spleen, kidney and liver for RNA extraction and qRT-PCR. PHZ-treated zebrafish revealed greatly enlarged spleen with a dark brown color, suggesting active EP to clear the damaged RBCs. The kidney and livers were pale compared to the untreated controls. The gastrointestinal cavity accumulated large amounts of green substances which could be bilirubin, a heme degradation byproduct. qRT-PCR revealed that *hrg1a* and *hrg1b* mRNA expression were upregulated in the kidneys, the major adult hematopoietic tissue, with 2.8 and 3.6-fold, respectively ($p < 0.05$, t-test) (**Fig 4.6A**). While *hrg1a* is 5 times upregulated in the spleen ($p < 0.05$, t-test), expression of *hrg1b* mRNA is not significantly upregulated ($p = 0.4$, t-test) (**Fig 4.6B**). We did not detect any significant changes in *hrg1a* or *hrg1b* expression in the liver (**Fig 4.6C**). As expected, *hmox1* mRNA was greatly upregulated in the kidney, spleen and liver, upon PHZ treatment ($p < 0.05$, t-test) (**Fig 4.6D**), implying that these tissues could play a role in heme breakdown. Comparison of *hmox1* expression levels in the kidney, spleen, and liver reveals that the spleen has the highest expression of *hmox1* ($p < 0.0001$, t-test) (**Fig 4.6D**). Based on the upregulation of *hmox1* and *hrg1*, it is possible that the kidney and spleen may be the most active tissues for RBC degradation in the adult zebrafish.

We next performed DAB-enhanced iron staining on histological sections from PHZ-treated adult zebrafish. Large amount of iron accumulated in the kidney and spleen, with no obvious differences in the liver (**Fig. 4.7A**).

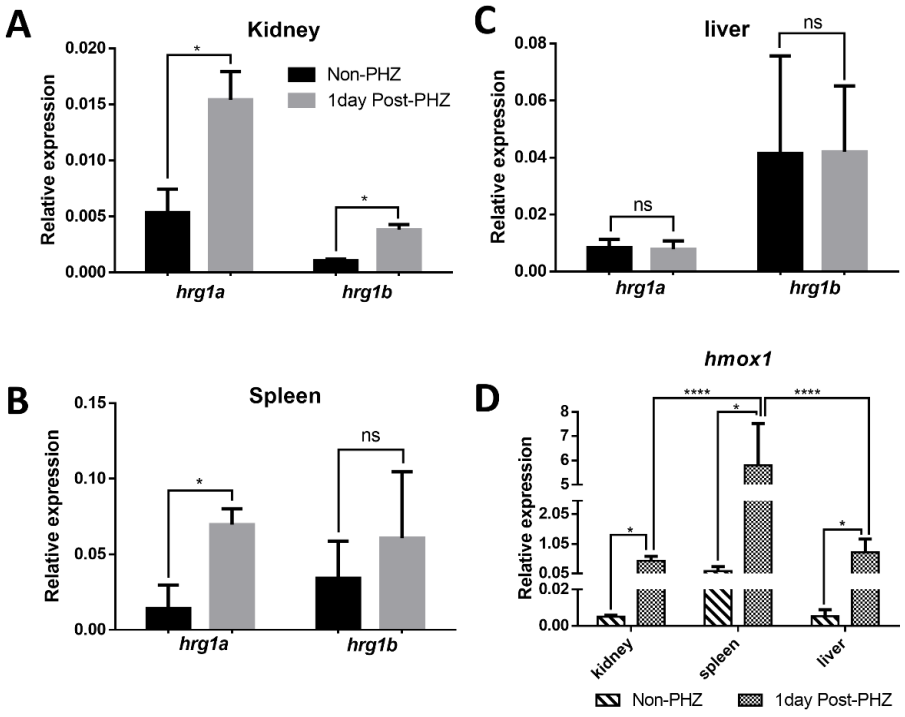

Figure 4.6 *Hrg1* mRNA is upregulated upon acute hemolysis induced by PHZ

A). qRT-PCR of *hrg1a* and *hrg1b* mRNA expression in kidneys from control (non-PHZ treatment) and 1 day post-PHZ treatment adult zebrafish.

B). qRT-PCR of *hrg1a* and *hrg1b* expression in spleens from control (non-PHZ treatment) and 1 day post-PHZ treatment adult zebrafish.

C). qRT-PCR of *hrg1a* and *hrg1b* expression in livers from control (non-PHZ treatment) and 1 day post-PHZ treatment adult zebrafish.

D). Comparison of *hmox1* mRNA level in kidneys, spleens and livers from control (non-PHZ treatment) and 1 day post-PHZ treatment adult zebrafish.

Statistical analysis: Multi-t test. *: p-value < 0.05; **: p-value < 0.01; ****: p-value < 0.0001

Relative expressions are normalized to *ef1a* as reference gene. Each group have 3 biological cohorts, each cohort is pooled from 3 adult zebrafish.

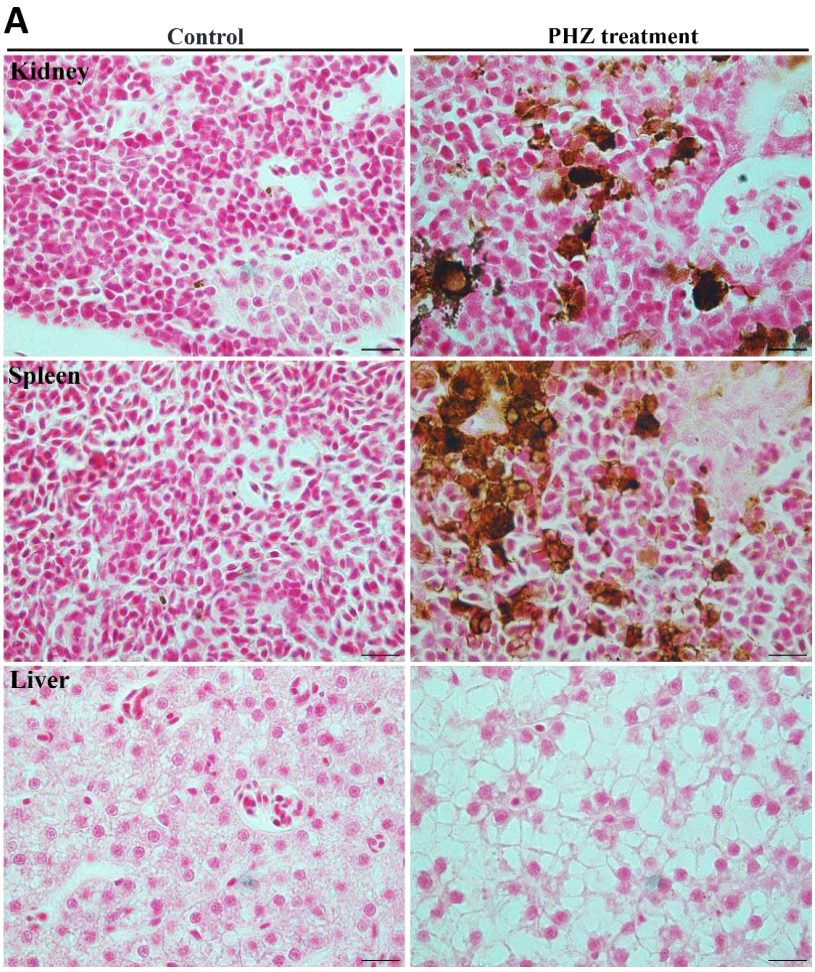

Figure 4.7 Iron is accumulated in kidney and spleen upon PHZ treatment A). DAB-enhanced Perl's iron staining on kidney, spleen, and liver sections. Adult zebrafish were treated with PHZ, then fixed and sectioned 3 days after PHZ treatment. DAB enhanced Perl's staining were showed on sectioned slides with brown staining. Scale Bar: 20 μm.

Delineating heme-iron recycling during hemolysis in *hrg1* mutant zebrafish

Macrophages are predominantly involved in heme-iron recycling during EP and defects in HRG1 causes failure in upregulation of *HMOX1* in mouse BMDMs with accumulation of heme in the erythrophagosome (92). We therefore delineated whether *hrg1a*$^{iq261/iq261}$*; hrg1b*$^{iq361/iq361}$ mutants are defective in heme-iron recycling when challenged with PHZ. qRT-PCR on mRNA from kidneys and spleens of adult zebrafish at 1 day post-PHZ treatment revealed no significant differences in *hmox1* mRNA induction between double heterozygotes (*Hets*), *hrg1a*$^{iq261/iq261}$, *hrg1b*$^{iq361/iq361}$ and *hrg1a*$^{iq261/iq261}$*; hrg1b*$^{iq361/iq361}$ mutants, although there was a trend for *hmox1* mRNA was to be lower in the double mutant (**Fig. 4.8A**). At 3 days post-PHZ treatment, *hmox1* expression is lower in the kidney of *hrg1a*$^{iq261/iq261}$*; hrg1b*$^{iq361/iq36}$ ($p < 0.05$, t-test), but not in the spleen (**Fig. 4.8B**). Histological analysis with DAB-enhanced Perl's staining reveals no obvious differences in iron accumulation in the spleen at 3 days post-PHZ treatment (**Fig. 4.9A**). However, Perl's staining revealed that unlike the WT kidney which showed iron accumulation in both renal tubules and macrophages, the double mutant showed iron staining predominantly localized in renal tubules in the *hrg1a*$^{iq261/iq261}$*; hrg1b*$^{iq361/iq361}$ (**Fig. 4.9B**). This result suggests that in the absence of functional Hrg1, the kidneys are unable to efficiently recycle heme-iron derived from damaged RBCs.

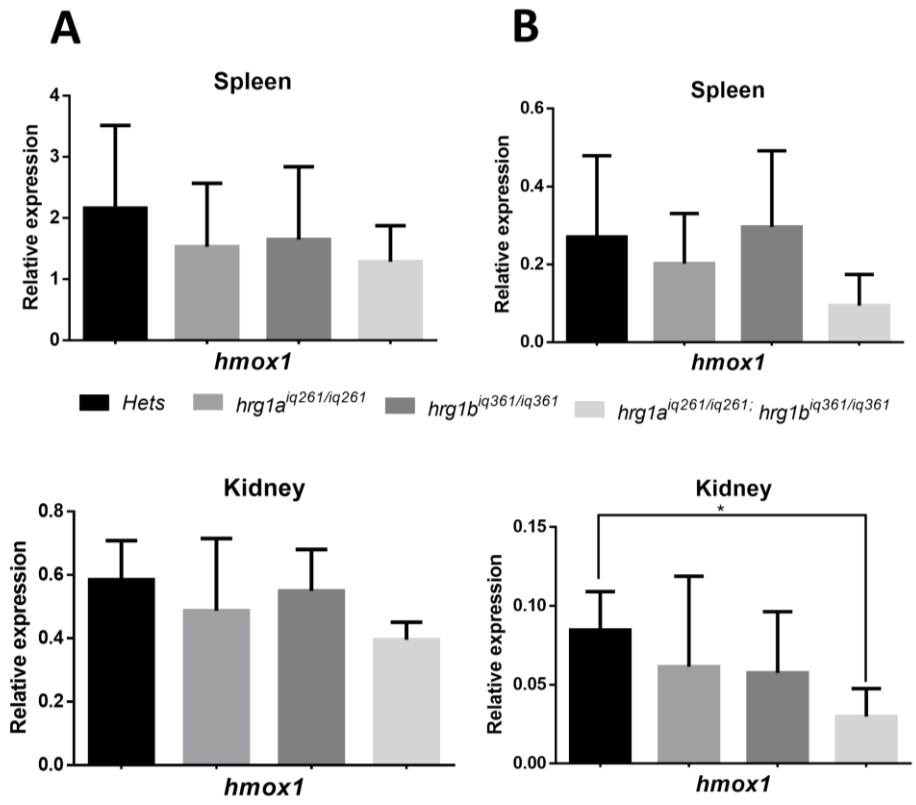

Figure 4.8 Expression of *hmox1* upon PHZ treatment

A). qRT-PCR of *hmox1* mRNA in spleen and kidney at 1day post-PHZ treatment.

B). qRT-PCR of *hmox1* mRNA in spleen and kidney at 3day post-PHZ treatment.

Statistical analysis: t-test. *: $p < 0.05$. Relative expressions are normalized to *ef1a* as reference gene. Each group have 3 biological cohorts, each cohort is pooled from 3 adult zebrafish.

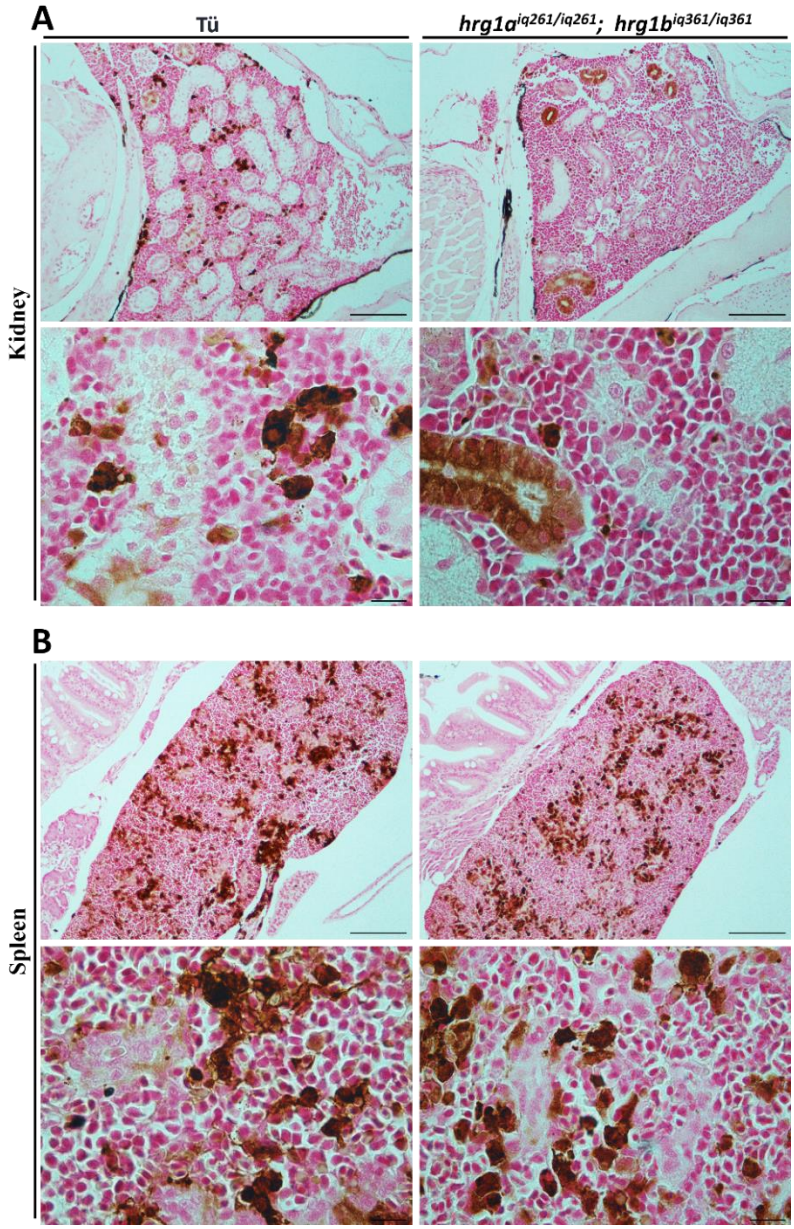

Figure 4.9 Iron is accumulated in kidney and spleen after PHZ treatment.

A). DAB-enhanced Perl's iron staining on kidneys of WT and *hrg1a*$^{iq261/iq261}$*; hrg1b*$^{iq361/iq361}$ at 3 days post-PHZ treatment. Scale Bar: 200 µm.

B). DAB-enhanced Perl's iron staining on spleens of WT and *hrg1a*$^{iq261/iq261}$*; hrg1b*$^{iq361/iq361}$ at 3 days post-PHZ treatment. Scale Bar: 200 µm.

Discussion

In this chapter, we aimed to delineate the function of Hrg1 in heme-iron recycling of adult zebrafish. First, we disrupted primitive erythrocytes by PHZ and found that the recovery of circulating definitive RBCs are the same between WT and mutants. Whether any heme-iron recycling occurs in the developing embryos is unclear, for the following reasons: a) zebrafish embryos retain large amount of maternal iron for embryogenesis and *fpn1* is proposed to transport maternal iron to the developing embryos (134); and b) zebrafish *merlot* (*mot*) mutants with hemolytic anemia seem to get rid of heme and degradation products from hemolysis of primitive RBCs into the bile as dark pigments during early embryogenesis without undergoing recycling (181). We have also detected the same dark pigment around the yolk extension tube of PHZ-treated embryos. Thus, a heme-iron recycling system might not be required or in existence in early embryos.

However, *mot* mutants can survive to adulthood and adult mutants suffer from prominent phenotypes including enlarged spleen, and hypercellular kidneys with high bilirubin levels, a byproduct of heme catabolism, suggesting an active heme-iron recycling pathway in adult fish (181). It also has been shown that *fpn1*, an iron exporter, is critical in iron recycling during adult erythropoiesis, and mutation in *fpn1* causes iron accumulation in the macrophages of liver and kidney (135). The zebrafish kidney marrow is the major hematopoietic tissue and the spleen is a niche for EP (114, 115). It is noteworthy that Hrg1a and Hrg1b is relatively highly expressed in the kidney marrow and spleen, thus it is possible that zebrafish Hrg1 is involved in adult heme-iron recycling during definitive erythropoiesis or in stressed conditions such hemolysis. Indeed, RNAseq results suggest a possible defect in macrophage function and consequently immune response in the *hrg1* mutant fish. Moreover, since there may be a disruption in recycling damaged RBCs, which involves catabolism of large amount of proteins and lipids from RBCs, gene expression of proteolysis and lipid transport pathways are therefore mis-regulated in the absence of Hrg1.

Hrg1a and *hrg1b* mRNA are upregulated in zebrafish kidney upon PHZ-induced hemolysis. Similar upregulation also occurs in the spleen for *hrg1a*. Zebrafish spleen is relatively tiny, and the size and morphology varies in adult zebrafish. Although we used 3 biological replicates and each replicate contain 3 adult spleen, the variation in qPCR results is still large. Zebrafish kidney and spleen are the predominant sites for heme-iron recycling, based on the following facts: a) PHZ causes iron accumulation in the spleen and kidney as shown by DAB-enhance Perl's staining; and b) *hmox1* shows high upregulation during hemolysis. Further studies with $hrg1a^{iq261/iq261}$; $hrg1b^{iq361/iq361}$ is necessary to establish zebrafish as a c concrete model to study EP.

Chapter 5: MRP5/ABCC5, a heme exporter, and its paralog MRP9/ABCC12 alter zebrafish erythropoiesis

Summary

Using *C.elegans* as an animal model of heme auxotroph, we have previously showed that *mrp-5* is a heme exporter expressing on the basolateral membranes of the worm's intestine. Zebrafish *mrp*5/*abcc*5 is the ortholog of *C.elegans mrp*-5. We have previously shown that zebrafish Hrg1 paralogs (*hrg1a* and *hrg1b*) can rescue the growth of *hem1*Δ strain in the presence of low heme, indicating that they are *bone fide* heme importers. In this chapter, we show that zebrafish Mrp5 is capable of transporting heme. Expression of zebrafish *mrp*5 decreases growth of *hem1Δ* yeast, suggesting that heme is transported out of yeast by zebrafish Mrp5. WISH reveals that zebrafish *mrp*5 is ubiquitously expressed throughout the developing embryo with high expression in the central nervous system. Morpholino knockdown of *mrp*5 in zebrafish shows severe anemia in developing embryos with loss of *gata1* expression, a transcription factor for erythroid specification. Additionally, anemic phenotypes in *mrp*5 morphants can be rescued by co-injection of in-vitro transcribed recoded *mrp*-5 capped RNA, indicating that zebrafish Mrp5 is necessary for erythropoietic development. Unlike two paralogs (ohnologues) for *hrg1* in zebrafish genome, the closest homolog of *mrp5* is *mrp*9/*abcc*12 by multiple sequence alignment and phylogenetic analysis. Yeast growth assay revealed that both zebrafish Mrp5 and Mrp9 are capable of heme export. *Mrp9* mRNA is ubiquitously expressed in zebrafish embryos at different developing stages and maternal *mrp*9 mRNA is deposited into oocytes. Similar to *mrp*5, knockdown of *abcc*12 in zebrafish also causes anemia and loss of hemoglobinized RBCs. These results suggest that both *mrp*5 and *mrp*9 are required for RBC development in zebrafish embryos. Subsequent generation and characterization of *mrp*5 and *mrp*9 mutants by CRISPR/Cas9 gene editing will further define the function of Mrp5 and Mrp9 in zebrafish development.

Results

Expression of Zebrafish Mrp5 alters heme homeostasis in a heterologous yeast system

Zebrafish *mrp*5/*abcc*5 is located across ~56kb on chromosome 18 in the zebrafish genome, with overall 28 exons encoding a 1,426 aa protein (**Fig. 5.1A**). Like the canonical multidrug resistant protein (MRP), zebrafish Mrp5 contains 12 transmembrane domains and 2 nucleotide binding domains (NBD) with ATP-hydrolysis activity for energy-driven substrate transport. To determine whether zebrafish Mrp5 transports heme, we exploited the well-established assays in yeast. Expression of *C. elegans* heme importers HRG-4 (CeHRG-4) or HRG-1 (CeHRG-1) increases yeast growth compared to control yeast grown on heme-supplemented plates (**Fig. 5.1B**). When *hem1Δ* yeast cells express the *C.elegans* heme exporter, CeMRP-5, their growth is reduced compared to control group. Similarly, the growth of *hem1Δ* yeast expressing zebrafish Mrp5 (ZfMrp5) is decreased in the presence of heme (**Fig. 5.1B**), suggesting that Mrp5 is decreasing intracellular heme and therefore worsening the growth of a heme deficient yeast strain.

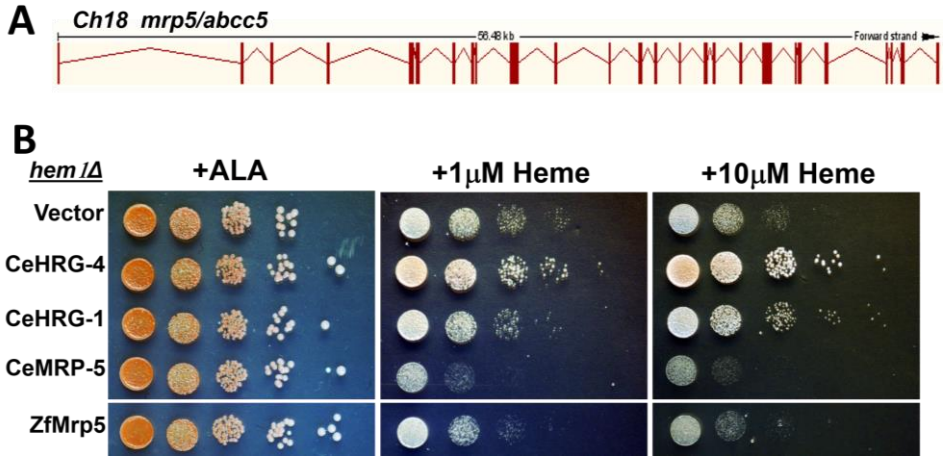

Figure 5.1 Expression of zebrafish Mrp5 reduces growth of heme deficient yeast stain in the presence of exogenous heme

A). Structure of *mrp5* in its gene locus on chromosome 18. Exons are shown as brown boxes and introns are shown as lines. The overall length of zebrafish mrp5 gene is ~56kb.

B). Inhibition of yeast growth by zebrafish Mrp5 when expression in mutant *hemΔ1* strain. The *hem1Δ* yeast strain was transformed with indicated constructs and grown overnight in SC medium without ALA and spotted in serial dilutions on 2 % raffinose SC (-Ura, +0.4 % galactose) plates supplemented with indicated concentrations of ALA or hemin. Plates were incubated 3 days prior to imaging

Expression of zebrafish *mrp5/abcc5* in developing zebrafish embryos

RT-PCR of total mRNA extracted from embryos at single cell stage to 4 dpf showed that *mrp5* mRNA is not expressed in the early stage embryos but only after 18 hpf (**Fig. 5.2A**). To determine the temporospatial expression profile of *mrp5* mRNA in zebrafish embryos, we generated anti-sense RNA probe and WISH analysis revealed that *mrp*5 mRNA is ubiquitously expressed all through the developing embryo with greater expression in the central nervous system **(Fig. 5.2B)**.

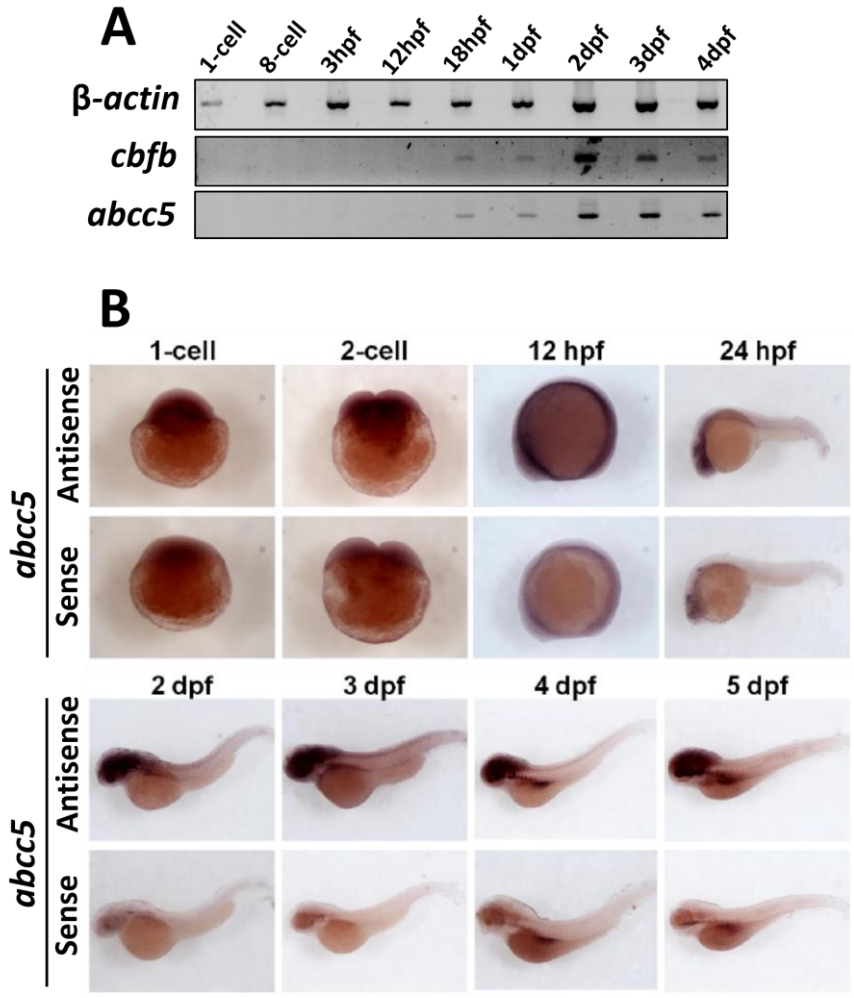

Figure 5.2 Expression of *mrp5* in developing zebrafish embryos

A). RT-PCR of *mrp5/abcc5* in embryos at different developmental stages. *ß-actin* is the control for house-keeping gene; *cbfb*, an established transcription factor which is only turned on around 18 hpf.

B). WISH of *mrp5/abcc5* in embryos at different developmental stages. Anterior is to the left. Anti-sense probe is used to detect mRNA expression; sense probe is shown to indicate background staining.

Mopholino knockdown of *mrp*5 in zebrafish embryos causes severe anemia and developmental defects

To knockdown *mrp5/abcc5*, we injected fish embryos with morpholinos specifically targeting against the ATG start codon of *mrp5/abcc5* (*mrp5_MO*) mRNA. Embryos injected with *mrp5_MO* show severe anemia with few *o*-dianisidine-positive RBCs compared to embryos injected with *control_MO* (**Fig. 5.3A**). *Mrp5_MO* morphants also exhibited developmental malformations including body axis curvature defects and enlarged hearts. To quantify the severe anemia phenotype, we compared levels of globin-expressing RBCs in the *control_MO* and *mrp5_MO* morphants. Transgenic zebrafish expressing GFP from the globin locus control region (globinLCR:GFP) were injected with either *control_MO* or *mrp5_MO* morpholinos, and the blood was analyzed 2 dpf embryos for GFP expression. Zebrafish embryos injected with *mrp5_MO* showed significantly less GFP-positive RBCs compared to *control_MO* morphants (**Fig 5.3B**). The *mrp5_MO* anemia is indeed due to Mrp5/Abcc5 deficiency, as co-injecting zebrafish embryos with *mrp5/abcc5* capped mRNA (cRNA) significantly corrected the anemia phenotype (**Fig 5.3C**). Taken together, these data indicate that *mrp5* is critical for zebrafish erythropoiesis, and that MRP5 regulation of systemic heme homeostasis is likely conserved from worms to vertebrates.

To further confirm the anemic phenotype, we used another splice-blocking morpholino targeting the intron-exon junction of exon 26. Similar to translation blocking morpholino *mrp5_MO*, *Mrp5_E26_MO* also resulted in significantly higher portion of morphants with anemia, suggesting that the anemic phenotypes are likely due to *mrp5* knockdown (**Fig. 5.4A and B**). RT-PCR analysis revealed that *Mrp5_E26_MO* morphants expressed a mis-spliced form of *mrp*5 mRNA with a deletion in exon 26 (**Appendix V**) (**Fig. 5.4C**).

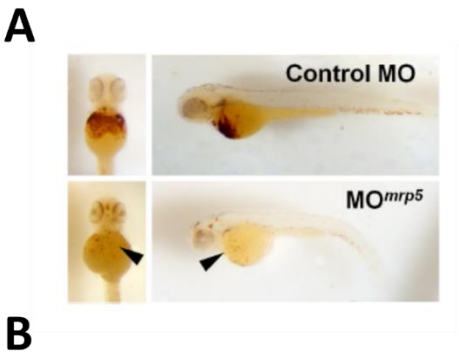
A
Control MO
MO^{mrp5}
B
Control MO
Mrp5 MO
36.2%
10.9%
FSC-A
GFP-A
GFP-Positive Cells Normalized to Control MO
100
50
0
**
Control MO
MO^{mrp5}
C
MO^{mrp5} + Zf *mrp5* RNA
Percent Anemic (%)
100
50
0
***
**
Control MO
MO^{mrp5}
MO^{mrp5} + Zf *mrp5* RNA

Figure 5.3 Morpholino knockdown of *mrp5* alters zebrafish erythropoiesis.

A). Knockdown of zebrafish *mrp5* using morpholinos (*mrp5_MO*) results in severe anemia, as indicated by reduced staining of *o*-dianisidine-positive red cells.

B). Knockdown of zebrafish *mrp-5* using *mrp5_MO* results in reduced red cell formation. Transgenic embryos expressing GFP from the globinLCR: GFP were injected with *control_MO* or *mrp5_MO*. LEFT: On 3 dpf, percent GFP-positive RBCs was analyzed by FACS. X and Y axes measure GFP and forward scatter, respectively; boxed area indicates gate for RBCs. RIGHT: Quantification of morphants shown at left. For *Mrp5_MO* injection, error bars indicate SEM of four independent experiments. ***P<0.001 for *Mrp5_MO* morphants compared to control morphants under identical conditions. (One-way ANOVA, Tukey post-tests.).

C). *O*-dianisidine staining and quantification of anemia rescue in zebrafish embryos co-injected with *mrp5* cRNA. For *Mrp5_MO* injection, error bars indicate SEM of four independent experiments. ***P<0.001 for *Mrp5_MO* morphants compared to control morphants under identical conditions. For *Mrp5_MO* co-injection with rescue mRNA, error bars indicate SEM of three independent experiments. **P<0.01 for *mrp5* morphants co-injected with rescue mRNA when compared to *mrp5* morphants with no rescue mRNA under identical conditions (One-way ANOVA, Tukey post-tests.)

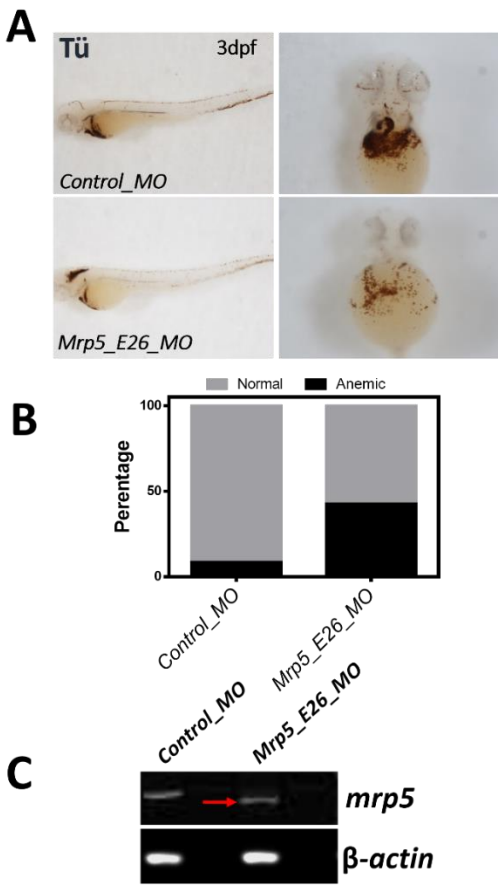

Figure 5.4 Knockdown of *mrp5* by splice-blocking morpholino alters zebrafish erythropoiesis.

A). Knockdown of zebrafish *mrp5* using *mrp5_E26_MO* results in severe anemia, as indicated by reduced staining of *o*-dianisidine-positive red cells.

B). Quantification of anemic embryos in *control_MO* or *mrp5_E26_MO.*

C). RT-PCR of *control_MO* and *mrp5_E26_MO* for *mrp5* expression. Red arrow shows the mis-spliced *mrp5* mRNA.

Mrp5 knockdown results in deficiency in erythroid specification

To investigate whether the anemic phenotypes of *mrp*5 morphants are due to differentiation of erythroid progenitor cells or RBC maturation, we perform WISH on *gata1*, a transcription factor required for primitive erythropoiesis in zebrafish. While *gata1* mRNA was robustly expressed in WT embryos and *control_MO* morphants, positive *gata1* staining was rarely observed in the *mrp5_MO* morphants (**Fig. 5.5A**). We also injected *mrp5_MO* to *gata1*: GFP transgenic embryos, in which GFP expression is driven by gata1 promoter. Knockdown of *mrp5* causes *gata1:* GFP to be significantly impaired (**Fig. 5.5A**). These results suggest that the anemic phenotypes in the *mrp5_MO* morphants are due to defects in erythropoietic differentiation during early erythropoiesis.

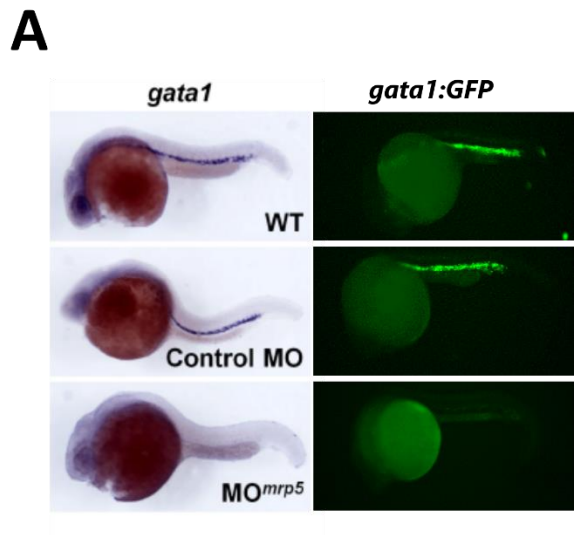

Figure 5.5 Knockdown of *mrp5* results in loss of *gata1* expression in zebrafish embryos

A). Lateral view of zebrafish embryos in WT, *control MO*, and *Mrp5_MO* morphants by whole mount *in situ* hybridization using anti-sense *gata1* probe or *gata1*:GFP at 24 hpf. Anterior is to the left.

Mrp9/Abcc12 is a functional homolog of Mrp5/Abcc5

Multiple sequences alignment and phylogenetic analysis reveal that *mrp*5/*abcc*5, and has another close homolog *mrp*9/*abcc*12 in zebrafish, mouse and human genome **(Fig. 5.6A)**. Zebrafish *mrp*9/*abcc*12 is located in chromosome 16 spanning 26 kb with 31 exons encoding a 1,368 aa protein (**Fig. 5.6B**). Zebrafish Mrp9 also contains 12 transmembrane domains and two nucleotide-biding domains with ATP-hydrolysis activity.

To assess the heme transport activity of zebrafish Mrp9, we performed the yeast growth assay in *hem1*Δ mutant. Similar to expression zebrafish Mrp5, expression of zebrafish Mrp9 retards the growth of *hem1*Δ yeast suggesting that both Mrp5 and Mrp9 could be potential heme exporters (**Fig. 5.6C**).

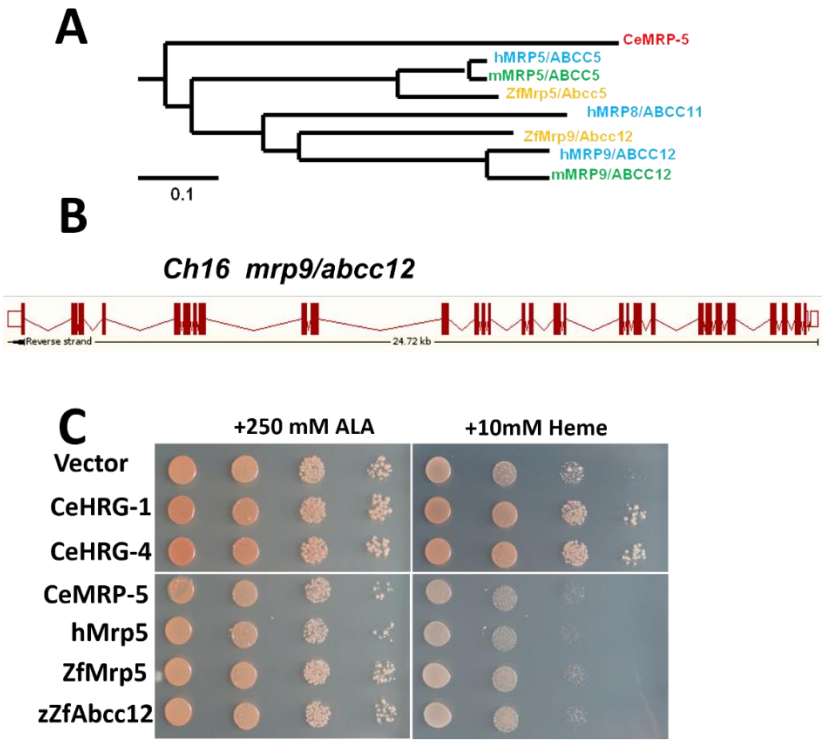

Figure 5.6 Mrp9/Abcc12 is a functional homolog to Mrp5/Abcc5

A). Phylogenetic analysis of MRP5/ABCC5 clade in *C. elegans*, zebrafish, mice, and humans. Sequences were aligned using ClustalW2 and a phylogenetic tree was generated using the Neighbor-Joining method in MEGA5.

B). Structure of mrp9 in its gene locus on chromosome 16.. Exons are showed as brown boxes and introns are shown as lines. The overall length of zebrafish mrp9 gene is ~27kb.

C). Inhibition of yeast growth by zebrafish Mrp9 when expression in *hemΔ1* strain. The *hem1Δ* yeast strain was transformed with indicated constructs and grown overnight in SC medium without ALA and spotted in serial dilutions on 2 % glycerol-lactate (-Ura, +0.4 % galactose for induction before plating) plates supplemented with indicated concentrations of ALA or hemin. Plates were incubated 3 days prior to imaging.

RNA expression of zebrafish *mrp9/abcc12* in developing zebrafish embryos

To determine the localization of *mrp*9/*abcc*12 expression, total mRNA was extracted from one-cell stage to 4 dpf. Compared to its homolog *mrp*5/*abcc5*, RT-PCR analysis revealed that *mrp9* mRNA is maternally deposited in the developing embryos (**Fig. 5.7A**). WISH analysis using anti-sense RNA probe for *abcc12* mRNA revealed that *mrp*9 mRNA is ubiquitously expressed all over the developing embryos with strong expression in the central nervous system, but unlike *mrp5*, *mrp9* showed strong staining in the early stage embryos, which correlated with the RT-PCR results.

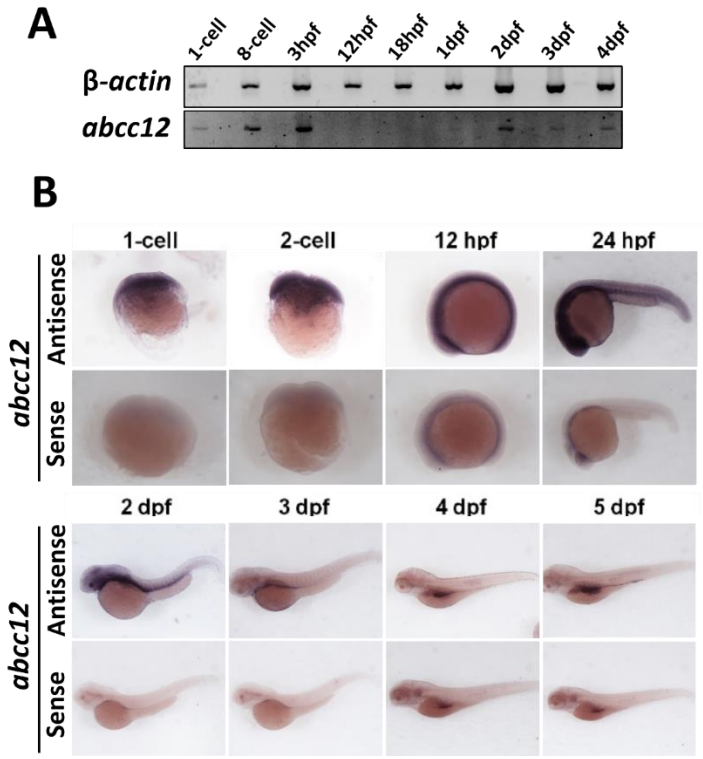

Figure 5.7 Expression of *mrp9* in developing zebrafish embryos.

A). Semi-quantitative RT-PCR of *mrp9/abcc12* in embryos at different developmental stages. *ß-actin* is the control for house-keeping gene; *cbfb*, an established transcription factor which is only turned on around 18 hpf.

B). WISH of *mrp5* expression in embryos at different stages. Anterior is to the left. Anti-sense probe is used to detect mRNA expression; sense probe is shown to indicate background staining.

Mopholino knockdown of *mrp*9/*abcc*12 in zebrafish embryos causes anemia

To knockdown *mrp9/abcc12*, zebrafish embryos were injected with morpholinos targeting against either the ATG start codon (*abcc12_ATG_MO*) or exon-intron junction (*abcc12_E29_MO*) of *mrp9/abcc12* mRNA. Knockdown of *mrp9*/*abcc*12 by both *abcc12_ATG-MO* and *abcc12_E29_MO* revealed few *o*-dianisidine positive RBCs compared to embryos injected with *control_MO* (**Fig. 5.8A**). Quantification of injected embryos revealed a significant number of *mrp*9 morphants is anemic compared to *control_MO* morphants (**Fig. 5.8B**). RT-PCR analysis showed that *abcc12_E29_MO* morphants express a misspliced form of *mrp*9/*abcc*12 mRNA as a larger-size PCR product was detected. Subsequent DNA sequencing of this product revealed that *abcc12_E29_MO* blocked splicing thereby causing retention of exon 29 in the morphants (**Appendix VI**) (**Fig. 5.8C**). These data collectively indicate that, similar to *mrp*5/*abcc*5, zebrafish *mrp*9/*abcc*12 is necessary for normal hemoglobinization of RBCs in early embryonic development.

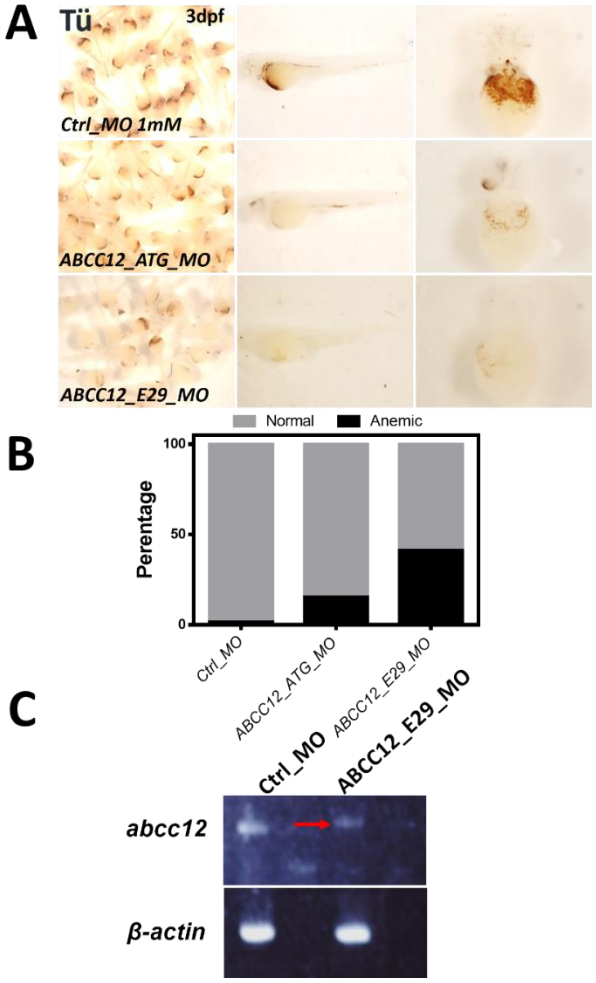

Figure 5.8 Knockdown of *mrp9/abcc12* alters zebrafish erythropoiesis

A). Morpholino knockdown of zebrafish *mrp9/abcc12* results in severe anemia, as indicated by reduced staining of *o*-dianisidine-positive red cells.

B). Quantification of anemic embryos in *control_MO* or *mpr9/abcc12* morphants.

C). RT-PCR of *control_MO* and *abcc12_E29_MO* for *mrp9* expression. Red arrow shows the mis-spliced *mrp9* mRNA with retention of exon 29.

Discussion

Mrp5 (ABC-transports subfamily C) has been extensively studied as an exporter of cancer drugs, organic anions and nucleoside metabolites. However, the physiological substrates for Mrp5 are unknown (182). Here we show that zebrafish *mrp5* is widely expressed during early zebrafish development and that loss of Mrp5 leads to severe anemia and developmental defects. We also show that zebrafish Mrp5, and human MRP5 inhibit heme-dependent growth when expressed in the *hem1Δ* yeast mutant.

By using subcellular HRP heme reporters, our lab previously showed that both *C. elegans* MRP-5 and human MRP5 reduces heme availability in the cytosol with a concomitant increase in heme availability in the secretory pathway (64). When expressed in yeast, both worm and human MRP5 localizes to intracellular membranes which are distinct from the vacuole or plasma membrane (64). These results suggest that MRP5 proteins are capable of transporting heme from the cytosol into the secretory pathway in yeast. Results from yeast growth assays indicate that zebrafish Mrp5 is capable of mediating heme transport and is comparable to the *C.elegans* and human MRP-5. It is therefore reasonable to predict that zebrafish Mrp5 may also localize to intracellular membranes and efflux heme into secretory pathway.

Mouse and Human Mrp5 are ~39 % identical to *C. elegans* MRP-5, while zebrafish Mrp5 is ~74 % identical to mammalian MRP5. Morpholino knockdown of *mrp5* results in severe anemia and developmental defects, which can be specifically rescued by co-injection with recoded zebrafish *mrp5* mRNA. Loss of the erythropoietic-specific transcription factor in *mrp5* morphants indicates that *mrp5* is required for specification of RBCs. While the mechanism whereby loss of *mrp5* results in anemia remains unknown, these results suggest that heme transport plays a critical role in early development and erythropoiesis in zebrafish.

Multiple sequences alignments and phylogenetic identify another member of ABC-transport subfamily C, Mrp9/Abcc12. Expression of Mrp9 also inhibited heme-dependent

growth of *hem1*Δ yeast mutants. Both *mrp5* and *mrp9* mRNA are widely expressed in the zebrafish embryo. Interestingly, unlike *mrp5*, mrp9 mRNA is maternally deposited to zebrafish embryos, suggesting its possible role in maternal heme delivery. Knockdown of Mrp9 in zebrafish embryos also caused anemic phenotypes. Further experiments are necessary to elucidate the subcellular localization of Mrp9 and the underlying mechanism of anemia in *mrp9* morphants.

One caveat is that we have not measured direct heme transport by Mrp5 and it is possible that the heme-dependent phenotypes are indirect. Since Mrp5 and Mrp9 localize to subcellular compartments, it is difficult to measure heme transport at a subcellular level. Expression of Mrp5 and Mrp9 in a reconstituted membrane system may permit transport measurement.

Our functional studies for Mrp5 and Mrp9 are based on heterologous expression and morpholino knockdown. While morpholino is a good tool for gene knockdown, it is possible that there could be off-target effects. Current studies are being conducted with CRISPR/Cas9 to generate null alleles for *mrp5* and *mrp9* in zebrafish and in mice, to further functionally characterize *mrp5*, *mrp9* and *mrp5; mrp9* mutants.

Chapter 6: Conclusions and future directions

Conclusions

Heme and iron metabolism are closely intertwined to maintain homeostasis and our results reveal that heme transporters significantly contribute to regulate intercellular and intracellular heme levels. HRG1 and MRP5 were identified as heme importer and exporter, respectively, using the power of *C. elegans* genetics. The objective of the current study was to dissect the function of heme transporters in red-cell development and heme-iron recycling by exploiting zebrafish as an *in vivo* vertebrate animal model. The major findings of this study are listed and discussed as follows:

Hrg1

1). *Hrg1* is duplicated in the zebrafish genome. Two ohnologues (paralogs) are found, *hrg1a* (*slc48a1b*) and *hrg1b* (*slc48a1a*). Hrg1a and Hrg1b are functional orthologs to worm, mouse and human HRG1, with similar topology comprising of four transmembrane domains, cytoplasmic N- and C-terminus. Expression of Hrg1a and Hrg1b can ameliorate the growth of a heme-deficient yeast strain upon heme supplementation.

2). *Hrg1a* and *hrg1b* are widely expressed throughout the zebrafish embryo and both mRNAs are maternally deposited during oogenesis. RT-PCR reveals that *hrg1a* and *hrg1b* mRNA are expressed in various adult tissues including the kidney and spleen, the major hematopoietic organs in zebrafish. Expression of fluorescence-tagged Hrg1a and Hrg1b proteins in mammalian cells reveals that Hrg1a and Hrg1b localize to the endo-lysosomal compartments and co-localize with LAMP1, a lysosomal marker.

3). Injection of *hrg1a_I2E3_MO2* morpholino into zebrafish embryos causes severe anemia in addition to morphological defects, even though *hrg1a* mRNA was only partially affected. However, knockdown of *hrg1a* or *hrg1b* with other morpholinos did not result in severe anemia.

4). *Hrg1a*$^{iq261/iq261}$; *hrg1b*$^{iq361/iq361}$ zebrafish mutants generated by CRISPR/Cas9 show no detectable Hrg1 proteins and double mutant embryos show no hematological defects. Knockdown of *hrg1a* in *hrg1b* mutants or *vice versa* do not impair erythropoiesis in zebrafish embryos. These genetic studies suggest that Hrg1 is not required for primitive erythropoietic development in zebrafish embryos.

5). The anemic phenotypes of *hrg1a_I2E3_MO2* morpholino cannot recapitulate the genetic muants in *hrg1*. Thus, the morpholino phenotype could be due to a dominant negative affect of the mis-spliced mRNA product or or an off-target effect.

6). Zebrafish RES is responsible for clearing damaged RBCs and for recycling heme-iron under hemolytic conditions. *Hrg1a* and *hrg1b* mRNA are upregulated in the zebrafish spleen and kidney upon PHZ-induced hemolysis, concomitant with *hmox1*, a heme-degrading enzyme essential for heme-iron recycling.

7). Whole transcriptome sequencing of mRNA extracted from the spleen and kidney reveals significant differentially expressed genes in immune response, lipid transport, oxidation-reduction processes, and proteolysis. This result indicates that *hrg1a*$^{iq261/iq261}$*; hrg1b*$^{iq361/iq361}$ mutants have aberrant recycling of heme-iron derived from damaged RBCs in the absence of functional Hrg1.

8). qRT-PCR on mRNA from kidneys and spleens of adult zebrafish at 1 day post-PHZ treatment reveal no significant differences in *hmox1* induction between double heterozygotes (*Hets*), single mutants (*hrg1a*$^{iq261/iq261}$ *and hrg1b*$^{iq361/iq361}$), and double mutants (*hrg1a*$^{iq261/iq261}$*; hrg1b*$^{iq361/iq361}$); a noticeable trend was observed for *hmox1* mRNA, which was lower in the double mutants. Perl's histochemical staining for iron reveal that iron is mis-localized to renal tubules in *hrg1* double mutants compared to WT kidney, which reveals iron accumulation mainly in macrophages.

Mrp5

1). Zebrafish Mrp5/Abcc5 encodes a 1,426 aa protein with twelve transmembrane and two NBD domains. Zebrafish Mrp5 shows ~32% homology to *C. elegans* MRP-5 and ~74% homology to mammalian MRP5. Expression of Mrp5 worsens the growth of heme-deficient *hem1*Δ mutant yeast, similar to *C. elegans* MRP-5, indicating that these Mrp5 proteins may serve similar functions as heme exporters.

2). Zebrafish *mrp5* mRNA is ubiquitously expressed throughout the zebrafish embryo and is detectable at ~18 hpf. Morpholino knockdown of *mrp5* results in severe anemia and developmental defects, which can be specifically rescued by co-injection with recoded zebrafish *mrp5* cRNA. Reduced expression of the erythropoietic-specific transcription factor *gata1* in 1 dpf *mrp5* morphant embryos indicate that Mrp5 is required for differentiation of RBCs. Accordingly, the number of RBCs was lower in 3 dpf *mrp5* morphants. While the mechanism whereby loss of *mrp5* results in anemia remains unknown, these results indicate that Mrp5 plays a role in regulating heme homeostasis and erythropoiesis.

3). Zebrafish Mrp9/Abcc12 encodes a 1,368 aa protein with twelve transmembrane and two NBD domains, similar to Mrp5. Phylogenetic analysis reveal that Mrp9 is the closest

homolog to Mrp5 in the zebrafish genome. Expression of Mrp9 in the *hem1*Δ yeast mutant shows reduced growth indicating that Mrp9 may have similar function as Mrp5.

4). Zebrafish *mrp9* is expressed throughout the embryo including at the one-cell stage suggesting that *mrp9* mRNA is maternally deposited during oogenesis. Knockdown of *mrp9* by both translation- and splice-blocking morpholinos results in less *o*-dianisidine staining of embryos. These results indicate that Mrp9 may be involved in the early development of RBCs in the zebrafish embryos. However, whether Mrp9 and Mrp5 functions synergistically or independently is unclear.

Future Directions

Localization of Hrg1 in RES of adult zebrafish

While qRT-PCR revealed that *hrg1a* and *hrg1b* mRNA are both expressed in zebrafish RES and upregulated during PHZ-induced hemolysis, localization of Hrg1a and Hrg1b proteins in the tissue context needs to be addressed especially in macrophages. We have tried to generate transgenic zebrafish with Hrg1a and Hrg1b tagged with fluorescent proteins using BAC (Bacterial Artificial chromosome) transgenesis. However, owing to the low efficiency and possible position effects by random insertion of the transgene, we did not successfully obtain a transgenic line with strong transgene expression. Our lab has generated custom HRG1 antibodies using the C-terminus 17-aa from human HRG1 as the immunogen. Although the customized HRG1 antibody can recognize zebrafish Hrg1, IHC (immunohistochemistry) staining in zebrafish sections with HRG1 antibody showed high background staining. To overcome this technical hurdle, we can adopt CRISPR/Cas9 technology to generate transgenic zebrafish by inserting GFP into the *hrg1a* or *hrg1b* genomic locus using homology-directed repair and creating a Hrg1::GFP translational protein

fusion (6). We have successfully used this strategy to generate a HRG1::GFP mouse. These transgenic Hrg1::GFP fish can then be used to check the localization of Hrg1a and Hrg1b protein using intra-vital imaging and co-localizing the protein either with IHC or genetic crosses with other transgenic zebrafish expressing fluorescent-tagged macrophage or other hematopoietic lineage markers (below). We can also perform flow cytometry with the transgenic fish to analyze the expression of Hrg1 in hematopoietic tissues and erythroid cells. Moreover, if we obtain the translational fusions with Hrg1a::GFP or Hrg1b::mCherry, we can intercross them to obtain double transgenic fish in which we can evaluate the biological role of both Hrg1 proteins concurrently.

Generating transgenic fish with hematopoietic markers in *hrg1* mutants

The transparency of the zebrafish embryo facilitates label-free visualization of cellular components in intact embryos. To better characterize *hrg1* mutant zebrafish, we can cross the established transgenic fish with hematopoietic lineages marked with fluorescent tags, such as globinLCR: GFP for RBCs; *gata1*: GFP for erythropoietic progenitor cells; and *mpeg1*: GFP for macrophages, to *hrg1a* and *hrg1b* double mutant. Flow cytometry analysis can be performed to check the expression profiles of these markers in *hrg1* mutants (154). Additionally, we can specifically quantify the hematopoietic cell profiles by FACS analysis of adult kidney, the major hematopoietic tissue for zebrafish, in *hrg1* mutants (183).

Histological staining of heme and iron

We propose that *hrg1* mutant zebrafish may have a defect in heme-iron recycling in RES macrophage. We can perform histological staining to examine the potential heme or iron accumulation in RES macrophages in the absence of functional Hrg1.

Iron restriction diets in zebrafish

In human, heme-iron recycling from senescent RBCs contributes to more than 90% of daily iron requirement, while dietary iron accounts for the remaining 10% (5, 6). This is in stark contrast to the well-studied mouse model which relies equally on dietary iron absorption and macrophage heme-iron recycling. The individual contribution of iron/heme absorption versus recycling is poorly understood in teleosts. The zebrafish is typically fed a diet of brine shrimp and dry food extracts everyday which is likely to be iron-loaded. Indeed, a typical mouse is fed chow containing 200 ppm of iron which is at least 10 times more than what is required for normal growth and development. Therefore, one possible explanation for why the *hrg1* mutants lack overt hematopoietic phenotypes could be because zebrafish can obtain sufficient iron from dietary absorption, or plausibly through its gills to overcome a block in heme-iron recycling by the RES macrophages (184). Few studies have been published to date on how to iron-restrict zebrafish. One way would be to formulate a custom fish diet with low iron and heme to limit dietary iron, in addition to restricting iron in the water by supplementing the water with a non-toxic iron chelator. If Hrg1 is the major heme-iron transporter, we may be able to tease-out the specific contribution of Hrg1 using these strategies.

Functional characterization of Hrg1 interacting proteins

The long-term goals of our laboratory are to identify potential components in eukaryotic heme trafficking network. One way to identify components in HRG1-dependent heme trafficking pathway is to analyze interacting proteins that co-immunoprecipitate with HRG1 by multidimensional protein identification technology (MudPIT) using a defined mammalian cell culture system. Once these interactors are identified, they need to be further confirmed and characterized *in cellula* and *in vivo*. In this regard, WT and *hrg1* mutant

zebrafish can be exploited to define the *in vivo* requirements of these interacting proteins by assessing their temporospatial expression and the effect of gene knockdowns in zebrafish embryos to assess synthetic or interacting phenotypes. CRISPR/Cas9 can be used to generate mutants for the most credible HRG1-interacting protein(s).

Generation and characterization of *mrp5/mrp9* mutants zebrafish

We have used CRISPR/Cas9 to generate *mrp5* and *mrp9* mutant zebrafish. Ian Chambers, a graduate student in our laboratory, is currently genotyping and screening to retrieve null alleles of *mrp5* and *mrp9* in zebrafish. He has genotyped F0 founder fish containing *mrp5* and *mrp9* mutations and is in the process of generating *mrp5; mrp9* double mutants. Future work with mutant zebrafish will determine the role of Mrp5/Mrp9 in maternal-fetal nutrient heme transfer, embryonic development, and differentiation of erythroid cells in zebrafish. Moreover, all the proposed experiments for Hrg1 delinated above are also applicable for characterizing Mrp5 and Mrp9.

Genetic pathway analysis with Hrg1 and Mrp5/Mrp9

Hrg1 and Mrp5 are identified as heme importer and exporter respectively. To genetically delineate the functional relationship of Hrg1 and Mrp5/Mrp9, we can morpholino knockdown *hrg1* in *mrp5/mrp9* transgenic fish to examine the alternation of *mrp5* and *mrp9* expression, or *vice versa* since it will be technically challenging and time-consuming to generate a quadruple knockout i.e. *hrg1a; hrg1b*; *mrp5; mrp9* mutant.

Interrogating heme trafficking in zebrafish by heme-sensors

One advantage of the zebrafish embryos is the *ex utero* transparency of early stage embryos. Our lab have developed heme reporters using HRP (horseradish peroxidase) and

APX (ascorbate peroxidase)-based subcellular probes, and genetically-encoded fluorescent sensors to interrogate the intra- and inter- cellular heme trafficking (185, 186). We can generate transgenic zebrafish expressing these heme sensors/reporters to directly visualize heme trafficking in the transparent embryos at the maternal-embryonic interface and between tissues and organs.

Significance

The current paradigm dictates that erythroblasts are self-sufficient, *i.e.* they produce large amounts of hemoglobin by simply upregulating endogenous heme synthesis. However, terminal erythroid maturation includes loss of intracellular organelles including mitochondria, the site for heme synthesis. Therefore, exogenous heme uptake may compensate for loss of heme synthesis in the maturing red cell. We postulate that during this terminal maturation, erythroid cells import exogenous heme through Hrg1, to maxmize hemoglobin production during RBCs maturation. It is possible that a portion of heme within maturing RBCs is derived from inter-cellular transport from nurse macrophages in EBIs to support the continuing hemoglobinization of RBCs, especially under conditions such as stress erythropoiesis. Understanding how Hrg1 is involved in the terminal RBC maturation may shed light on anemia.

Majority of the daily iron needs are fulfilled by heme-iron recycling via RES macrophages. Deficiency in heme-iron recycling concomitantly results in heme accumulation in macrophages and iron deficiency, as revealed by *hmox1*$^{-/-}$ mice, a heme degrading enzyme which functions downstream of *hrg1* during heme-iron recycling through EP (86). Moreover, transplantation of WT macrophage in *hmox1*$^{-/-}$ mice corrects the phenotypes (187). As heme accumulation is toxic and can be pro-inflammatory, blocking Hrg1-mediated heme transport upstream from Hmox1 may prove to be an effective therapeutic strategy in certain hemolytic disorders.

Additionally, heme export by MRP5 is conserved among metazoans. Knockdown of Mrp5 in zebrafish embryos results in developmental defects and decreased RBCs formation. Previous studies revealed that Flvcr1, a heme exporter, is required for cell survival and development of erythroid progenitors (53, 143). We envisage that cellular heme levels are maintained by a combination of heme export and heme degradation. Thus, understanding pathways of inter- and intra-cellular heme export may be relevant to specific conditions of aberrant heme and iron homeostasis, erythroid survival, and pathological conditions of hemolysis.

Appendix I

Sequences of morpholinos

Morpholino Name	Sequence
hrg1a_ATG_MO	5'-ATACGTCTTATTGAACGCCATTCCT -3'
hrg1a_E2I2_MO1	5'-CAGCCAAGGAATTACCTGATAATC -3'
hrg1a_I2E3_MO2	5'-CCATAATGCCAAAACTCCTGAAAAA -3'
hrg1b_ATG_MO	5'-GTAGATCCTGTTTGGACCCATTGAT -3'
hrg1b_E2I2_MO	5'-CCGTCAATGTCAAAGTACTCACACT -3'
hrg1b_I1E2_MO2	5'-CCAGAGCGCCAGGACTCCTGTAGAT -3'
Mrp5_ATG_MO	5'-CCCAAATCATGTCCTTTCATCTTCT -3'
Mrp5_E26_MO	5'-ACATGGATTTTGACTCACCTTGCAC -3'
Abcc12_ATG_MO	5'-GGGAAGTCCTTCATTTTTACTATAG -3'
Abcc12_E29_MO	5'-TTGTGTTTTTACTTTGGAGTTGCGC -3'
alas2_MO	5'-CAGTGATGCAGAAAAGCAGACATGA -3'
p53_MO	5'- GCGCCATTGCTTTGCAAGAATTG -3'
standard_control	5'- CCTCTTACCTCAGTTACAATTTATA -3'

Appendix II

Sequencing of *hrg1a* transcripts by *hrg1a_E2I2_MO1*

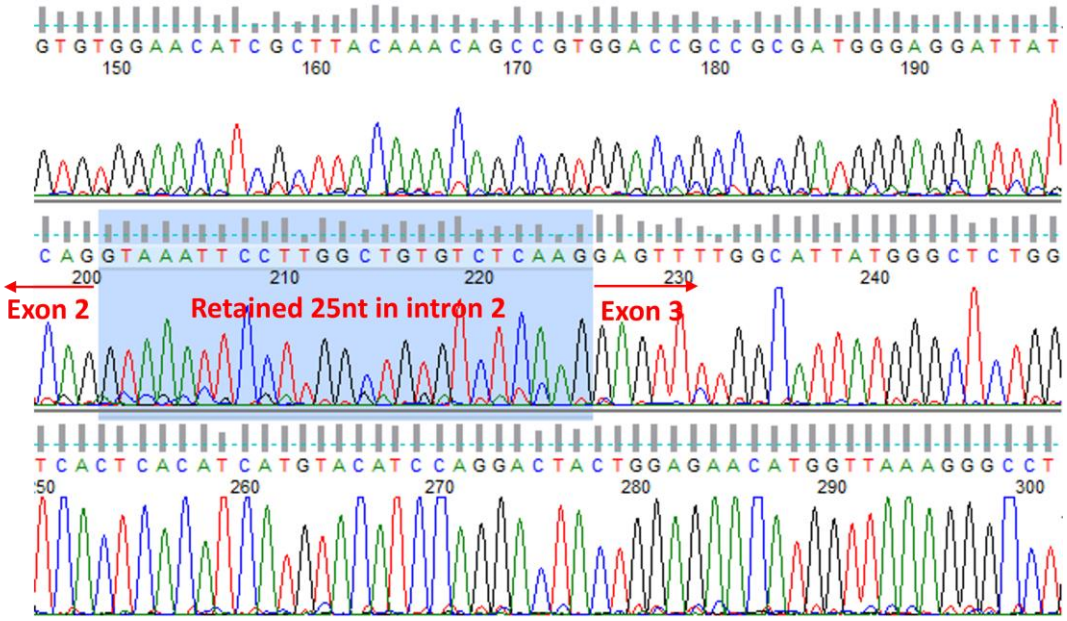

Appendix III

Sequening of *hrg1a* transcripts by *hrg1a_I2E3_MO2*

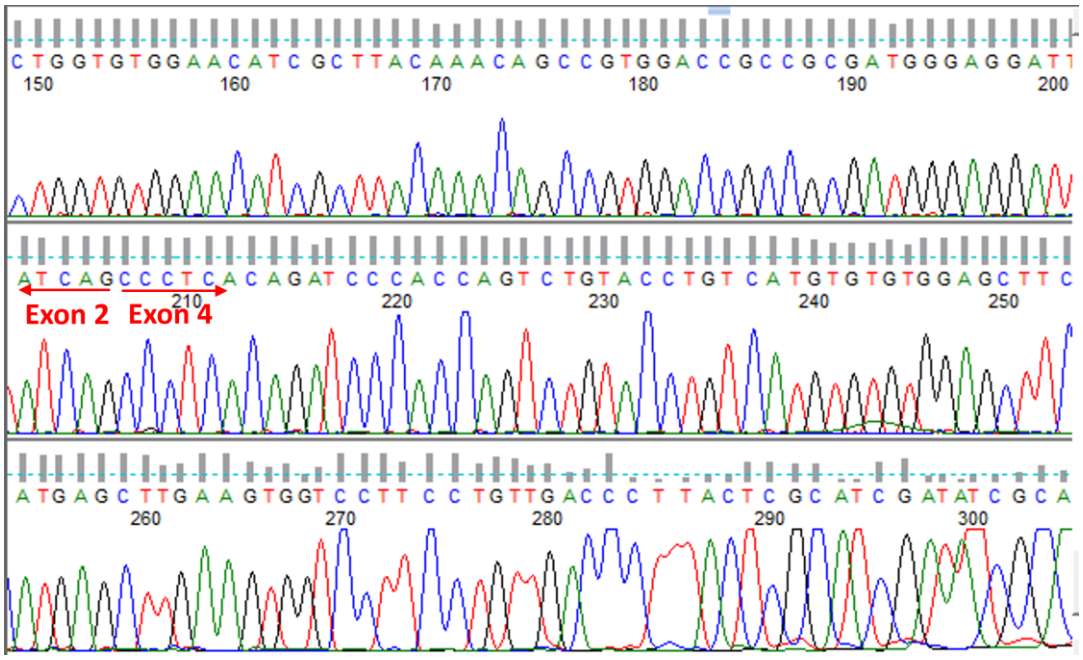

Appendix IV

Sequencing of *hrg1b* transcripts by *hrg1b_E2I3_MO*

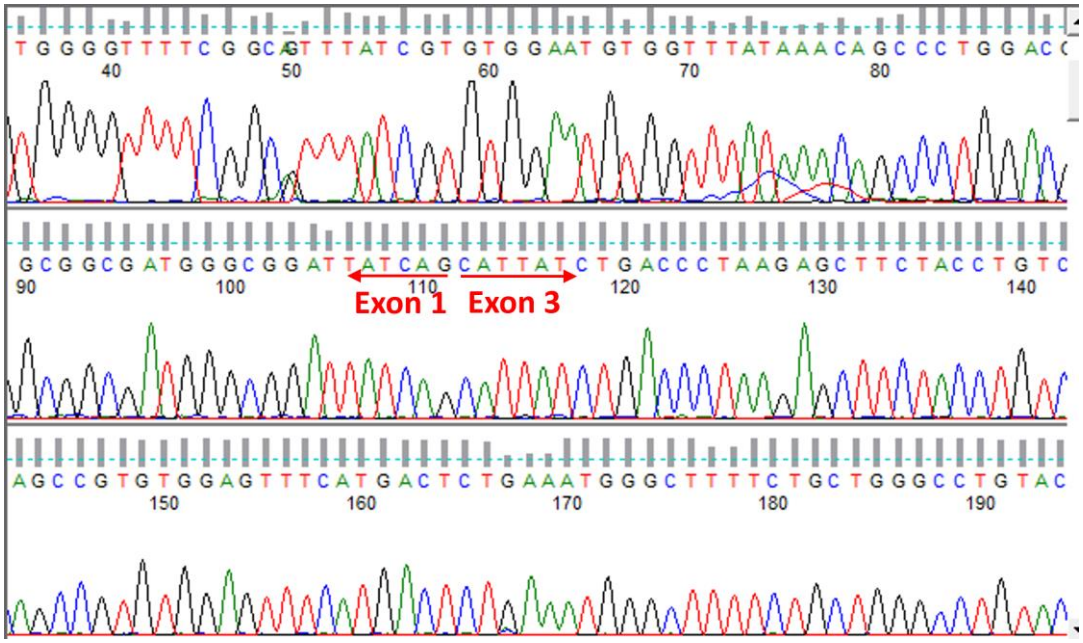

Appendix V

Sequencing of *mrp5* transcripts by *mrp5_E26_MO*

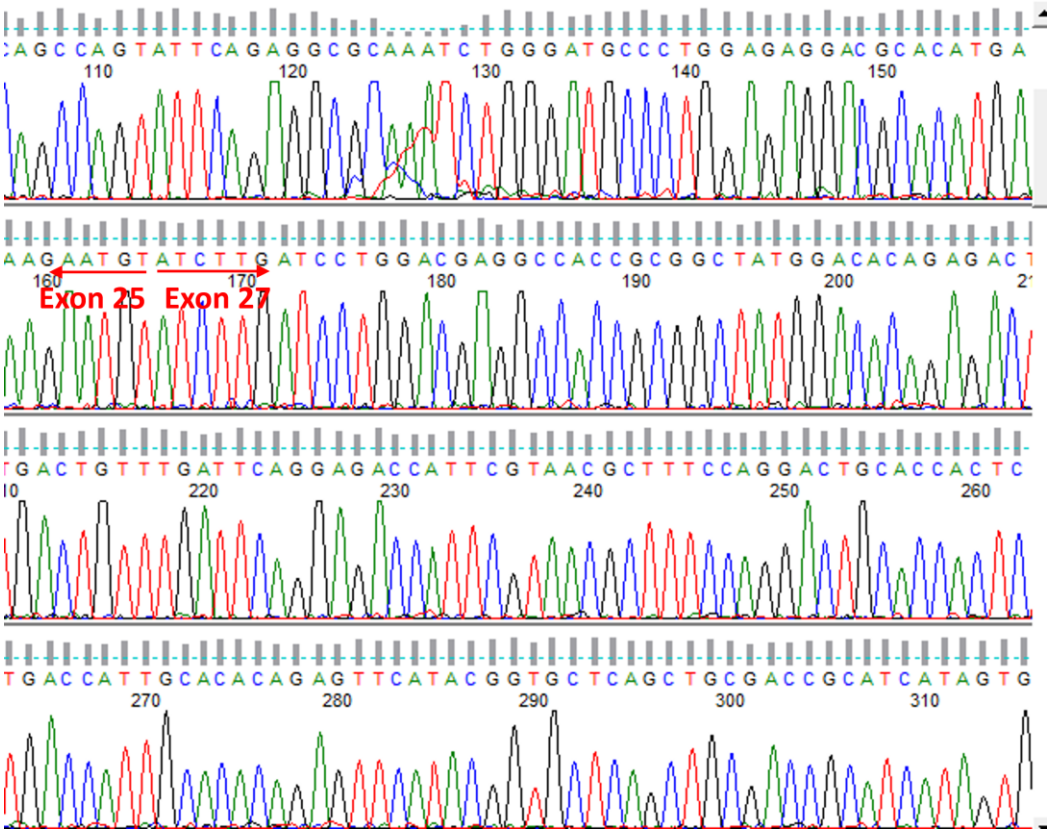

Appendix VI

Sequencing of *mrp9* transcripts by *abcc12_E29_MO*

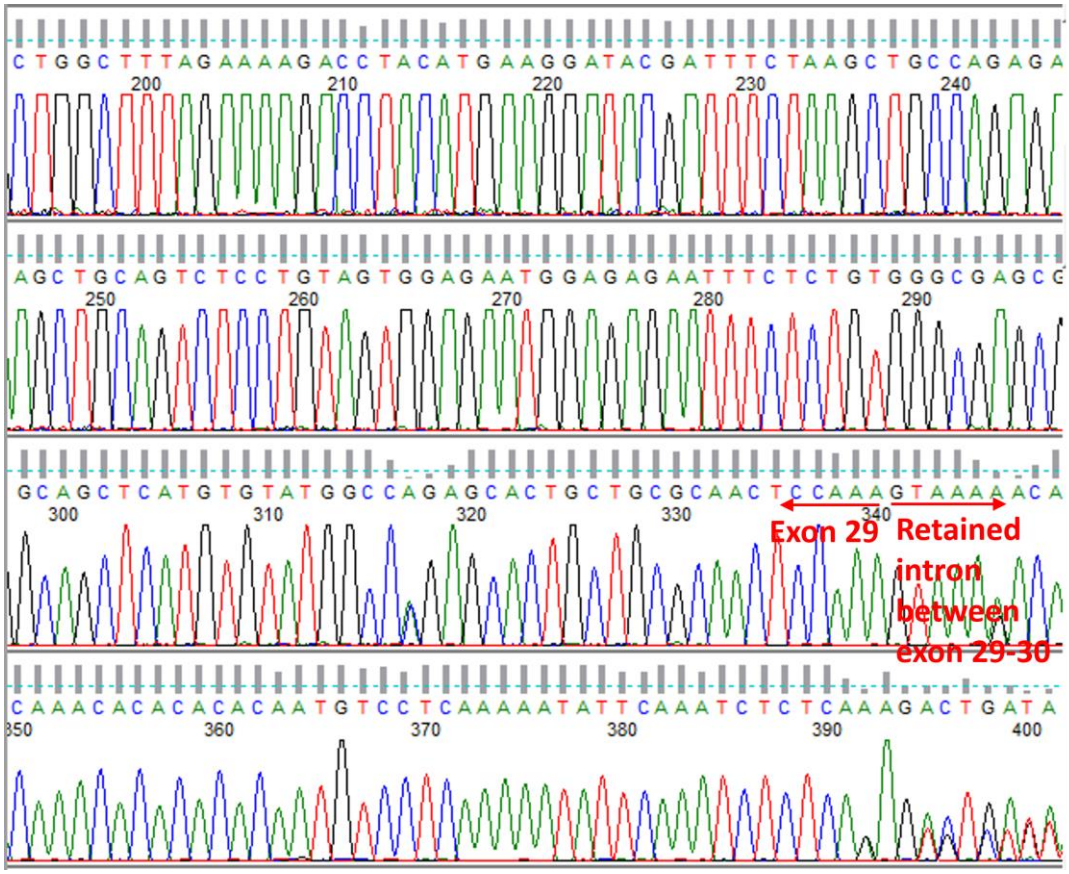

Appendix VII

Genotyping primers of *hrg1a* and *hrg1b* mutants

Genotyping Primers	Sequence
zf1a_TALE1&2_fwd_PstI_1(Exon2)	AAG CTA CAC TGC AG GTGGCGATAACAACTACAGCTGG
zfhrg1a-_HindIII_TALE1&2_rev(Exon2)	GAA TTA TCA AGC TT CACATCACAGGCTCTTTCCGAG
zfhrg1a_PstI_TAL_E3_fwd(Exon3)	AAG CTA CAC TGC AG CAGAGATGTGTTTGCTTATTGTGTG
zfhrg1a_HindIII_TAL_E3_rev(Exon3)	GAA TTA TCA AGC TT GATATGGGAGTGATTGCATCTGTAC
hrg1b_E1_BamHI_fwd(Exon1)	actgcataGGATCC CTCATCGATGGTGTAATCCTTCTC
hrg1b_E1_HindIII_rev(Exon1)	actgcatcAAGCTT CCCTGTCCTAGACCCATGCAAAC
hrg1b_E3_BamHI_fwd(Exon3)	actgcataGGATCC CCCTTTAAAGTGTGTTATCATGTG
hrg1b_E3_XhoI_rev(Exon3)	GCagactc ctcgag CTTCCTACTACAGGGCCTGAATC

Appendix VIII

Sequence chromatogram of *hrg1a* and *hrg1b* mutants

***hrg1a*^{iq261}**

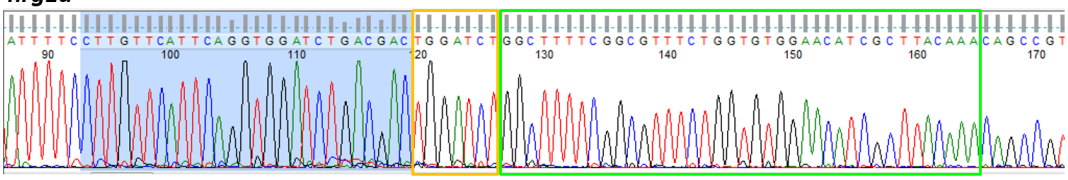

TGGATCT (-61, +7nt)

TCATTCAGGTGGATCTGACGACAGGAATGGCGTTCAATAAGACGTATATTCGCGTGGCCTACT

CGTGTATGGGGATGCTGGTGGGCTTTTCGGCGTTTC TGGTGTGGAACATCGCTTACAAA

Wild Type *hrg1a* sequence

***hrg1b*^{iq361}**

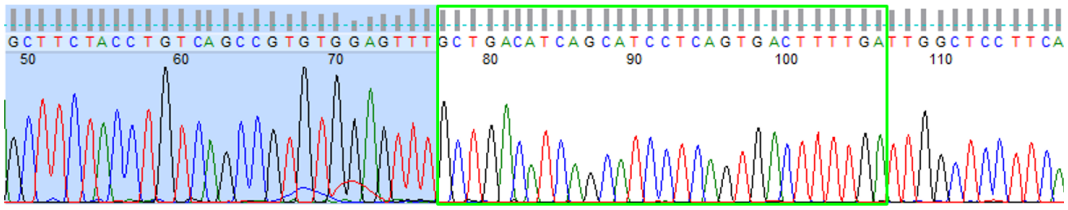

-61nt

GCTTCTACCTGTCAGCCGTGTGGAGTTTCATGACTCTGAAATGGGCTTTTCTGCTGGGCCTG

TACTCCTACCGCTACCGCCAGGAGTTTGCTGACATCAGCATCCTCAGTGACTTTTGATTGGC

TCCT **Wild Type *hrg1b* sequence**

Appendix IX

Summary of Bioanalyzer electrophoresis

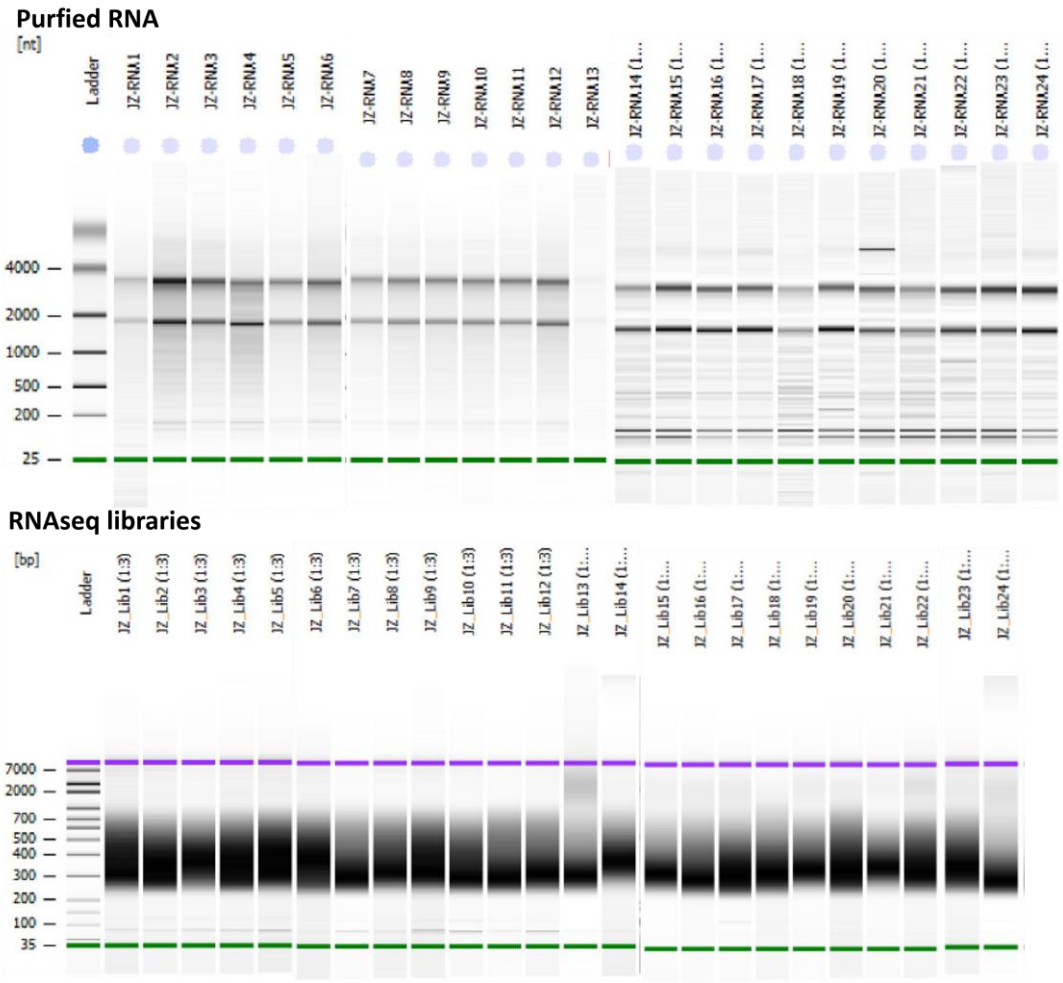

Appendix X

Bioanalyzer plots for RNA integrity

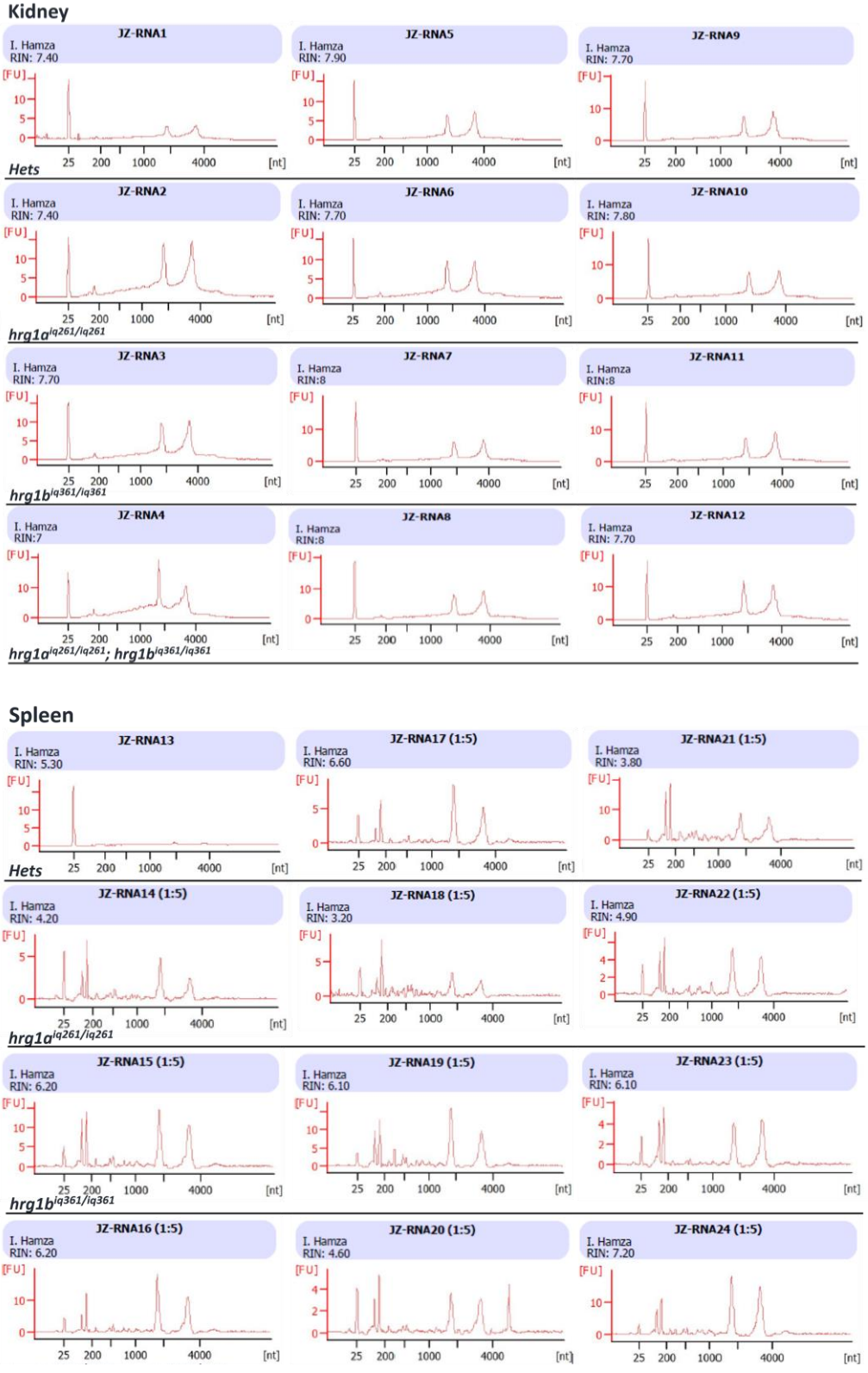

Appendix XI

Bioanalyzer plots for RNAseq library qulification

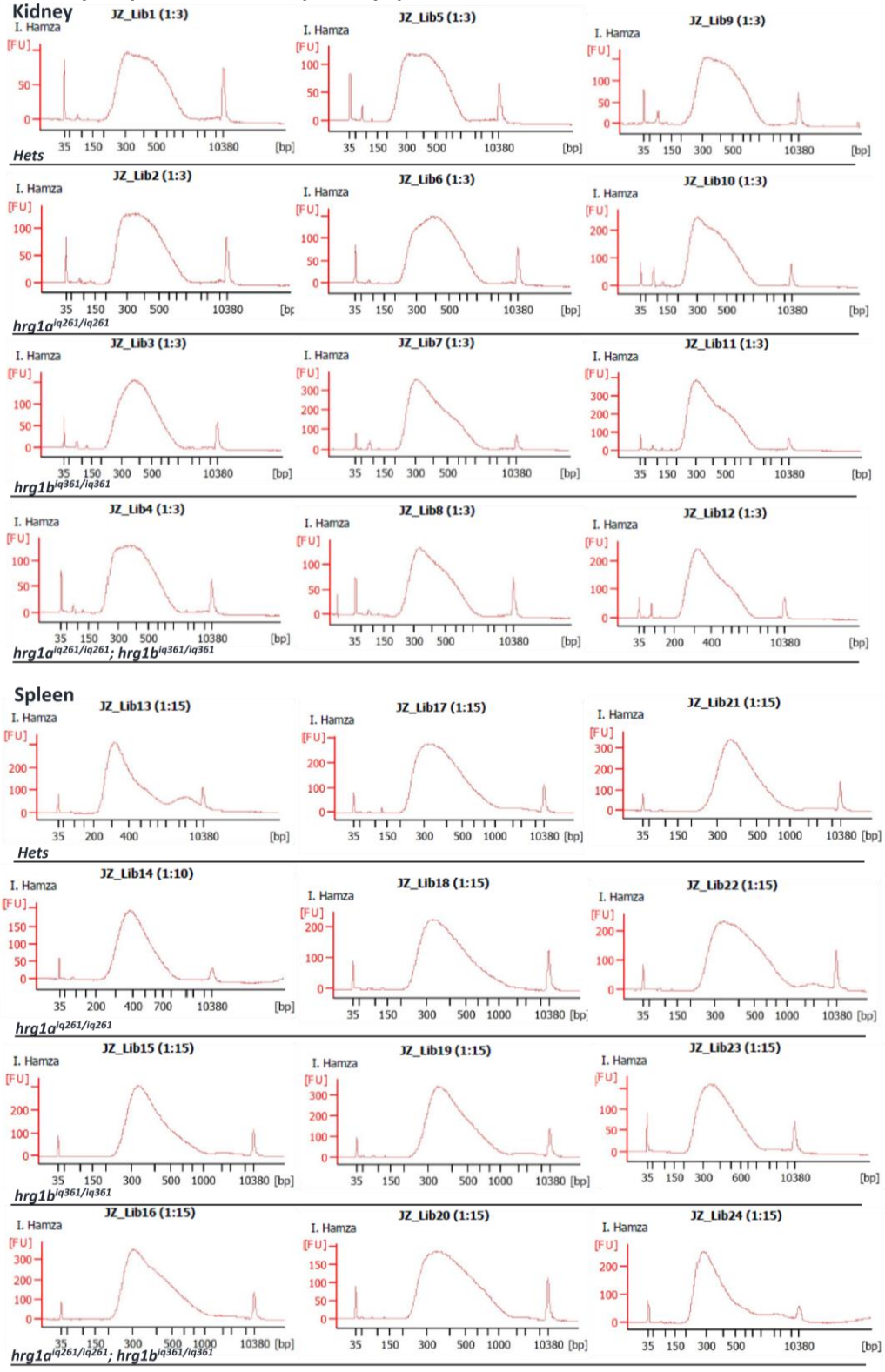

References

1. PONKA, P. (1999) Cell Biology of Heme. *Am. J. Med. Sci.*
2. Severance, S., and Hamza, I. (2009) Trafficking of Heme and Porphyrins in Metazoa
3. WHO | Micronutrient deficiencies [online] http://www.who.int/nutrition/topics/ida/en/#.U2-1-ED6P4o.mendeley (Accessed May 11, 2014)
4. Uzel, C., and Conrad, M. E. (1998) Absorption of heme iron. *Semin. Hematol.* **35**, 27–34
5. Ganz, T., and Nemeth, E. (2012) Iron Metabolism: Interactions with Normal and Disordered Erythropoiesis. *Cold Spring Harb. Perspect. Med.*
6. Muñoz, M., Villar, I., and García-Erce, J. A. (2009) An update on iron physiology. *World J. Gastroenterol.* **15**, 4617–4626
7. Miller, J. L. (2013) Iron Deficiency Anemia: A Common and Curable Disease. *Cold Spring Harb. Perspect. Med.*
8. Dailey, H. A., and Meissner, P. N. (2013) Erythroid heme biosynthesis and its disorders. *Cold Spring Harb. Perspect. Med.*
9. Richardson, D. R., Ponka, P., and Vyoral, D. (1996) Distribution of iron in reticulocytes after inhibition of heme synthesis with succinylacetone: examination of the intermediates involved in iron metabolism. *Blood* . **87**, 3477–88
10. Zhang, A.-S., Sheftel, A. D., and Ponka, P. (2005) Intracellular kinetics of iron in reticulocytes: evidence for endosome involvement in iron targeting to mitochondria. *Blood* . **105**, 368–375
11. Muñoz, M., García-Erce, J. A., and Remacha, Á. F. (2011) Disorders of iron metabolism. Part II: iron deficiency and iron overload. *J. Clin. Pathol.* **64**, 287–296
12. Hunter, G. A., and Ferreira, G. C. (2011) Molecular enzymology of 5-

Aminolevulinate synthase, the gatekeeper of heme biosynthesis. *Biochim. Biophys. Acta - Proteins Proteomics*. **1814**, 1467–1473

13. May, B. K., Dogra, S. C., Sadlon, T. J., Bhasker, C. R., Cox, T. C., and Bottomley, S. S. (1995) Molecular Regulation of Heme Biosynthesis in Higher Vertebrates. *Prog. Nucleic Acid Res. Mol. Biol.* **51**, 1–51

14. Sadlon, T. J., Dell'Oso, T., Surinya, K. H., and May, B. K. (1999) Regulation of erythroid 5-aminolevulinate synthase expression during erythropoiesis. *Int. J. Biochem. Cell Biol.* **31**, 1153–1167

15. Weiss, M. J., Yu, C., and Orkin, S. H. (1997) Erythroid-cell-specific properties of transcription factor GATA-1 revealed by phenotypic rescue of a gene-targeted cell line. *Mol. Cell. Biol.* **17**, 1642–51

16. Tanimura, N., Miller, E., Igarashi, K., Yang, D., Burstyn, J. N., Dewey, C. N., and Bresnick, E. H. (2015) Mechanism governing heme synthesis reveals a GATA factor/heme circuit that controls differentiation. *EMBO Rep.* **17**, 1–17

17. Zhang, Y., Zhang, J., An, W., Wan, Y., Ma, S., Yin, J., Li, X., Gao, J., Yuan, W., Guo, Y., Engel, J. D., Shi, L., Cheng, T., and Zhu, X. (2016) Intron 1 GATA site enhances ALAS2 expression indispensably during erythroid differentiation. *Nucleic Acids Res.* 10.1093/nar/gkw901

18. Wilkinson, N., and Pantopoulos, K. (2014) The IRP/IRE system in vivo: insights from mouse models . *Front. Pharmacol.* . **5**, 176

19. Tugores, A., Magness, S. T., and Brenner, D. A. (1994) A single promoter directs both housekeeping and erythroid preferential expression of the human ferrochelatase gene. *J. Biol. Chem.* . **269**, 30789–30797

20. Crooks, D. R., Ghosh, M. C., Haller, R. G., Tong, W.-H., and Rouault, T. A. (2010) Posttranslational stability of the heme biosynthetic enzyme ferrochelatase is dependent on iron availability and intact iron-sulfur cluster assembly machinery.

Blood. **115**, 860-869

21. Magness, S. T., Tugores, A., and Brenner, D. A. (2000) Analysis of ferrochelatase expression during hematopoietic development of embryonic stem cells. *Blood*. **95**, 3568-3577

22. Chan, R. Y. Y., Schulman, H. M., and Ponka, P. (1993) Expression of ferrochelatase mRNA in erythroid and non-erythroid cells. *Biochem. J.* **292**, 343-349

23. Tahara, T., Sun, J., Nakanishi, K., Yamamoto, M., Mori, H., Saito, T., Fujita, H., Igarashi, K., and Taketani, S. (2004) Heme Positively Regulates the Expression of β-Globin at the Locus Control Region via the Transcriptional Factor Bach1 in Erythroid Cells. *J. Biol. Chem.* **279**, 5480–5487

24. Aisen, P., Leibman, A., and Zweier, J. (1978) Stoichiometric and site characteristics of the binding of iron to human transferrin. *J. Biol. Chem.* . **253**, 1930–1937

25. Ohgami, R. S., Campagna, D. R., Greer, E. L., Antiochos, B., McDonald, A., Chen, J., Sharp, J. J., Fujiwara, Y., Barker, J. E., and Fleming, M. D. (2005) Identification of a ferrireductase required for efficient transferrin-dependent iron uptake in erythroid cells. *Nat Genet*. **37**, 1264–1269

26. Gunshin, H., Mackenzie, B., Berger, U. V, Gunshin, Y., Romero, M. F., Boron, W. F., Nussberger, S., Gollan, J. L., and Hediger, M. A. (1997) Cloning and characterization of a mammalian proton-coupled metal-ion transporter. *Nature*. **388**, 482–488

27. Prus, E., and Fibach, E. (2011) Uptake of non-transferrin iron by erythroid cells. *Anemia*. 10.1155/2011/945289

28. Winterbourn, C. C. (1995) Toxicity of iron and hydrogen peroxide: the Fenton reaction. *Toxicol. Lett.* **82**–**83**, 969–974

29. Leidgens, S., Bullough, K. Z., Shi, H., Li, F., Shakoury-Elizeh, M., Yabe, T., Subramanian, P., Hsu, E., Natarajan, N., Nandal, A., Stemmler, T. L., and Philpott, C. C. (2013) Each Member of the Poly-r(C)-binding Protein 1 (PCBP) Family Exhibits

Iron Chaperone Activity toward Ferritin. *J. Biol. Chem.* . **288**, 17791–17802

30. Ryu, M., Zhang, D., Protchenko, O., Shakoury-Elizeh, M., and Philpott, C. C. (2017) PCBP1 and NCOA4 regulate erythroid iron storage and heme biosynthesis. *J. Clin. Invest.* 10.1172/JCI90519

31. Shaw, G. C., Cope, J. J., Li, L., Corson, K., Hersey, C., Ackermann, G. E., Gwynn, B., Lambert, A. J., Wingert, R. a, Traver, D., Trede, N. S., Barut, B. a, Zhou, Y., Minet, E., Donovan, A., Brownlie, A., Balzan, R., Weiss, M. J., Peters, L. L., Kaplan, J., Zon, L. I., and Paw, B. H. (2006) Mitoferrin is essential for erythroid iron assimilation. *Nature*. **440**, 96–100

32. Troadec, M.-B. B., Warner, D., Wallace, J., Thomas, K., Spangrude, G. J., Phillips, J., Khalimonchuk, O., Paw, B. H., Ward, D. M., and Kaplan, J. (2011) Targeted deletion of the mouse Mitoferrin1 gene: from anemia to protoporphyria. *Blood*. **117**, 5494–502

33. Das, A., Nag, S., Mason, A. B., and Barroso, M. M. (2016) Endosome–mitochondria interactions are modulated by iron release from transferrin. *J. Cell Biol.* **214**, 831-845

34. Rouault, T. A. (2006) The role of iron regulatory proteins in mammalian iron homeostasis and disease. *Nat Chem Biol*. **2**, 406–414

35. Moroishi, T., Nishiyama, M., Takeda, Y., Iwai, K., and Nakayama, K. I. (2011) The FBXL5-IRP2 Axis Is Integral to Control of Iron Metabolism In Vivo. *Cell Metab.* **14**, 339–351

36. Reichard, J. F., Motz, G. T., and Puga, A. (2007) Heme oxygenase-1 induction by NRF2 requires inactivation of the transcriptional repressor BACH1. *Nucleic Acids Res.* **35**, 7074–7086

37. Fujita, H., and Sassa, S. (1989) The rapid and decremental change in haem oxygenase mRNA during erythroid differentiation of murine erythroleukaemia cells. *Br. J. Haematol.* **73**, 557–560

38. Garcia-Santos, D., Schranzhofer, M., Horvathova, M., Jaberi, M. M., Bogo Chies, J.

A., Sheftel, A. D., and Ponka, P. (2014) Heme oxygenase 1 is expressed in murine erythroid cells where it controls the level of regulatory heme. *Blood*. **123**, 2269–2277

39. Hintze, K. J., and Theil, E. C. (2005) DNA and mRNA elements with complementary responses to hemin, antioxidant inducers, and iron control ferritin-L expression. *Proc. Natl. Acad. Sci. U. S. A.* **102**, 15048–15052

40. McEwen, E., Kedersha, N., Song, B., Scheuner, D., Gilks, N., Han, A., Chen, J.-J., Anderson, P., and Kaufman, R. J. (2005) Heme-regulated Inhibitor Kinase-mediated Phosphorylation of Eukaryotic Translation Initiation Factor 2 Inhibits Translation, Induces Stress Granule Formation, and Mediates Survival upon Arsenite Exposure. *J. Biol. Chem.* . **280**, 16925–16933

41. Han, A.-P., Yu, C., Lu, L., Fujiwara, Y., Browne, C., Chin, G., Fleming, M., Leboulch, P., Orkin, S. H., and Chen, J.-J. (2001) Heme-regulated eIF2α kinase (HRI) is required for translational regulation and survival of erythroid precursors in iron deficiency. *EMBO J.* **20**, 6909–6918

42. Khan, A. a, and Quigley, J. G. (2011) Control of intracellular heme levels: heme transporters and heme oxygenases. *Biochim. Biophys. Acta*. **1813**, 668–82

43. Guernsey, D. L., Jiang, H., Campagna, D. R., Evans, S. C., Ferguson, M., Kellogg, M. D., Lachance, M., Matsuoka, M., Nightingale, M., Rideout, A., Saint-Amant, L., Schmidt, P. J., Orr, A., Bottomley, S. S., Fleming, M. D., Ludman, M., Dyack, S., Fernandez, C. V, and Samuels, M. E. (2009) Mutations in mitochondrial carrier family gene SLC25A38 cause nonsyndromic autosomal recessive congenital sideroblastic anemia. *Nat. Genet.* **41**, 651–653

44. Fernández-Murray, J. P., Prykhozhij, S. V, Dufay, J. N., Steele, S. L., Gaston, D., Nasrallah, G. K., Coombs, A. J., Liwski, R. S., Fernandez, C. V, Berman, J. N., and McMaster, C. R. (2016) Glycine and Folate Ameliorate Models of Congenital Sideroblastic Anemia. *PLOS Genet.*

45. Krishnamurthy, P. C., Du, G., Fukuda, Y., Sun, D., Sampath, J., Mercer, K. E., Wang, J., Sosa-Pineda, B., Murti, K. G., and Schuetz, J. D. (2006) Identification of a mammalian mitochondrial porphyrin transporter. *Nature*. **443**, 586–589

46. Ulrich, D. L., Lynch, J., Wang, Y., Fukuda, Y., Nachagari, D., Du, G., Sun, D., Fan, Y., Tsurkan, L., Potter, P. M., Rehg, J. E., and Schuetz, J. D. (2012) ATP-dependent Mitochondrial Porphyrin Importer ABCB6 Protects against Phenylhydrazine Toxicity. *J. Biol. Chem.* . **287**, 12679–12690

47. Wang, L., He, F., Bu, J., Liu, X., Du, W., Dong, J., Cooney, J. D., Dubey, S. K., Shi, Y., Gong, B., Li, J., McBride, P. F., Jia, Y., Lu, F., Soltis, K. A., Lin, Y., Namburi, P., Liang, C., Sundaresan, P., Paw, B. H., Li, D. Y., Phillips, J. D., and Yang, Z. (2012) ABCB6 Mutations Cause Ocular Coloboma. *Am. J. Hum. Genet.* **90**, 40–48

48. Kiss, K., Brozik, A., Kucsma, N., Toth, A., Gera, M., Berry, L., Vallentin, A., Vial, H., Vidal, M., and Szakacs, G. (2012) Shifting the paradigm: The putative mitochondrial protein ABCB6 resides in the lysosomes of cells and in the plasma membrane of erythrocytes. *PLoS One*.

49. Transport, C. I. (2010) Iron and Porphyrin Trafficking in Heme Biogenesis *. **285**, 26753–26759

50. Liesa, M., Qiu, W., and Shirihai, O. S. (2012) Mitochondrial ABC transporters function: The role of ABCB10 (ABC-me) as a novel player in cellular handling of reactive oxygen species. *Biochim. Biophys. Acta - Mol. Cell Res.* **1823**, 1945–1957

51. Chen, W., Dailey, H. A., and Paw, B. H. (2010) Ferrochelatase forms an oligomeric complex with mitoferrin-1 and Abcb10 for erythroid heme biosynthesis. *Blood*. **116**, 628-630

52. Quigley, J. G., Yang, Z., Worthington, M. T., Phillips, J. D., Sabo, K. M., Sabath, D. E., Berg, C. L., Sassa, S., Wood, B. L., and Abkowitz, J. L. (2004) Identification of a human heme exporter that is essential for erythropoiesis. *Cell*. **118**, 757–66

53. Keel, S. B., Doty, R. T., Yang, Z., Quigley, J. G., Chen, J., Knoblaugh, S., Kingsley, P. D., De Domenico, I., Vaughn, M. B., Kaplan, J., Palis, J., and Abkowitz, J. L. (2008) A heme export protein is required for red blood cell differentiation and iron homeostasis. *Sci. (New York, NY)*. **319**, 825–828

54. Chiabrando, D., Marro, S., Mercurio, S., Giorgi, C., Petrillo, S., Vinchi, F., Fiorito, V., Fagoonee, S., Camporeale, A., Turco, E., Merlo, G. R., Silengo, L., Altruda, F., Pinton, P., and Tolosano, E. (2012) The mitochondrial heme exporter FLVCR1b mediates erythroid differentiation. **122**, 4569–4579

55. Quigley, J. G., Burns, C. C., Anderson, M. M., Lynch, E. D., Sabo, K. M., Overbaugh, J., and Abkowitz, J. L. (2000) Cloning of the cellular receptor for feline leukemia virus subgroup C (FeLV-C), a retrovirus that induces red cell aplasia. *Blood*. **95**, 1093-1099

56. Yang, Z., Philips, J. D., Doty, R. T., Giraudi, P., Ostrow, J. D., Tiribelli, C., Smith, A., and Abkowitz, J. L. (2010) Kinetics and Specificity of Feline Leukemia Virus Subgroup C Receptor (FLVCR) Export Function and Its Dependence on Hemopexin. *J. Biol. Chem.* **285**, 28874–28882

57. Alves, L. R., Costa, E. S., Sorgine, M. H. F., Nascimento-Silva, M. C. L., Teodosio, C., B??rcena, P., Castro-Faria-Neto, H. C., Bozza, P. T. P. T., Orfao, A., Oliveira, P. L., Maya-Monteiro, C. M., Bárcena, P., Castro-Faria-Neto, H. C., Bozza, P. T. P. T., Orfao, A., Oliveira, P. L., and Maya-Monteiro, C. M. (2011) Heme-oxygenases during erythropoiesis in K562 and human bone marrow cells. *PLoS One*.

58. Krishnamurthy, P., and Schuetz, J. D. (2005) The ABC Transporter Abcg2/Bcrp: Role in Hypoxia Mediated Survival. *Biometals*. **18**, 349–358

59. Yamamoto, K., Suzu, S., Yoshidomi, Y., Hiyoshi, M., Harada, H., and Okada, S. (2007) Erythroblasts highly express the ABC transporter Bcrp1/ABCG2 but do not show the side population (SP) phenotype. *Immunol. Lett.* **114**, 52–8

60. Desuzinges-Mandon, E., Arnaud, O., Martinez, L., Huché, F., Di Pietro, A., and Falson, P. (2010) ABCG2 Transports and Transfers Heme to Albumin through Its Large Extracellular Loop. *J. Biol. Chem.* **285**, 33123–33133

61. Saison, C., Helias, V., Ballif, B. A., Peyrard, T., Puy, H., Miyazaki, T., Perrot, S., Vayssier-Taussat, M., Waldner, M., Le Pennec, P.-Y., Cartron, J.-P., and Arnaud, L. (2012) Null alleles of ABCG2 encoding the breast cancer resistance protein define the new blood group system Junior. *Nat Genet*. **44**, 174–177

62. Zelinski, T., Coghlan, G., Liu, X.-Q., and Reid, M. E. (2012) ABCG2 null alleles define the Jr(a-) blood group phenotype. *Nat Genet*. **44**, 131–132

63. Rao, A. U., Carta, L. K., Lesuisse, E., and Hamza, I. (2005) Lack of heme synthesis in a free-living eukaryote. *Proc. Natl. Acad. Sci. U. S. A.* **102**, 4270–4275

64. Korolnek, T., Zhang, J., Beardsley, S., Scheffer, G. L. L., and Hamza, I. (2014) Control of metazoan heme homeostasis by a conserved multidrug resistance protein. *Cell Metab.* **19**, 1008–1019

65. Shayeghi, M., Latunde-Dada, G. O., Oakhill, J. S., Laftah, A. H., Takeuchi, K., Halliday, N., Khan, Y., Warley, A., McCann, F. E., Hider, R. C., Frazer, D. M., Anderson, G. J., Vulpe, C. D., Simpson, R. J., and McKie, A. T. (2005) Identification of an Intestinal Heme Transporter. *Cell*. **122**, 789–801

66. Le Blanc, S., Garrick, M. D., and Arredondo, M. (2012) Heme carrier protein 1 transports heme and is involved in heme-Fe metabolism. *AJP Cell Physiol.* **302**, 1780–1785

67. Salojin, K. V, Cabrera, R. M., Sun, W., Chang, W. C., Lin, C., Duncan, L., Platt, K. A., Read, R., Vogel, P., Liu, Q., Finnell, R. H., and Oravecz, T. (2011) A mouse model of hereditary folate malabsorption: deletion of the PCFT gene leads to systemic folate deficiency. *Blood*

68. Laftah, A. H., Latunde-Dada, G. O., Fakih, S., Hider, R. C., Simpson, R. J., and

McKie, A. T. (2008) Haem and folate transport by proton-coupled folate transporter/haem carrier protein 1 (SLC46A1). *Br. J. Nutr.* **101**, 1150–1156

69. Rajagopal, A., Rao, A. U., Amigo, J., Tian, M., Upadhyay, S. K., Hall, C., Uhm, S., Mathew, M. K., Fleming, M. D., Paw, B. H., Krause, M., and Hamza, I. (2008) Haem homeostasis is regulated by the conserved and concerted functions of HRG-1 proteins. *Nature*. **453**, 1127–31

70. O'Callaghan, K. M., Ayllon, V., O'Keeffe, J., Wang, Y., Cox, O. T., Loughran, G., Forgac, M., and O'Connor, R. (2010) Heme-binding Protein HRG-1 Is Induced by Insulin-like Growth Factor I and Associates with the Vacuolar H(+)-ATPase to Control Endosomal pH and Receptor Trafficking. *J. Biol. Chem.* **285**, 381–391

71. An, X., Schulz, V. P., Li, J., Wu, K., Liu, J., Xue, F., Hu, J., Mohandas, N., and Gallagher, P. G. (2014) Global transcriptome analyses of human and murine terminal erythroid differentiation Global Transcriptome Analyses of Human and Murine Terminal Erythroid Differentiation. **123**, 3466–3478

72. de Back, D. Z., Kostova, E. B., van Kraaij, M., van den Berg, T. K., and van Bruggen, R. (2014) Of macrophages and red blood cells; A complex love story. *Front. Physiol.*

73. Korolnek, T., and Hamza, I. (2015) Macrophages and iron trafficking at the birth and death of red cells. *Blood.* **125**, 2893–2897

74. Palis, J. (2014) Primitive and definitive erythropoiesis in mammals. *Front. Physiol.*

75. An, X., and Mohandas, N. (2011) Erythroblastic islands, terminal erythroid differentiation and reticulocyte maturation. *Int. J. Hematol.* **93**, 139–143

76. YOKOYAMA, T., KITAGAWA, H., TAKEUCHI, T., TSUKAHARA, S., and KANNAN, Y. (2002) No Apoptotic Cell Death of Erythroid Cells of Erythroblastic Islands in Bone Marrow of Healthy Rats. *J. Vet. Med. Sci.* **64**, 913–919

77. S. H. LEE, P. R. CROCKER, S. WESTABY, N.Key, D. Y. M. (1988) Isolation and immunocytochemical characterization of human bone marrow stromal macrophages in

hemopoietic clusters. *J. Exp. Med.* **168**, 1193–1198

78. Fraser, S. T., Midwinter, R. G., Coupland, L. A., Kong, S., Berger, B. S., Yeo, J. H., Andrade, O. C., Cromer, D., Suarna, C., Lam, M., Maghzal, G. J., Chong, B. H., Parish, C. R., and Stocker, R. (2015) Heme oxygenase-1 deficiency alters erythroblastic Island formation, steady-state erythropoiesis and red blood cell lifespan in mice. *Haematologica*. **100**, 601–610

79. Giger, K. M., and Kalfa, T. A. (2015) Phylogenetic and Ontogenetic View of Erythroblastic Islands. *Biomed Res. Int.* 10.1155/2015/873628

80. McGrath, K. E., Kingsley, P. D., Koniski, A., Porter, R. L., Bushnell, T. P., and Palis, J. (2015) Enucleation of Primitive Erythroid Cells Generates a Transient Population of "Pyrenocytes" in the Mammalian Fetus. *Blood*. **110**, 425-425

81. Rhodes, M. M., Kopsombut, P., Bondurant, M. C., Price, J. O., and Koury, M. J. (2008) Adherence to macrophages in erythroblastic islands enhances erythroblast proliferation and increases erythrocyte production by a different mechanism than erythropoietin. *Blood*. **111**, 1700–1708

82. Leimberg, M. J., Prus, E., Konijn, A. M., and Fibach, E. (2008) Macrophages function as a ferritin iron source for cultured human erythroid precursors. *J. Cell. Biochem.* **103**, 1211–1218

83. Shemin, D., and Rittenberg, D. (1946) THE LIFE SPAN OF THE HUMAN RED BLOOD CELL. *J. Biol. Chem.* . **166**, 627–636

84. VAN PUTTEN, L. M., and Croon, F. (1958) The Life Span of Red Cells in the Rat and the Mouse as Determined by Labeling with DFP³² in Vivo. *Blood*. **13**, 789-794

85. Poss, K. D., and Tonegawa, S. (1997) Heme oxygenase 1 is required for mammalian iron reutilization. *Proc. Natl. Acad. Sci. U. S. A.* **94**, 10919–10924

86. Kovtunovych, G., Eckhaus, M. A., Ghosh, M. C., Ollivierre-Wilson, H., and Rouault,

T. A. (2010) Dysfunction of the heme recycling system in heme oxygenase 1–deficient mice: effects on macrophage viability and tissue iron distribution. *Blood.* **116**, 6054–6062

87. Soe-Lin, S., Apte, S. S., Andriopoulos, B., Andrews, M. C., Schranzhofer, M., Kahawita, T., Garcia-Santos, D., and Ponka, P. (2009) Nramp1 promotes efficient macrophage recycling of iron following erythrophagocytosis in vivo. *Proc. Natl. Acad. Sci. U. S. A.* **106**, 5960–5965

88. Yoshida, T., and Sato, M. (1989) Posttranslational and direct integration of heme oxygenase into microsomes. *Biochem. Biophys. Res. Commun.* **163**, 1086–1092

89. Gottlieb, Y., Truman, M., Cohen, L. A., Leichtmann-Bardoogo, Y., and Meyron-Holtz, E. G. (2012) Endoplasmic reticulum anchored heme-oxygenase 1 faces the cytosol. *Haematologica*. **97**, 1489–1493

90. Liu, Y., Ortiz de Montellano, P. R., Yoshida, T., and Sato, M. (2000) Reaction Intermediates and Single Turnover Rate Constants for the Oxidation of Heme by Human Heme Oxygenase-1. *J. Biol. Chem.* . **163**, 1086–1092

91. Delaby, C., Rondeau, C., Pouzet, C. C., Willemetz, A., Pilard, N., Desjardins, M., and Canonne-Hergaux, F. F. (2012) Subcellular localization of iron and heme metabolism related proteins at early stages of erythrophagocytosis. *PLoS One*.

92. White, C., Yuan, X., Schmidt, P. J., Bresciani, E., Samuel, T. K., Campagna, D., Hall, C., Bishop, K., Calicchio, M. L., Lapierre, A., Ward, D. M., Liu, P., Fleming, M. D., and Hamza, I. (2013) HRG1 is essential for heme transport from the phagolysosome of macrophages during erythrophagocytosis. *Cell Metab.* **17**, 261–270

93. Theurl, I., Hilgendorf, I., Nairz, M., Tymoszuk, P., Haschka, D., Asshoff, M., He, S., Gerhardt, L. M. S., Holderried, T. A. W., Seifert, M., Sopper, S., Fenn, A. M., Anzai, A., Rattik, S., McAlpine, C., Theurl, M., Wieghofer, P., Iwamoto, Y., Weber, G. F., Harder, N. K., Chousterman, B. G., Arvedson, T. L., McKee, M., Wang, F., Lutz, O.

M. D., Rezoagli, E., Babitt, J. L., Berra, L., Prinz, M., Nahrendorf, M., Weiss, G., Weissleder, R., Lin, H. Y., and Swirski, F. K. (2016) On-demand erythrocyte disposal and iron recycling requires transient macrophages in the liver. *Nat. Med.* **22**, 945–951

94. Kohyama, M., Ise, W., Edelson, B. T., Wilker, P. R., Hildner, K., Mejia, C., Frazier, W. A., Murphy, T. L., and Murphy, K. M. (2009) Critical role for Spi-C in the development of red pulp macrophages and splenic iron homeostasis. *Nature*. **457**, 318–321

95. Haldar, M., Kohyama, M., So, A. Y.-L., Kc, W., Wu, X., Briseño, C. G., Satpathy, A. T., Kretzer, N. M., Arase, H., Rajasekaran, N. S., Wang, L., Egawa, T., Igarashi, K., Baltimore, D., Murphy, T. L., and Murphy, K. M. (2014) Heme-mediated SPI-C induction promotes monocyte differentiation into iron-recycling macrophages. *Cell*. **156**, 1223–1234

96. Lieschke, G. J., and Currie, P. D. (2007) Animal models of human disease: zebrafish swim into view. *Nat Rev Genet*. **8**, 353–367

97. Davidson, A. J., and Zon, L. I. The /`definitive/' (and /`primitive/') guide to zebrafish hematopoiesis. *Oncogene*. **23**, 7233–7246

98. Galloway, J. L., and Zon, L. I. (2003) 3 Ontogeny of hematopoiesis: Examining the emergence of hematopoietic cells in the vertebrate embryo (Biology, B. T.-C. T. in D. ed), pp. 139–158, Academic Press, Volume **53**, 139–158

99. Ransom, D. G., Haffter, P., Odenthal, J., Brownlie, a, Vogelsang, E., Kelsh, R. N., Brand, M., van Eeden, F. J., Furutani-Seiki, M., Granato, M., Hammerschmidt, M., Heisenberg, C. P., Jiang, Y. J., Kane, D. a, Mullins, M. C., and Nüsslein-Volhard, C. (1996) Characterization of zebrafish mutants with defects in embryonic hematopoiesis. *Development*. **123**, 311–319

100. Jill L.O. de Jong and Leonard I. Zon (2005) Use of the Zebrafish System to Study Primitive and Definitive Hematopoiesis. *Annu. Rev. Genet.* **39**, 481–501

101. Lyons, S. E., Lawson, N. D., Lei, L., Bennett, P. E., Weinstein, B. M., and Liu, P. P. (2002) A nonsense mutation in zebrafish gata1 causes the bloodless phenotype in vlad tepes. *Proc. Natl. Acad. Sci.* . **99**, 5454–5459

102. Long, Q., Meng, a, Wang, H., Jessen, J. R., Farrell, M. J., and Lin, S. (1997) GATA-1 expression pattern can be recapitulated in living transgenic zebrafish using GFP reporter gene. *Development*. **124**, 4105–4111

103. Cumano, A. and I. G. (2007) Ontogeny of the Hematopoietic System. *Annu. Rev. Immunol.* **25**, 745–785

104. Burns, C. E., DeBlasio, T., Zhou, Y., Zhang, J., Zon, L., and Nimer, S. D. (2002) Isolation and characterization of runxa and runxb, zebrafish members of the runt family of transcriptional regulators. *Exp. Hematol.* **30**, 1381–1389

105. Willett, C. E., Cortes, A., Zuasti, A., and Zapata, A. G. (1999) Early hematopoiesis and developing lymphoid organs in the zebrafish. *Dev. Dyn.* **214**, 323–336

106. Murayama, E., Kissa, K., Zapata, A., Mordelet, E., Briolat, V., Lin, H.-F., Handin, R. I., and Herbomel, P. (2006) Tracing Hematopoietic Precursor Migration to Successive Hematopoietic Organs during Zebrafish Development. *Immunity*. **25**, 963–975

107. Jin, H., Xu, J., and Wen, Z. (2007) Migratory path of definitive hematopoietic stem/progenitor cells during zebrafish development. *Blood*. **109**, 5208-5214

108. Liao, E. C., Trede, N. S., Ransom, D., Zapata, A., Kieran, M., and Zon, L. I. (2002) Non-cell autonomous requirement for the bloodless gene in primitive hematopoiesis of zebrafish. *Development*. **129**, 649-659

109. Chan, F.-Y., Robinson, J., Brownlie, A., Shivdasani, R. A., Donovan, A., Brugnara, C., Kim, J., Lau, B.-C., Witkowska, H. E., and Zon, L. I. (1997) Characterization of Adult α- and β-Globin Genes in the Zebrafish. *Blood*. **89**, 688-700

110. Brownlie, A., Hersey, C., Oates, A. C., Paw, B. H., Falick, A. M., Witkowska, H. E., Flint, J., Higgs, D., Jessen, J., Bahary, N., Zhu, H., Lin, S., and Zon, L. (2003)

Characterization of embryonic globin genes of the zebrafish. *Dev. Biol.* **255**, 48–61

111. Traver, D., Paw, B. H., Poss, K. D., Penberthy, W. T., Lin, S., and Zon, L. I. (2003) Transplantation and in vivo imaging of multilineage engraftment in zebrafish bloodless mutants. *Nat Immunol*. **4**, 1238–1246

112. Traver, D., Winzeler, A., Stern, H. M., Mayhall, E. A., Langenau, D. M., Kutok, J. L., Look, A. T., and Zon, L. I. (2004) Effects of lethal irradiation in zebrafish and rescue by hematopoietic cell transplantation. *Blood*. **104**, 1298-1305

113. Carradice, D., and Lieschke, G. J. (2008) Zebrafish in hematology: sushi or science? *Blood*. **111**, 3331–3342

114. Lieschke, G. J., Oates, A. C., Crowhurst, M. O., Ward, A. C., and Layton, J. E. (2001) Morphologic and functional characterization of granulocytes and macrophages in embryonic and adult zebrafish. *Blood*. **98**, 3087-3096

115. Menke, A. L., Spitsbergen, J. M., Wolterbeek, A. P. M., and Woutersen, R. a (2011) Normal anatomy and histology of the adult zebrafish. *Toxicol. Pathol.* **39**, 759–775

116. Howe, K., Clark, M. D., Torroja, C. F., Torrance, J., Berthelot, C., Muffato, M., Collins, J. E., Humphray, S., McLaren, K., Matthews, L., McLaren, S., Sealy, I., Caccamo, M., Churcher, C., Scott, C., Barrett, J. C., Koch, R., Rauch, G.-J., White, S., Chow, W., Kilian, B., Quintais, L. T., Guerra-Assunção, J. a, Zhou, Y., Gu, Y., Yen, J., Vogel, J.-H., Eyre, T., Redmond, S., Banerjee, R., Chi, J., Fu, B., Langley, E., Maguire, S. F., Laird, G. K., Lloyd, D., Kenyon, E., Donaldson, S., Sehra, H., Almeida-King, J., Loveland, J., Trevanion, S., Jones, M., Quail, M., Willey, D., Hunt, A., Burton, J., Sims, S., McLay, K., Plumb, B., Davis, J., Clee, C., Oliver, K., Clark, R., Riddle, C., Elliot, D., Eliott, D., Threadgold, G., Harden, G., Ware, D., Mortimore, B., Mortimer, B., Kerry, G., Heath, P., Phillimore, B., Tracey, A., Corby, N., Dunn, M., Johnson, C., Wood, J., Clark, S., Pelan, S., Griffiths, G., Smith, M., Glithero, R., Howden, P., Barker, N., Stevens, C., Harley, J., Holt, K., Panagiotidis, G., Lovell, J.,

Beasley, H., Henderson, C., Gordon, D., Auger, K., Wright, D., Collins, J., Raisen, C., Dyer, L., Leung, K., Robertson, L., Ambridge, K., Leongamornlert, D., McGuire, S., Gilderthorp, R., Griffiths, C., Manthravadi, D., Nichol, S., Barker, G., Whitehead, S., Kay, M., Brown, J., Murnane, C., Gray, E., Humphries, M., Sycamore, N., Barker, D., Saunders, D., Wallis, J., Babbage, A., Hammond, S., Mashreghi-Mohammadi, M., Barr, L., Martin, S., Wray, P., Ellington, A., Matthews, N., Ellwood, M., Woodmansey, R., Clark, G., Cooper, J. D., Cooper, J., Tromans, A., Grafham, D., Skuce, C., Pandian, R., Andrews, R., Harrison, E., Kimberley, A., Garnett, J., Fosker, N., Hall, R., Garner, P., Kelly, D., Bird, C., Palmer, S., Gehring, I., Berger, A., Dooley, C. M., Ersan-Ürün, Z., Eser, C., Geiger, H., Geisler, M., Karotki, L., Kirn, A., Konantz, J., Konantz, M., Oberländer, M., Rudolph-Geiger, S., Teucke, M., Osoegawa, K., Zhu, B., Rapp, A., Widaa, S., Langford, C., Yang, F., Carter, N. P., Harrow, J., Ning, Z., Herrero, J., Searle, S. M. J., Enright, A., Geisler, R., Plasterk, R. H. a, Lee, C., Westerfield, M., de Jong, P. J., Zon, L. I., Postlethwait, J. H., Nüsslein-Volhard, C., Hubbard, T. J. P., Roest Crollius, H., Rogers, J., Stemple, D. L., Begum, S., Lloyd, C., Lanz, C., Raddatz, G., and Schuster, S. C. (2013) The zebrafish reference genome sequence and its relationship to the human genome. *Nature*. **496**, 498–503

117. Driever, W., Solnica-Krezel, L., Schier, A. F., Neuhauss, S. C., Malicki, J., Stemple, D. L., Stainier, D. Y., Zwartkruis, F., Abdelilah, S., Rangini, Z., Belak, J., and Boggs, C. (1996) A genetic screen for mutations affecting embryogenesis in zebrafish. *Development*. **123**, 37-46

118. Sumanas, S., and Larson, J. D. (2002) Morpholino phosphorodiamidate oligonucleotides in zebrafish: a recipe for functional genomics? *Brief. Funct. Genomic. Proteomic.* **1**, 239–256

119. Huang, P., Xiao, A., Zhou, M., Zhu, Z., Lin, S., and Zhang, B. (2011) Heritable gene

targeting in zebrafish using customized TALENs. *Nat. Biotechnol.* **29**, 699–700

120. Jao, L.-E., Wente, S. R., and Chen, W. (2013) Efficient multiplex biallelic zebrafish genome editing using a CRISPR nuclease system. *Proc. Natl. Acad. Sci. U. S. A.* **110**, 13904–13909

121. Brownlie, a, Donovan, a, Pratt, S. J., Paw, B. H., Oates, a C., Brugnara, C., Witkowska, H. E., Sassa, S., and Zon, L. I. (1998) Positional cloning of the zebrafish sauternes gene: a model for congenital sideroblastic anaemia. *Nat. Genet.* **20**, 244–250

122. Kardon, J. R., Yien, Y. Y., Huston, N. C., Branco, D. S., Hildick-Smith, G. J., Rhee, K. Y., Paw, B. H., and Baker, T. A. (2015) Mitochondrial ClpX activates a key enzyme for heme biosynthesis and erythropoiesis. *Cell*. **161**, 858–867

123. Sakamoto, D., Kudo, H., Inohaya, K., Yokoi, H., Narita, T., Naruse, K., Mitani, H., Araki, K., Shima, A., Ishikawa, Y., Imai, Y., and Kudo, A. (2004) A mutation in the gene for delta-aminolevulinic acid dehydratase (ALAD) causes hypochromic anemia in the medaka, Oryzias latipes. *Mech. Dev.* **121**, 747–752

124. Noguchi, C. T., and Schechter, A. N. (1981) The intracellular polymerization of sickle hemoglobin and its relevance to sickle cell disease. *Blood*. **58**, 1057 LP-1068

125. Wang, H., Long, Q., Marty, S. D., Sassa, S., and Lin, S. (1998) A zebrafish model for hepatoerythropoietic porphyria. *Nat. Genet.* **20**, 239–243

126. Childs, S., Weinstein, B. M., Mohideen, M. a, Donohue, S., Bonkovsky, H., and Fishman, M. C. (2000) Zebrafish dracula encodes ferrochelatase and its mutation provides a model for erythropoietic protoporphyria. *Curr. Biol.* **10**, 1001–1004

127. Wingert, R. a, Galloway, J. L., Barut, B., Foott, H., Fraenkel, P., Axe, J. L., Weber, G. J., Dooley, K., Davidson, A. J., Schmid, B., Paw, B. H., Shaw, G. C., Kingsley, P., Palis, J., Schubert, H., Chen, O., Kaplan, J., and Zon, L. I. (2005) Deficiency of glutaredoxin 5 reveals Fe-S clusters are required for vertebrate haem synthesis. *Nature*. **436**, 1035–1039

128. Rodríguez-Manzaneque, M. T., Tamarit, J., Bellí, G., Ros, J., and Herrero, E. (2002) Grx5 Is a Mitochondrial Glutaredoxin Required for the Activity of Iron/Sulfur Enzymes. *Mol. Biol. Cell*. **13**, 1109–1121

129. Camaschella, C., Campanella, A., De Falco, L., Boschetto, L., Merlini, R., Silvestri, L., Levi, S., and Iolascon, A. (2007) The human counterpart of zebrafish shiraz shows sideroblastic-like microcytic anemia and iron overload. *Blood*. **110**, 1353–1358

130. Chung, J., Anderson, S. A., Gwynn, B., Deck, K. M., Chen, M. J., Langer, N. B., Shaw, G. C., Huston, N. C., Boyer, L. F., Datta, S., Paradkar, P. N., Li, L., Wei, Z., Lambert, A. J., Sahr, K., Wittig, J. G., Chen, W., Lu, W., Galy, B., Schlaeger, T. M., Hentze, M. W., Ward, D. M., Kaplan, J., Eisenstein, R. S., Peters, L. L., and Paw, B. H. (2014) Iron Regulatory Protein-1 Protects against Mitoferrin-1-deficient Porphyria. *J. Biol. Chem.* . **289**, 7835–7843

131. Fleming, M. D., Trenor III, C. C., Su, M. A., Foernzler, D., Beier, D. R., Dietrich, W. E., and Andrews, N. C. (1997) Microcytic anaemia mice have a mutation in Nramp2, a candidate iron transporter gene. *Nat. Genet.* **16**, 383–386

132. Donovan, A., Brownlie, A., Dorschner, M. O., Zhou, Y., Pratt, S. J., Paw, B. H., Phillips, R. B., Thisse, C., Thisse, B., and Zon, L. I. (2002) The zebrafish mutant gene chardonnay (cdy) encodes divalent metal transporter 1 (DMT1). *Blood*. **100**, 4655–4659

133. Mims, M. P., Guan, Y., Pospisilova, D., Priwitzerova, M., Indrak, K., Ponka, P., Divoky, V., and Prchal, J. T. (2005) Identification of a human mutation of DMT1 in a patient with microcytic anemia and iron overload. *Blood*. **105**, 1337–1342

134. Donovan, a, Brownlie, a, Zhou, Y., Shepard, J., Pratt, S. J., Moynihan, J., Paw, B. H., Drejer, a, Barut, B., Zapata, a, Law, T. C., Brugnara, C., Lux, S. E., Pinkus, G. S., Pinkus, J. L., Kingsley, P. D., Palis, J., Fleming, M. D., Andrews, N. C., and Zon, L. I. (2000) Positional cloning of zebrafish ferroportin1 identifies a conserved vertebrate

iron exporter. *Nature*. **403**, 776–781

135. Fraenkel, P. G., Traver, D., Donovan, A., Zahrieh, D., and Zon, L. I. (2005) Ferroportin1 is required for normal iron cycling in zebrafish. *J. Clin. Invest.* **115**, 1532–1541

136. Donovan, A., Lima, C. A., Pinkus, J. L., Pinkus, G. S., Zon, L. I., Robine, S., and Andrews, N. C. (2005) The iron exporter ferroportin/Slc40a1 is essential for iron homeostasis. *Cell Metab.* **1**, 191–200

137. Fraenkel, P. G., Gibert, Y., Holzheimer, J. L., Lattanzi, V. J., Burnett, S. F., Dooley, K. A., Wingert, R. A., and Zon, L. I. (2009) Transferrin-a modulates hepcidin expression in zebrafish embryos. *Blood*. **113**, 2843–2850

138. Goldwurm, S., Casati, C., Venturi, N., Strada, S., Santambrogio, P., Indraccolo, S., Arosio, P., Cazzola, M., Piperno, A., Masera, G., and Blondi, A. (2000) Biochemical and genetic defects underlying human congenital hypotransferrinemia. *Hematol. J.* **1**, 390–398

139. Wingert, R. a, Brownlie, A., Galloway, J. L., Dooley, K., Fraenkel, P., Axe, J. L., Davidson, A. J., Barut, B., Noriega, L., Sheng, X., Zhou, Y., and Zon, L. I. (2004) The chianti zebrafish mutant provides a model for erythroid-specific disruption of transferrin receptor 1. *Development*. **131**, 6225–6235

140. Postlethwait, J. H., Yan, Y.-L. L., Gates, M. a, Horne, S., Amores, A., Brownlie, A., Donovan, A., Egan, E. S., Force, A., Gong, Z., Goutel, C., Fritz, A., Kelsh, R., Knapik, E., Liao, E., Paw, B., Ransom, D., Singer, A., Thomson, M., Abduljabbar, T. S., Yelick, P., Beier, D., Joly, J.-S. S., Larhammar, D., Rosa, F., Westerfield, M., Zon, L. I., Johnson, S. L., and Talbot, W. S. (1998) Vertebrate genome evolution and the zebrafish gene map. *Nat Genet*. **18**, 345–349

141. Amores, A., Force, A., Yan, Y.-L., Joly, L., Amemiya, C., Fritz, A., Ho, R. K., Langeland, J., Prince, V., Wang, Y.-L., Westerfield, M., Ekker, M., and Postlethwait,

J. H. (1998) Zebrafish hox Clusters and Vertebrate Genome Evolution. *Science (80-.).* **282**, 1711-1714

142. Levy, J. E., Jin, O., Fujiwara, Y., Kuo, F., and Andrews, N. C. (1999) Transferrin receptor is necessary for development of erythrocytes and the nervous system. *Nat. Genet.* **21**, 396–399

143. Mercurio, S., Petrillo, S., Chiabrando, D., Bassi, Z. I., Gays, D., Camporeale, A., Vacaru, A., Miniscalco, B., Valperga, G., Silengo, L., Altruda, F., Baron, M. H., Santoro, M. M., and Tolosano, E. (2015) The heme exporter Flvcr1 regulates expansion and differentiation of committed erythroid progenitors by controlling intracellular heme accumulation. *Haematologica*. **100**, 720–729

144. Byon, J. C. H., Chen, J., Doty, R. T., and Abkowitz, J. L. (2013) FLVCR is necessary for erythroid maturation, may contribute to platelet maturation, but is dispensable for normal hematopoietic stem cell function. *Blood*. **122**, 2903–2910

145. Doty, R. T., Phelps, S. R., Shadle, C., Sanchez-Bonilla, M., Keel, S. B., and Abkowitz, J. L. (2015) Coordinate expression of heme and globin is essential for effective erythropoiesis. *J. Clin. Invest.* **125**, 4681–4691

146. Cannon, J. E., Place, E. S., Eve, a M. J., Bradshaw, C. R., Sesay, a, Morrell, N. W., and Smith, J. C. (2013) Global analysis of the haematopoietic and endothelial transcriptome during zebrafish development. *Mech. Dev.* **130**, 122–131

147. Westerfield, M. (2000) *The zebrafish book. A guide for the laboratory use of zebrafish (Danio rerio)*, 4th Ed., Univ. of Oregon Press, Eugene

148. Thisse, C., and Thisse, B. (2008) High-resolution in situ hybridization to whole-mount zebrafish embryos. *Nat. Protoc.* **3**, 59–69

149. Gupta, T., and Mullins, M. C. (2010) Dissection of organs from the adult zebrafish. *J. Vis. Exp.* 10.3791/1717

150. Cermak, T., Doyle, E. L., Christian, M., Wang, L., Zhang, Y., Schmidt, C., Baller, J.

A., Somia, N. V., Bogdanove, A. J., and Voytas, D. F. (2011) Erratum: Efficient design and assembly of custom TALEN and other TAL effector-based constructs for DNA targeting (Nucleic Acids Research (2011) 39 (e82) DOI: 10.1093/nar/gkr218). *Nucleic Acids Res.* **39**, 7879

151. Wilkinson, R. N., Elworthy, S., Ingham, P. W., and van Eeden, F. J. M. (2013) A method for high-throughput PCR-based genotyping of larval zebrafish tail biopsies. *Biotechniques*. **55**, 314–316

152. Iuchi, I., and Yamamoto, M. (1983) Erythropoiesis in the developing rainbow trout, Salmo gairdneri irideus: histochemical and immunochemical detection of erythropoietic organs. *J. Exp. Zool.* **226**, 409–417

153. Lumsden, A. L., Henshall, T. L., Dayan, S., Lardelli, M. T., and Richards, R. I. (2007) Huntingtin-deficient zebrafish exhibit defects in iron utilization and development. *Hum. Mol. Genet.* **16**, 1905–1920

154. Manoli, M., and Driever, W. (2012) Fluorescence-activated cell sorting (FACS) of fluorescently tagged cells from zebrafish larvae for RNA isolation. *Cold Spring Harb. Protoc.* **7**, 879–886

155. Chen, C., Garcia-Santos, D., Ishikawa, Y., Seguin, A., Li, L., Fegan, K. H., Hildick-Smith, G. J., Shah, D. I., Cooney, J. D., Chen, W., King, M. J., Yien, Y. Y., Schultz, I. J., Anderson, H., Dalton, A. J., Freedman, M. L., Kingsley, P. D., Palis, J., Hattangadi, S. M., Lodish, H. F., Ward, D. M., Kaplan, J., Maeda, T., Ponka, P., and Paw, B. H. (2013) Snx3 regulates recycling of the transferrin receptor and iron assimilation. *Cell Metab.* **17**, 343–352

156. Protchenko, O., Shakoury-Elizeh, M., Keane, P., Storey, J., Androphy, R., and Philpott, C. C. (2008) Role of PUG1 in Inducible Porphyrin and Heme Transport in Saccharomyces cerevisiae . *Eukaryot. Cell* . **7**, 859–871

157. Protchenko, O., Rodriguez-Suarez, R., Androphy, R., Bussey, H., and Philpott, C. C.

(2006) A Screen for Genes of Heme Uptake Identifies the FLC Family Required for Import of FAD into the Endoplasmic Reticulum. *J. Biol. Chem.* . **281**, 21445–21457

158. Ito, H., Fukuda, Y., Murata, K., and Kimura, A. (1983) Transformation of intact yeast cells treated with alkali cations. *J. Bacteriol.* **153**, 163–168

159. Yuan, X., Protchenko, O., Philpott, C. C., and Hamza, I. (2012) Topologically conserved residues direct heme transport in HRG-1-related proteins. *J. Biol. Chem.* **287**, 4914–4924

160. Tadros, W., and Lipshitz, H. D. (2009) The maternal-to-zygotic transition: a play in two acts. *Dev.* . **136**, 3033–3042

161. Cade, L., Reyon, D., Hwang, W. Y., Tsai, S. Q., Patel, S., Khayter, C., Joung, J. K., Sander, J. D., Peterson, R. T., and Yeh, J.-R. J. (2012) Highly efficient generation of heritable zebrafish gene mutations using homo- and heterodimeric TALENs. *Nucleic Acids Res.* **40**, 8001–8010

162. Smith et al., 2006 (2015) High-throughput gene targeting and phenotyping in zebrafish using CRISPR / Cas9. 10.1101/gr.186379.114.

163. Robu, M. E., Larson, J. D., Nasevicius, A., Beiraghi, S., Brenner, C., Farber, S. A., and Ekker, S. C. (2007) P53 Activation By Knockdown Technologies. *PLoS Genet.* **3**, 787–801

164. Kaufman, C. K., White, R. M., and Zon, L. (2009) Chemical Genetic Screening in the Zebrafish Embryo. *Nat. Protoc.* **4**, 1422–1432

165. Ebert, P. S., Hess, R. A., Frykholm, B. C., and Tschudy, D. P. (1979) Succinylacetone, a potent inhibitor of heme biosynthesis: Effect on cell growth, heme content and δ-aminolevulinic acid dehydratase activity of malignant murine erythroleukemia cells. *Biochem. Biophys. Res. Commun.* **88**, 1382–1390

166. Chen, C., Samuel, T. K., Sinclair, J., Dailey, H. a, and Hamza, I. (2011) An intercellular heme-trafficking protein delivers maternal heme to the embryo during

development in C. elegans. *Cell*. **145**, 720–731

167. Bill, B. R., Petzold, A. M., Clark, K. J., Schimmenti, L. a, and Ekker, S. C. (2009) A primer for morpholino use in zebrafish. *Zebrafish*. **6**, 69–77

168. Schulte-Merker, S., and Stainier, D. Y. R. (2014) Out with the old, in with the new: reassessing morpholino knockdowns in light of genome editing technology. *Development*. **141**, 3103–3104

169. Kok, F. O., Shin, M., Ni, C. W., Gupta, A., Grosse, A. S., vanImpel, A., Kirchmaier, B. C., Peterson-Maduro, J., Kourkoulis, G., Male, I., DeSantis, D. F., Sheppard-Tindell, S., Ebarasi, L., Betsholtz, C., Schulte-Merker, S., Wolfe, S. A., and Lawson, N. D. (2015) Reverse genetic screening reveals poor correlation between morpholino-induced and mutant phenotypes in zebrafish. *Dev. Cell*. **32**, 97–108

170. Kettleborough, R. N. W., Busch-Nentwich, E. M., Harvey, S. a, Dooley, C. M., de Bruijn, E., van Eeden, F., Sealy, I., White, R. J., Herd, C., Nijman, I. J., Fényes, F., Mehroke, S., Scahill, C., Gibbons, R., Wali, N., Carruthers, S., Hall, A., Yen, J., Cuppen, E., and Stemple, D. L. (2013) A systematic genome-wide analysis of zebrafish protein-coding gene function. *Nature*. **496**, 494–497

171. Rossi, A., Kontarakis, Z., Gerri, C., Nolte, H., Hölper, S., Krüger, M., and Stainier, D. Y. R. (2015) Genetic compensation induced by deleterious mutations but not gene knockdowns. *Nature*. **Aug 13**, 230–233

172. Eve, A. M. J., Place, E. S., and Smith, J. C. (2017) Comparison of Zebrafish tmem88a mutant and morpholino knockdown phenotypes. *PLoS One*.

173. NCBI Resource Coordinators (2015) Database resources of the National Center for Biotechnology Information. *Nucleic Acids Res.* **43**, 6–17

174. Franken, L., Klein, M., Spasova, M., Elsukova, A., Wiedwald, U., Welz, M., Knolle, P., Farle, M., Limmer, A., and Kurts, C. (2015) Splenic red pulp macrophages are intrinsically superparamagnetic and contaminate magnetic cell isolates. *Nat. Publ. Gr.*

10.1038/srep12940

175. de Jong, J. L. O., and Zon, L. I. (2012) Histocompatibility and hematopoietic transplantation in the zebrafish. *Adv. Hematol.*

176. Esteban, M. Á., Cuesta, A., Chaves-Pozo, E., and Meseguer, J. (2015) Phagocytosis in Teleosts. Implications of the New Cells Involved. *Biology (Basel).* **4**, 907–22

177. Tschopp, J., Martinon, F., and Burns, K. (2003) NALPs: a novel protein family involved in inflammation. *Nat Rev Mol Cell Biol*. **4**, 95–104

178. Campbell, M. R., Karaca, M., Adamski, K. N., Chorley, B. N., Wang, X., and Bell, D. A. (2013) Novel hematopoietic target genes in the NRF2-Mediated transcriptional pathway. *Oxid. Med. Cell. Longev.*

179. Kanehisa, M., Araki, M., Goto, S., Hattori, M., Hirakawa, M., Itoh, M., Katayama, T., Kawashima, S., Okuda, S., Tokimatsu, T., and Yamanishi, Y. (2008) KEGG for linking genomes to life and the environment. *Nucleic Acids Res.* **36**, 480–484

180. McReynolds, L. J., Tucker, J., Mullins, M. C., and Evans, T. (2008) Regulation of hematopoiesis by the BMP signaling pathway in adult zebrafish. *Exp. Hematol.* **36**, 1604–1615

181. Shafizadeh, E., Paw, B. H., Foott, H., Liao, E. C., Barut, B. A., Cope, J. J., Zon, L. I., and Lin, S. (2002) Characterization of zebrafish merlot/chablis as non-mammalian vertebrate models for severe congenital anemia due to protein 4.1 deficiency. *Development*. **129**, 4359–4370

182. Borst, P., de Wolf, C., and van de Wetering, K. (2007) Multidrug resistance-associated proteins 3, 4, and 5. *Pflügers Arch. - Eur. J. Physiol.* **453**, 661–673

183. Ivanovski, O., Kulkeaw, K., Nakagawa, M., Sasaki, T., Mizuochi, C., Horio, Y., Ishitani, T., and Sugiyama, D. (2009) Characterization of kidney marrow in zebrafish (Danio rerio) by using a new surgical technique. *Prilozi*. **30**, 71–80

184. Cooper, C. A., Handy, R. D., and Bury, N. R. (2006) The effects of dietary iron

concentration on gastrointestinal and branchial assimilation of both iron and cadmium in zebrafish (Danio rerio). *Aquat. Toxicol.* **79**, 167–175

185. Yuan, X., Rietzschel, N., Kwon, H., Walter Nuno, A. B., Hanna, D. A., Phillips, J. D., Raven, E. L., Reddi, A. R., and Hamza, I. (2016) Regulation of intracellular heme trafficking revealed by subcellular reporters. *Proc. Natl. Acad. Sci.* . **113**, 5144–5152

186. Hanna, D. A., Harvey, R. M., Martinez-Guzman, O., Yuan, X., Chandrasekharan, B., Raju, G., Outten, F. W., Hamza, I., and Reddi, A. R. (2016) Heme dynamics and trafficking factors revealed by genetically encoded fluorescent heme sensors. *Proc. Natl. Acad. Sci.* . **113**, 7539–7544

187. Kovtunovych, G., Ghosh, M. C., Ollivierre, W., Weitzel, R. P., Eckhaus, M. A., Tisdale, J. F., Yachie, A., and Rouault, T. A. (2014) Wild-type macrophages reverse disease in heme oxygenase 1-deficient mice. *Blood*. **124**, 1522–1530